Electromagnetic Interference on Static Energy Meters Due to Residential Emissions

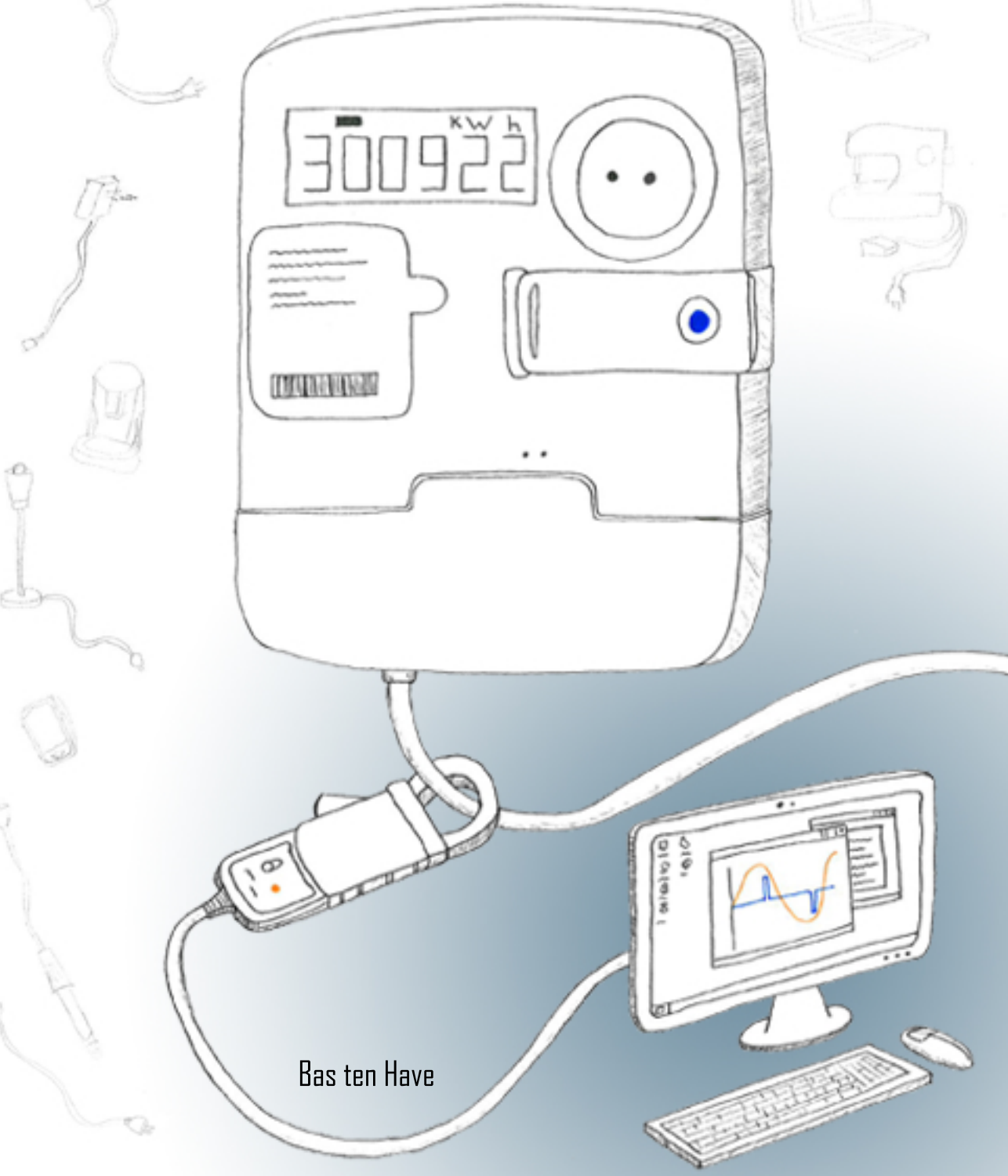

Bas ten Have

Electromagnetic Interference on Static Energy Meters Due to Residential Emissions

by

Bas ten Have

Members of the graduation committee:

Chairman & Secretary:

Prof. dr. J. N. Kok

Promoter:

Prof. dr. ir. ing. F. B. J. Leferink

Co-Promoter:

Dr. ir. D. J. G. Moonen

Internal Members:

Prof. dr. ir. G. Rietveld

Dr. ing. J. Popovic

External Members:

Prof. dr. ir. J. F. G. Cobben (Eindhoven University of Technology)

Prof. dr. F. Grassi (Politecnico di Milano)

Dr. M. Pous (Universitat Politècnica de Catalunya)

The research described in this thesis was carried out in the Power Electronics and Electromagnetic Compatibility Group, which is part of the Faculty of Electrical Engineering, Mathematics and Computer Science at the University of Twente, Enschede, The Netherlands.

The author's Ph.D. position in the project 17NRM02 MeterEMI has received funding from the EMPIR programme co-financed by the Participating States and from the European Union's Horizon 2020 research and innovation programme.

ISBN: 978-90-365-5413-8
DOI: 10.3990/1.9789036554138

Cover design by Birgit ten Have
Printed by Gildeprint
Typeset in LaTeX 2ε

Electromagnetic Interference on Static Energy Meters Due to Residential Emissions

Dissertation

to obtain
the degree of doctor at the University of Twente,
on the authority of the rector magnificus,
Prof. dr. ir. A. Veldkamp,
on account of the decision of the Doctorate Board,
to be publicly defended
on Friday 30th September 2022 at 12:45 hours

by

Bas ten Have

born on 2nd October 1994
in Zuidhorn, The Netherlands

This dissertation has been approved by:

The Promoter:	Prof. dr. ir. ing. F. B. J. Leferink
The Co-Promoter:	Dr. ir. D. J. G. Moonen

Summary

Nowadays, as part of the energy transition electricity is used more efficient and sustainable. Either by developing sustainable alternatives for other domains, such as photovoltaic installations and electric cars. Or by making equipment more efficient, for example by energy efficient lighting equipment. This will increase the energy usage, but moreover the connected loads in an electricity grid change from conventional linear towards non-linear time-variant loads. This has resulted in many conducted electromagnetic interference problems, especially in the frequency range from dc till 150 kHz. Of which the interference on static energy meters is an impactful case as it results in too high or too low energy bills for consumers. Therefore, this thesis aims to get a better understanding of the underlying problem by investigating the interfering cases and determining the extent of the problem. This is done by reviewing the electromagnetic compatibility standards for static energy meters. After which, the immunity of static energy meters is investigated in the lab by using various non-linear equipment. Then, measurement probes are characterized for an accurate capture of (on-site) pulsed currents. Next, the critical parameters that interfere with static energy meters are identified. And finally, the extent of the metering problem is investigated by capturing on-site current waveforms from individual equipment and of the complete system at the meter connection point. From which it is concluded that the electromagnetic interference on static energy meters is due to non-linear pulsed currents. Which have a high crest factor, narrow pulse width, high peak amplitude, low charge, and high slopes. Moreover, in the on-site many similar waveforms were found. In contrast, the test standards only cover frequency domain test methods, which are thus not representative for the interference waveforms.

Samenvatting

Vandaag de dag wordt elektriciteit duurzamer en efficiënter gebruikt als onderdeel van de energie transitie. Bijvoorbeeld door duurzame alternatieven voor andere domeinen te ontwikkelen, zoals zonnepanelen en elektrische auto's. Of door apparatuur efficiënter te maken, bijvoorbeeld met energie zuinige verlichtingsapparatuur. Dit zal het energieverbruik verhogen, maar bovendien zullen de belastingen in het elektriciteitsnet veranderen van lineair naar niet-lineaire tijd variërende belastingen. Dit heeft geresulteerd in veel elektromagnetische interferentie problemen, met name in het frequentiebereik van dc tot 150 kHz. Een aangrijpend probleem is de interferentie van statische energie meters dat resulteert in te hoge of te lage energierekeningen voor consumenten. Daarom is dit proefschrift bedoeld om het onderliggende probleem beter te begrijpen en de omvang van het probleem te bepalen. Dit is onderzocht door de elektromagnetische compatibiliteit standaarden voor statische energie meters te analyseren. Waarna de immuniteit van statische energie meters is onderzocht in het lab door verschillende niet-lineaire belastingen te gebruiken. Hierna worden meetsensoren voor het accuraat bemeten van pulserende stroomvormen gekarakteriseerd. Vervolgens worden de kritische parameters die interfereren met de statische energie meters geïdentificeerd. Tot slotte wordt de omvang van het probleem onderzocht door de stroomvormen die in het veld voorkomen bij individuele apparatuur en bij het complete systeem in de meterkast te bemeten. Hieruit kan geconcludeerd worden dat de elektromagnetische interferentie van statische energie meters wordt veroorzaakt door niet-lineaire pulserende belastingen. Deze hebben een hoge topfactor, smalle puls breedte, hoge piek amplitude, kleine lading, en steile helling. Bovendien hebben de veld metingen vergelijkbare golfvormen laten zien. Dit in tegenstelling tot de test standaarden die frequentiedomein test methodes bevatten, welke dus niet representatief zijn voor de interfererende golfvormen.

Table of contents

Abbreviations

APD amplitude probability distribution.

CFL compact fluorescent lighting.

COTS commercial off-the-shelf.

CT current transducer.

CW continuous wave.

DWT discrete wavelet transform.

EMC electromagnetic compatibility.

EMI electromagnetic interference.

EU European Union.

EUT equipment under test.

EV electric vehicle.

FFT fast Fourier transform.

GaN gallium-nitride.

IDW inverse distance weighting.

LED light emitting diode.

LISN line impedance stabilization network.

LTI linear time-invariant.

MID measuring instruments directive.

MOSFET metal-oxide-semiconductor field-effect transistor.

PELT pruned exact linear time.

PLC power line communication.

PV photovoltaic.

PWM pulse width modulation.

RCD residual-current device.

TEMPS time-domain EMI measurement and processing system.

TRIAC triode for alternating current.

Chapter 1

Introduction

1.1 Background and motivation

Over the last decades the electrical world is changing and many energy efficient solutions contribute to a more sustainable use of electricity. This is an important transition that aims to reduce the emission of greenhouse gasses and has an environmental impact, among others. According to the goal of the European Union (EU) which are committed to reduce its overall emissions by at least 55% compared to 1990, by 2030, and to achieve climate neutrality in 2050 [1]. This has resulted in the development of sustainable electrical alternatives for well known products from other domains, such as new sources of energy and energy efficient products. Examples of these sustainable alternatives are wind turbines, photovoltaic (PV) installations, electric cars, induction cookers, heat pumps and many more, which are replacing their coal-fired, combustion engine, or gas-based counterparts. Furthermore, already existing equipment such as lighting equipment is made more energy efficient. This energy transition, e.g. the increased use of electrical alternatives, means an increased use of electricity, which is expected to grow from 3500 TWh per year in 2020 to 4900 TWh per year in 2050 within the EU, according to Roadmap 2050 [2], initiated by the European Climate Foundation (ECF).

Furthermore, the electrical behavior of the loads (i.e. electrical equipment/appliances) is also changing, with the aim of using the electricity in an energy efficient manner. The loads that were used in a conventional electricity grid could be considered to be of a linear nature with some degree of capacitive or inductive behavior. Whereas, nowadays there is a large increase in loads that cannot be considered as linear time-invariant (LTI) [3], for example due to the introduction of switching power electronics. Where non-linear means that the equipment has a voltage varying impedance, and time-varying means that it is dependent on time.

These changes provide several technical challenges in the field of electromagnetic compatibility (EMC), for example due to the electrification and smart

grid technology as pinpointed in [4]. EMC is the ability to operate adequatly (being compatible) in the electromagnetic environment, i.e. without causing unwanted emissions and being immune to this environment. The classical description of electromagnetic interference (EMI) is visualized in Figure 1.1, the disturbance consists of a source creating the interference that propagates via a coupling path to a victim. Where the coupling path is either radiated or conducted. As opposed to radiated, conducted coupling is via a medium, being the coupling path in this thesis. In that sense, the electrification and increased use of non-linear loads is increasing the harmonic distortion. While, decreasing the linear loads which function as damping elements. Therefore, the harmonic levels are expected to increase in power supply systems [5].

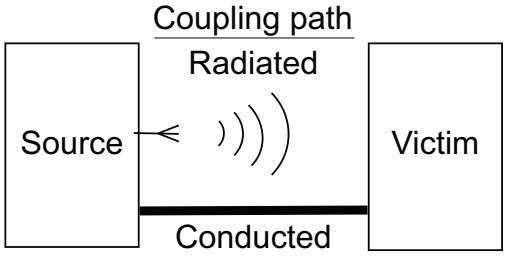

Figure 1.1. Classical description of the EMI problem.

In that sense, the conventional victim of conducted EMI was the distribution grid. Where the quality of the supply voltage is standardized using the EN 50160 [6], and disturbances that are considered are a voltage dip, voltage surge, voltage fluctuations, harmonic voltage distortion, transient voltage, and voltage unbalance [7]. These basic (conventional) conducted disturbances are shown in Figure 1.2. Where the voltage disturbances due to the current, e.g. inrush currents, were not considered as an EMI problem. The effect of current distortion on a weak supply grid was investigated in [8], it was shown that for low power loads connected to the generator, the supplied voltage waveform was heavily distorted, resulting in high harmonic distortion. Switching on multiple loads simultaneously resulted in high inrush currents causing stability problems of the generator. These high peak values could result in a crash of the generator thus indicating a complete shutdown of the system. Furthermore, the energy efficient equipment poses several problems in the frequency range from dc to 150 kHz. Actually most equipment malfunction originates from this frequency range [9]. An example is the switching of power electronics, usually operating from dc to 150 kHz, that draws pulsed currents with high peak values, and creates a high $\mathrm{d}v/\mathrm{d}t$ and $\mathrm{d}i/\mathrm{d}t$ [10]. Several other cases of conducted EMI issues are reported that include, but are not limited to problems with power converters [11], household equipment [12], for instance lighting equipment [13], television and radio receivers or a coffee machine [14], power line communication (PLC) [15], PV installations [16], and static energy meters [17]. In all these cases malfunctions or loss of performance are observed.

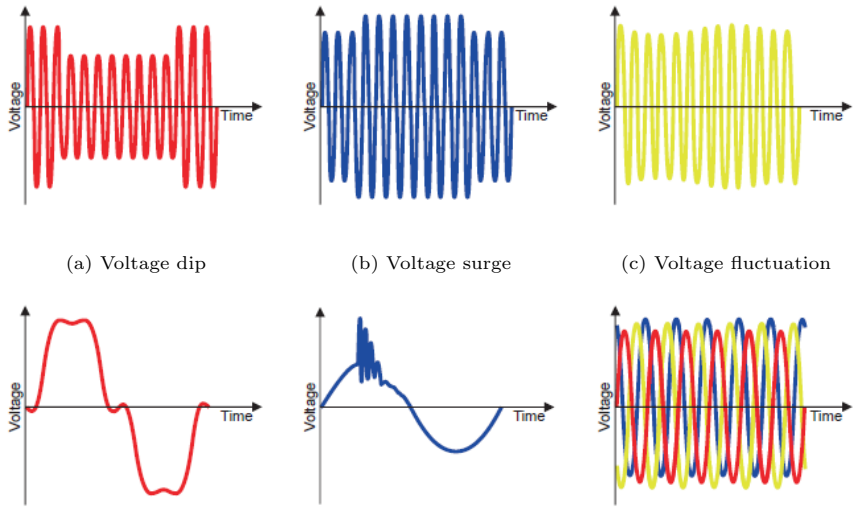

(a) Voltage dip (b) Voltage surge (c) Voltage fluctuation

(d) Harmonic voltage distortion (e) Transient voltage (f) Voltage unbalance

Figure 1.2. Basic conducted disturbances [7].

The latter EMI issue is an important issue as it affects society directly, as static energy meters are used to measure the electrical energy consumption in household situations for billing purposes. Static energy meters are electronic and replace conventional electromechanical (or Ferraris) meters. The static energy meter has no rotating parts such as the rotating disc of the electromechanical meter (rotating at a speed proportional to the power or rate of energy usage, according to the Ferraris principle) and are therefore called static. Despite the proper functioning of the electromechanical meter, as acknowledged by the utilities and consumers, replacing them by their electronic counterparts is useful as the electromechanical meter provides limited information, i.e. only the measured energy, and its lack of communication capabilities [18]. The static energy meter is also able to measure and record the rms voltages and currents, apparent power, and reactive power, among others. When the static energy meter is communicating automatically with the utility provider, i.e. a communication interface is added, the meter is called a smart meter. This communication can provide information in a smart grid to balance the supply and demand of energy [19], or even allows for appliance control based on the status of the grid [20]. An additional benefit is to adapt the energy pricing to the dynamic generation of energy. Furthermore, a static energy meter is a valuable tool for consumers to monitor and become aware of their energy consumption using specific monitoring applications. This can give an insight in their energy consumption and pinpoint large consuming loads. The static energy meters are

currently widely deployed throughout the EU [21], so potential EMI issues will affect a large group of consumers.

Interference problems with static energy meters were reported in various situations. These are summed up hereafter to indicate the size of the interference issues with static energy meters. Such as, considering harmonic disturbances in power systems as explored in [22], after which errors of static energy meters are presented in [23] and analyzed in dept in [24]. Where the errors seem to increase with the increase of the reactive energy in the test signal. Furthermore, interference of static energy meters from PV installations and power drive systems was found in Germany [25] in an on-site situation, after which a further elaboration showed that the meters could be affected in certain conditions [26]. Afterwards, laboratory measurements confirmed these errors [27], those measurements focused both on the standardized immunity tests as well as the emissions of inverters. Besides, cases of high interference levels generated by various modern appliances in Finland, Spain, and Sweden are listed in the CLC/TR50627 [14] technical report, which resulted in a loss of communication of static energy meters with their PLC system. These problems were, among others, due to: inverters, televisions, DVD players, computers, heat pumps, boilers, an uninterruptible power supply, a PLC homeplug modem, a frequency controlled ventilator, and a camera surveillance system. These observations, possibly combined with a higher number of complaints and failures, resulted in faster publication of the CLC/TR50579 [28] technical report and IEC 61000-4-19 standard [29]. Afterwards interference problems with modern household appliances are observed, based on consumer complaints. Such as, lighting equipment using light emitting diode (LED) and compact fluorescent lighting (CFL) technology has resulted in static energy meter misreadings [30]. These experiments were extended by the inclusion of more specimen of static energy meters in [31], and showed the existence of interference on a larger selection of meters. After which, [32] discusses the cause of the problem and shows that the Rogowski coil, which measures the time-derivative of the current, can result in errors as the measured signal needs to be integrated. These findings were confirmed by an independent research lab in [33]. Similar research in [34] tried to replicate the measurements for specimen of meters as used in North America, however this research could not find any errors outside the permissible limits of those tested meters. This means that only a selection of static energy meters will show interference problems, which was also stated in the other studies. Additionally, static energy meter performance in an on-site environment was considered in [35] by including various harmonic voltages and currents, this resulted in metering errors. Especially, when considering actual waveforms from light bulbs, errors up to 25% were reported. Other cases of interference due to modern appliances were reported, e.g. due to a speed-controlled water pump [36], resulting in errors up to 2675%, and multimedia equipment [37]. These interference cases will be explained in more detail in Chapter 3. The existence of more household appliances and their relation to metering errors was reported in [38]. In [39], the effect of frequency variations

affected the tested static energy meters, however those still complied with the accuracy limits. Also more recent studies on the effect of non-sinusoidal voltages and currents showed errors up to 8% of static energy meters, so outside the limits as included in the test standards [40]. And in [41], static energy meter errors are found due to undershoot and overshoot effects of the integrated circuit technology when using pulsed currents. Furthermore, interference from a missile early warnings system at RAF Fylingdales could not work together with a static energy meter [42]. Therefore a consumer living close to the missile system could not be equipped with a static energy meter. This is undesirable as the consumer wanted to charge its electric vehicle (EV) based on dynamic pricing as offered by its utility company, and consequently this issue costs him £26 every week. The previously listed interference cases indicate the large extent of the problem, which could have large societal implications by means of incorrect energy bills. This thesis analyzes the underlying problem by investigating the interference cases and aims at providing a better understanding of the problem. Furthermore, the investigated interference cases are placed into perspective by correlating them with typical waveforms that occur in residences.

1.2 The MeterEMI research project

The EMI problems resulting in misreadings of static energy meters are researched within the framework of the MeterEMI project [43]. This is an European research project where seven partners are collaborating within the project, of which five are metrology institutes and two are universities:

- National Physical Laboratory (United Kingdom),
- Cesky Metrologicky Institute (Czech Republic),
- Justervesenet (Norway),
- Eidgenössisches Institut für Metrologie METAS (Swiss),
- Van Swinden Lab B.V. (The Netherlands),
- Universitat Politècnica de Catalunya (Spain),
- University of Twente (The Netherlands).

The specific objectives of the project are split into work-packages (WP) as follows:

1. Provide measurement equipment that is able to determine the nature of the interference waveforms in lab and on-site situations. And to use it to find these interference signals. (WP1)
2. Develop measurement algorithms to accurately measure ac power and energy in the presence of highly impulsive current signals. And furthermore

develop algorithms to determine the parameters of typical disturbing currents to classify and re-generate them for type-testing of commercial static energy meters. And implement those algorithms in a tool suitable for diagnostic use by a non-specialist to analyze disturbing signals. (WP2)

3. Develop a standard measurement test-bed for testing static energy meters with a target uncertainty of better than 0.1 %, suitable for testing against disturbance signals from WP1 and WP2. (WP3)

4. Develop new type-tests and validated methods for determining the performance of a static energy meter. Including tests utilizing the test-bed from WP3. (WP4)

5. Contribute to the standards development work and the legal metrology organisations to ensure that the outputs of the project are aligned with their needs, communicated quickly to those developing the standards and to those who will use them, and in a form that can be incorporated into the standards at the earliest opportunity. (WP5)

The research of this thesis complements with the objectives of WP1 and WP2.

1.3 Research objectives

To address the EMI problems with static energy meters as introduced in Section 1.1, this thesis aims to get a better understanding of the underlying problem by investigating the interference cases. And aims to place them into perspective in order to determine the extent of this interference cases by a survey of the waveforms in a realistic on-site environment. In that sense, the thesis solely investigates the EMI resulting in (potential) incorrect energy readings of the static energy meter, and does not consider, for example, problems with the communication by PLC. That is, this thesis investigates the research objectives that are listed below:

- Review the EMC standards related to static energy meters and its electrical environment.
- Laboratory identification of the immunity of static energy meters due to non-linear equipment.
- Characterization of measurement probes for an accurate capture of (realistic) pulsed currents.
- Identify the critical parameters of the currents that interfere with static energy meters.
- Determine the extend of the metering problem by capturing realistic on-site current waveforms of individual appliances and the complete system at the meter connection point.

1.4 Outline of the thesis

The thesis is structured according to the research objectives stated in the previous section.

First, Chapter 2 reviews the relevant EMC standards based on the European directives. That is, both the EMC directive and the measuring instruments directive (MID) are analyzed. Furthermore, the harmonized standards that are related to the immunity and emission of the static energy meter, the grid, and the connected equipment are reviewed. So covering both the static energy meter and the electrical environment it is placed in.

Second, Chapter 3 presents several cases in which the static energy meter shows misreadings due to conducted EMI. It shows the measurement method that is used in a controlled laboratory environment. After which, several interference cases are presented including emissions from modern household appliances of a speed controlled water pump, lighting equipment, and multimedia equipment. Then, based on a consumers issue, different issues with a correctly functioning static energy meter are presented that are of interest from social point of view, as it can impact the energy billing of consumers.

Third, Chapter 4 describes a study on the applicability of a current transducer (CT) for the measurement of practical non-linear pulsed current waveforms in either a laboratory or on-site situation. This is done by characterizing CTs using pulsed currents rather than conventional methods that use frequency swept continuous wave (CW) signals. Those pulsed current test signals are based on the practical interference currents as identified in Chapter 3. It is shown that the characterization tests with pulsed currents result in similar results as the CW method without the need of exhaustive measurement equipment. Furthermore, the actual interference signals from Chapter 3 are used to test the response of the CTs. And discrepancies in the current response are observed, resulting in incorrect energy measurements when multiplying the measured current with the voltage.

Fourth, Chapter 5 provides a parametric waveform model to analyze the time-domain interference on static energy meters created by non-linear, pulsed currents. In that sense, the parametric waveform model aims at reducing the complexity of the waveforms description, while retraining the relevant critical features, in relation to static energy meter interference, of such a signal. So, it presents the critical features/parameters of the waveforms found to interfere with static energy meters in Chapter 3. Also this chapter shows how such a modelled version of the waveform could be used as a simplified artificial test waveform in future test standards.

Fifth, Chapter 6 presents a survey of the time-domain emissions that are generated by equipment in residential low-voltage networks. It analyzes the emissions from different (dimmed) lighting equipment in detail, and furthermore provides a statistical overview from all equipment classes included in the IEC 61000-3-2 [44] using the time-domain approach introduced in Chapter 5. At the end, a broad overview of emissions as created by modern appliances is

mapped.

Sixth, Chapter 7 presents typical current waveforms that are present at the static energy meter connection point in a residential situation. Thus portrays the realistic on-site situation where the static energy meter is placed in. The on-site waveforms are related to the critical waveforms that resulted in EMI problems with static energy meters in Chapter 3 by indicating similar features between those signals using the parametric modelling approach from Chapter 5. In order to find similarities between those signals and to estimated the interference of the on-site surveyed waveforms. In this way, the extend of the critical interference waveforms in a real-world environment is determined based on an on-site survey of three premises. Covering an EV charging station, a residence including a PV installation, and an apartment premise.

And finally, Chapter 8 will summarize and conclude the main findings of the work presented in this thesis. Furthermore, it aims at presenting directions for future work with respect to the interference of static energy meters.

Chapter 2

State of the art in standardization

In this chapter, the state of the art in standardization related to static energy meters, the equipment (or appliances) that is present in low-voltage grids, and the low-voltage grid is analyzed. The content of this chapter comprises the research that was earlier published in [45], [46].

2.1 Motivation

Problems with static energy meters resulting in incorrect billing of consumers are already discussed in the introduction of this thesis (Chapter 1). Therefore, it is of importance to ensure consumers confidence in the reliability of static energy meters and thus in their energy bill. The problem involves the static energy meter and the electromagnetic environment where the meter is placed in. Which includes the connected equipment and the low-voltage grid. The static energy meter should comply with the European directives to ensure a reliable measurement of energy, which is demonstrated by means of the corresponding harmonized standards. These are indicating the EMC limits for the products emission or immunity. In order to evaluate the feasibility of these directives and standards throughout this thesis, based on the measured waveforms of interference cases (Chapter 3), typical equipment (Chapter 6), and at residential metering connections (Chapter 7), this chapter aims to review the state of the art in standardization that is relevant for the interference on static energy meters.

In this regard, it is of importance to also review the frequency range from 2 kHz until 150 kHz, because there is a lack of civil standards in this frequency range as was already indicated in previous research [17]. For example, this gap was addressed considering the static energy meter [47], the smart grid components [48], or the connected equipment that consist of power electronic converters [49]. This frequency range has gained interest for the development

of standards for apparatus [50], as in this frequency range only a few standards exists and nearly no requirements are taken into account. While this is an important frequency range, as many power electronics switch in these frequencies [51], causing loads in low-voltage grids to include higher frequencies [52]. As a result the voltage and current waveforms may contain distortion for frequencies up to 150 kHz [53]. Also many EMC complaints of equipment malfunction due to interference in this frequency range are reported in [9], including problems with static energy meters as was introduced in Chapter 1 of this thesis. Furthermore, the interference signals that resulted in EMI problems with static energy meters in [31], represent quite wide-band signals. This is visualized in Figure 2.1 where the differential mode current and line-neutral voltage from a combination of dimmed CFL and LEDs is plotted in time and frequency-domain. The current harmonics up to 2 kHz are quite significant compared to the fundamental frequency of 50 Hz, but also the frequency content between 2 kHz

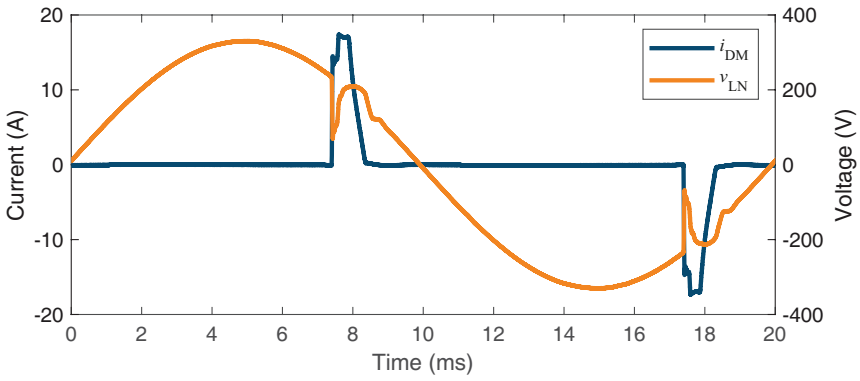

(a) Time-domain response

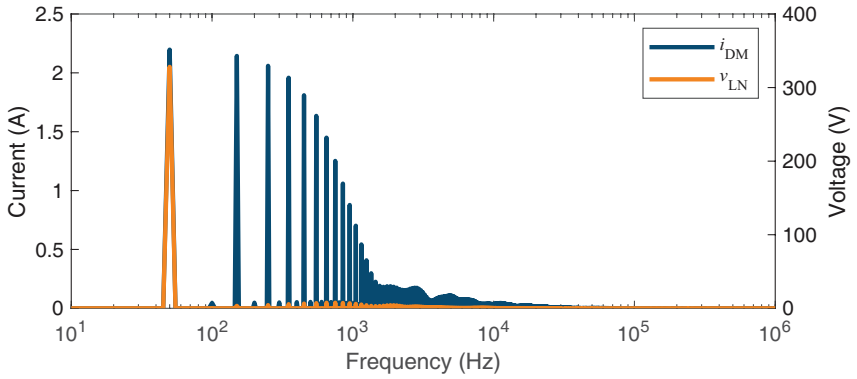

(b) Frequency-domain response

Figure 2.1. Waveforms from a combination of dimmed CFL and LEDs resulting in EMI problems with static energy meters [31].

and 150 kHz is still rather large, i.e. up to 10% of the current amplitude at the fundamental frequency.

The rest of this chapter discusses the applicable directives and standards. In Section 2.2 the European directives are be reviewed, i.e. the EMC directive and the MID. The harmonized standards specific for static energy meters are discussed in Section 2.3, the equipment (or appliances) connected to the meter in Section 2.4, and the low-voltage grid where the meter is installed in Section 2.5. Finally, in Section 2.6 this chapter ends with a discussion and conclusion about the feasibility of these standards, which will form a point of discussion throughout this whole thesis.

2.2 European directives

The European directives are a legal act of the EU to which all devices and systems available on the market should adhere. By means of harmonised standards manufacturers can demonstrate that the products/services/processes comply with the relevant EU legislation. Still, the European directives are the leading legal act [54].

When considering the EMC of products, all products available on the market should comply with the EMC directive 2014/30/EU [55]. The essential requirements of the EMC directive in point 1 of Annex 1 state that: *"Equipment shall be so designed and manufactured, having regard to the state of the art, as to ensure that:*

- *the electromagnetic disturbance generated does not exceed the level above which radio and telecommunications equipment or other equipment cannot operate as intended;*
- *it has a level of immunity to the electromagnetic disturbance to be expected in its intended use which allows it to operate without unacceptable degradation of its intended use."*

Furthermore, in point 2 it is stated that: *"A fixed installation shall be installed applying good engineering practices and respecting the information on the intended use of its components, with a view to meeting the essential requirements set out in point 1."* This means that you should not cause any interference and you should not be sensitive to interference. And the harmonized standards are only a tool to demonstrate the immunity or emissions. However, according to the MID, measuring instruments (such as the static energy meter) do not have to comply with the EMC directive, as the European MID 2014/32/EU [56] states the following: *"The performance of some measuring instruments is strongly influenced by the environment, especially the electromagnetic environment. Immunity to electromagnetic disturbances of measuring instruments should form an integral part of this Directive and the immunity requirements of Directive 2004/108/EU of the European Parliament and of the Council of 15*

December 2004 on the approximation of the laws of the Member States relating to electromagnetic compatibility, therefore do not apply." So measurement instruments can be affected by EMI, which is compromised in the MID, and therefore measurement instruments do not have to comply with the EMC directive.

Still, the requirements of the MID need to be taken into account, this directive is a conformity assessment to which all products (in this case measurement instruments) should adhere when those are placed on the market. The essential requirements in Annex I of this directive state the rated operating conditions as follows: *"The rated operating conditions are the values for the measurand and influence quantities making up the normal working conditions of an instrument."* Where it is clear that the "normal working conditions" are not sinusoidal, as was already addressed previously in [57]. Actually, the effect of non-sinusoidal conditions was already proven to interfere with static energy meters in [35], due to harmonic and on-site disturbances. In that sense, the equipment that is connected to the static energy meter in a real-world low-voltage grid should be seen as "normal working conditions" for the static energy meters. Furthermore, this annex also states that: *"Under rated operating conditions and in the absence of a disturbance, the error of measurement shall not exceed the maximum permissible error (MPE) value as laid down in the appropriate instrument-specific requirements."* Meaning that the static energy meter should measure correctly, i.e. comply, when placed in its "normal working conditions". For the interference example in [31], the dimmers and connected luminaries are present in a low-voltage grid and this situation is thus considered as a "normal working condition" for which the static energy meter should operate correctly.

2.3 Static energy meters

Next, the relevant harmonized standards are reviewed. Static energy meters have to comply with the product standard IEC 62053-21 [58] for meters with accuracy class 0.5, 1, and 2, or to the IEC 62053-22 [59] for transformer operated meters of accuracy classes 0.1 S, 0.2 S and 0.5 S. These standards refer back to the more general IEC 62052-11 [60] for electricity metering equipment. These have a similar structure and limits with the specific European requirements in the EN 50470-1 [61], for general metering equipment, and the EN 50470-3 [62], considering particular requirements for static energy meters. Static energy meters need to meet the maximum permissible limits for electricity meters with approval of the European MID 2014/32/EU [56], which are derived from the IEC 62053-21, IEC 62053-22, and EN 50470-3 standards. The approved accuracy limits are shown in Table 2.1.

Table 2.1. Maximum permissible error limits according to the European MID 2014/32/EU [56].

MID accuracy class	Maximum permissible error limits
Class A	2.5%
Class B	1.5%
Class C	0.5%

2.3.1 Harmonic voltages and currents

The IEC 62053-21 and EN 50470-3 standards include tests to verify the immunity of static energy meters to harmonic voltages and currents. In particular, even harmonics are tested using a half-wave rectified signal at mains frequency, as is visible in time and frequency-domain in Figure 2.2. Furthermore, odd harmonics are tested using a phase fired signal with firing points at 5 ms and 15 ms, i.e. 90°and 270°, with a rise time of 0.2 ms. This is shown in time and frequency-domain in Figure 2.3. However, these signals contain multiple frequency components, the harmonic content decays quite fast, and the signals are not comparable to the broadband pulse as was exemplified in Figure 2.1, that has a significant broader frequency spread.

2.3.2 Conducted common mode disturbances

For conducted measurements the general standard for electricity metering equipment, i.e. the IEC 62052-11, refers to the IEC 61000-4-6 [63]. However this standard only covers the frequency range from 150 kHz till 80 MHz and applies only common mode signals. Which covers higher frequencies than the frequency band of interest considering static energy meter interference, i.e. 2 kHz until 150 kHz. Next to this differential mode is more relevant compared to common mode [47].

2.3.3 Conducted differential mode disturbances

In addition to this, the IEC 61000-4-19 standard [29] applies for static energy meters, which was introduced in 2014 after the first complaints on static energy meter interference. The IEC 61000-4-19 standard, is used to test electrical and electronic equipment for immunity against conducted differential mode disturbances and signaling in the frequency range from 2 kHz to 150 kHz. The standard covers two test methods that consider CW signals and rectangular modulated CW signals. For the first test, a CW signal is applied to the equipment under test (EUT) and the frequency, f_i, is increased from 2 kHz to 150 kHz. The test cycle consists of a duration in which a CW of frequency f_i is applied and a pause where the signal is zero, after this the frequency is increased by a factor 1.02. This time-domain behavior is visualized in Figure 2.4(a).

The second test described in the standard is performed by applying a sequence of rectangular modulated CW pulses, with an increasing frequency from

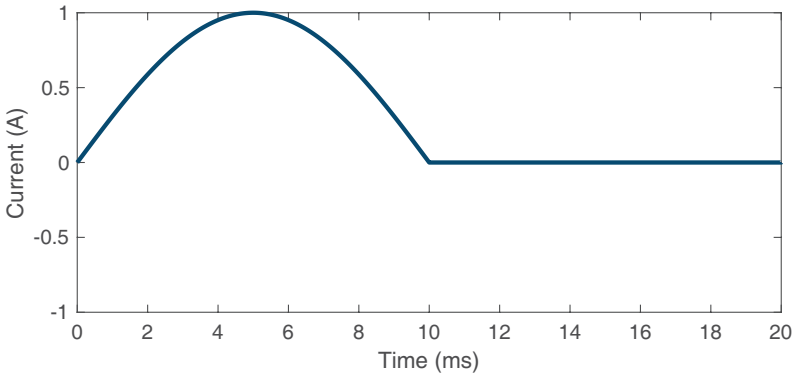

(a) Time-domain response

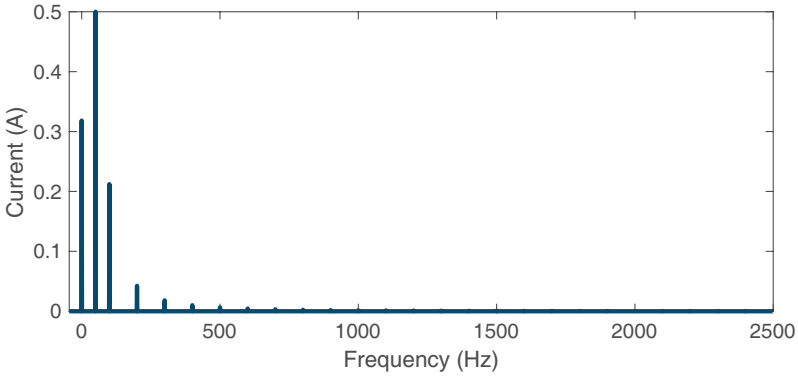

(b) Frequency-domain response

Figure 2.2. Test signals for even harmonic voltages and currents using a half-wave rectified signal, according to the IEC 62053-21 [58] and EN 50470-3 [62].

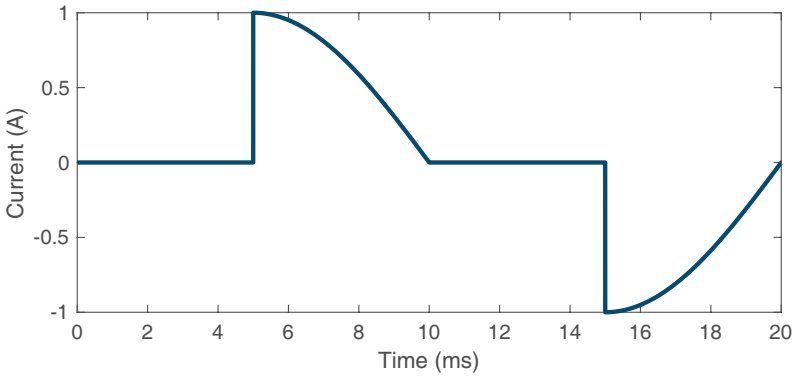

(a) Time-domain response

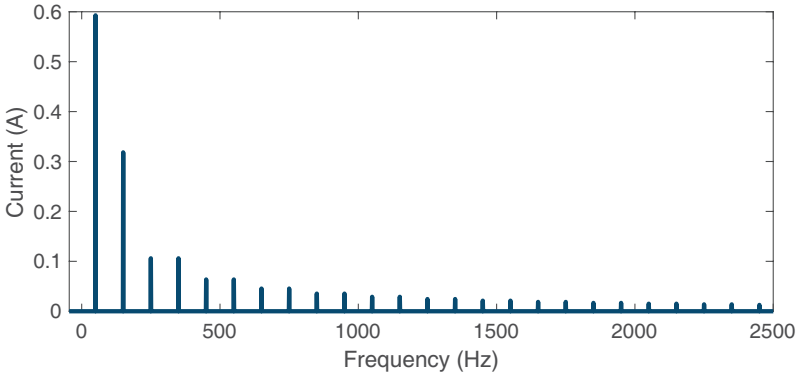

(b) Frequency-domain response

Figure 2.3. Test signals for odd harmonic voltages and currents using a phase fired signal at 90°and 270°, according to the IEC 62053-21 [58] and EN 50470-3 [62].

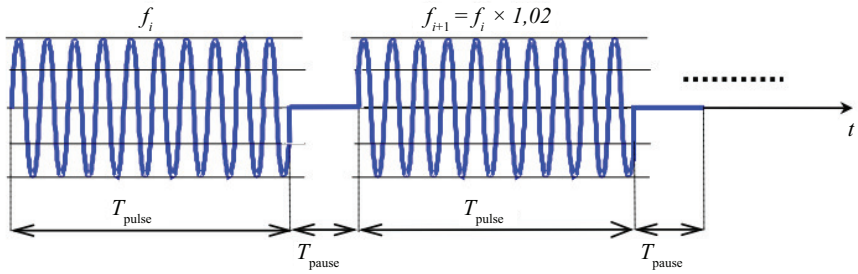

(a) CW pulses with pause

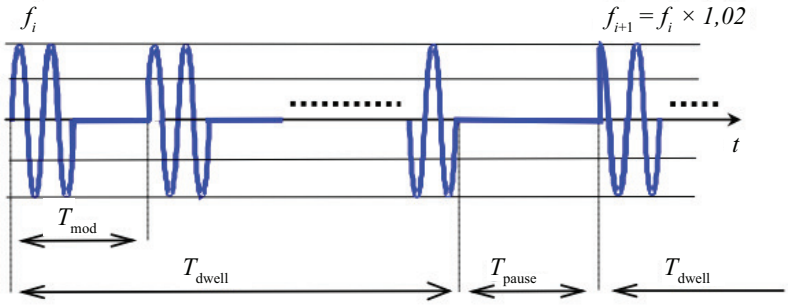

(b) Rectangular modulated pulses

Figure 2.4. Test wave profiles according to the IEC 61000-4-19 [29].

2 kHz to 150 kHz, to the EUT. The frequency is increased by a factor of 1.02 every step. This behavior is visualized in Figure 2.4(b).

The standard uses the frequency-domain, i.e. single tone testing, which is common among EMC compliance testing. It means that at any moment in time only one frequency is tested. Sweeping of frequencies is done to determine the system's transfer function, i.e. to determine how the system reacts to each frequency individually. From LTI theory it is known that the system's transfer function, $H(s)$, is related to the impulse response, $h(t)$, through the Laplace transform. Determining the impulse response is thus equivalent to the system's transfer function under the assumption that one is characterizing an LTI system. This means that the frequency-domain tests would hold in the situation of an LTI system. However, the problem is that the combination of all the systems within a household cannot be considered as LTI anymore. This is among others due to the non-linear elements within such a household. The connected loads in a household can be non-linear and time varying, which results in $H(s) \neq h(t)$. As the currents drawn are impulsive in nature, the system's response is more realistically described with its impulse response. These non-linear and time varying elements within the entire system result in the fact that the frequency-domain tests, like the IEC 61000-4-19, do not hold anymore,

as those are based on the LTI assumption.

2.4 Equipment

The connected equipment in low-voltage systems, where the static energy meter is also installed, should meet the EMC standards to ensure a proper function of all connected systems. In regard of the interference of static energy meters, the conducted emission limits of the equipment are of interest as it provides information about the maximum voltage and current levels generated by the equipment and measured by the installed static energy meter. An overview of the related EMC standards is provided in Figure 2.5 [64]. The harmonic current emissions of equipment with an input current lower than 16 A are regulated in the IEC 61000-3-2 [44], while input currents from 16 A to 75 A are covered by the IEC 61000-3-12 [65]. These standards cover the harmonic frequencies until the 40th harmonic, which is 2 kHz or 2.4 kHz for a 50 Hz and 60 Hz system, respectively. The IEC 61000-3-2 specifies the limits for different classes of equipment dependent on its usage and electrical working principle. It is remarkable that no emission limits apply for equipment with a rated power of 75 W or less, other than lighting equipment. This exception is resulting from the conventional connected loads, that are resistive, and consume more than 75 W, such that lower consuming loads could be considered as insignificant. However, nowadays most connected equipment is non-linear [3], made more energy efficient, and consumes less power. And thus, significant more modern equipment will have a lower consumption than 75 W. Furthermore, no limits apply for independent dimmers for lighting equipment. Which is also difficult to test as many luminaries can be combined with an independent

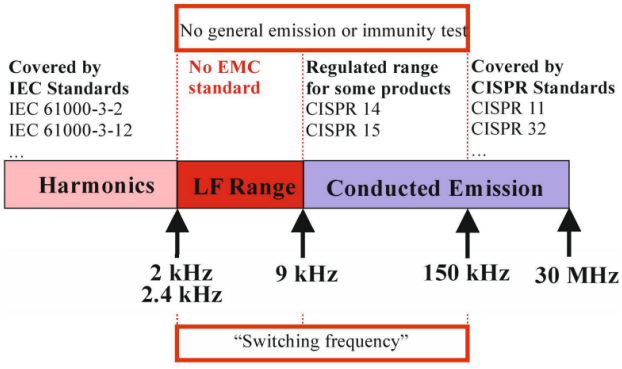

Figure 2.5. Overview of the frequency range covered by EMC standards for equipment [64].

dimmer, and interference problems might only occur in particular cases. But this is of particular interest, as a combination between dimming and lighting

equipment has been shown to generate highly distorted currents and could result in metering errors [31]. This emission was shown before in Figure 2.1, and it could be seen that the harmonic emissions are quite significant compared to the fundamental frequency. Beyond the frequencies covered by the IEC 61000-3-2, it is noted that no EMC standard exists in the region from 2 kHz till 9 kHz. From 9 kHz on-wards some product specific regulations hold, which are the CISPR 14-1 [66] and CISPR 14-2 [67] for emission and immunity of household appliances, electric tools and similar apparatus, respectively, and the CISPR 15 [68] for electrical lighting equipment. These standards specify disturbance voltage limits from 9 kHz till 150 kHz, but do not cover all connected equipment in low-voltage distribution systems. Furthermore, those standards only briefly address the frequency range from 9 kHz till 150 kHz and mainly focus on the emissions above 150 kHz. In addition, several other product standards have emission limits above 150 kHz, such as: the CISPR 11 [69] for industrial, scientific, and medical equipment, and the CISPR 32 [70] for multimedia equipment. So, this means that there is a lack of general emission limits in the frequency range from 2 kHz till 150 kHz to protect the electrical grid and connected equipment [71].

2.5 Low-voltage grid

Besides the EMC standards that apply for the static energy meter and the connected equipment, it is also important to know the electrical environment they are placed in or connected to, which is the low-voltage grid. And thus the limits stated for the low-voltage grid to ensure a compliant grid. This is regulated by means of the IEC 61000-2-2 [5] including compatibility limits for harmonic voltages, i.e. until 2 kHz, in the low-voltage grid. Besides, conducted limits for the frequency range 2 kHz till 150 kHz are included based on the CISPR 16-1-1 [72].

Next to the conducted limits for the low-voltage grid, it is also important to know the impedance of the grid, as it will affect, for example, the currents being drawn by the installed equipment. The reference impedances are specified by the IEC TR 60725 [73] for frequencies up to 2 kHz, the IEC 61000-4-7 [74] from 2 kHz to 9 kHz, and the EN 55016-1-2 [75] (or CISPR 16-1-2 [76]) from 9 kHz till 150 kHz. However, extensive impedance measurements in the low-voltage grid in Austria, Czech Republic, Germany, and Switzerland has shown that almost all measured impedances are below these reference impedances, as is made visible in Figure 2.6 [77]. Furthermore, the 50% percentile value is at one tenth of the reference impedances. This proves that the grid impedance is expected to be much lower than the conservative reference impedances as listed in the standards. This low impedance is due to the capacitive behavior of power supplies that are commonly used in low-voltage grids. Therefore, higher frequencies will flow more easily, and the grid voltage will be affected resulting in a distorted grid voltage. Consequently, the supply voltage that is used for example to test the harmonics of equipment in the IEC 61000-3-2

[44], which resembles a sinusoidal voltage, is not representative for the realistic on-site situation, and the drawn harmonic currents in a realistic on-site system are potentially much worse than in the tested situation.

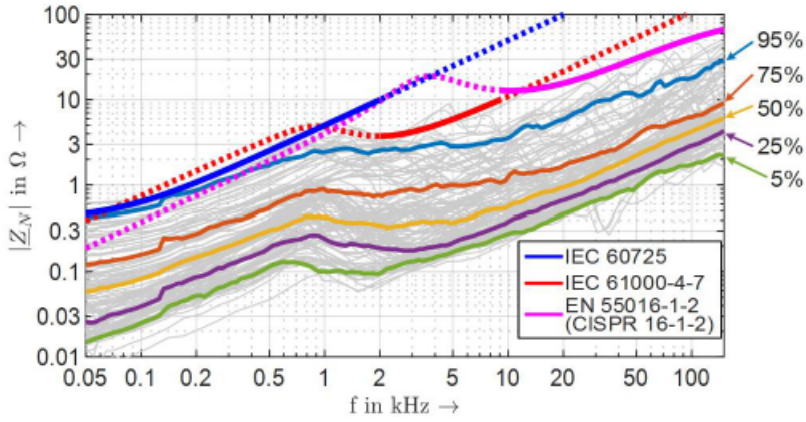

Figure 2.6. Measured impedance at typical public low-voltage grids (gray), including selected percentile curves and reference impedances [77].

2.6 Discussion and conclusion

This chapter summarizes all the relevant standards regarding the EMI problems with static energy meters, as is visualized in Figure 2.7. That is, it covers the relevant standards for static energy meters, the connected equipment, and the low-voltage grid where the meter is placed in. Furthermore, also the European directives were discussed, i.e. the EMC directive and the MID. The important observation here is that the EMC directive does not hold for measurement instruments, such as the static energy meter. Besides, the MID states that the measurement instrument shall not exceed any permissible error limits in its "normal working conditions". Where the latter is particular important as today's residential low-voltage grid cannot be considered as sinusoidal, and therefore the realistic on-site non-linear signals, i.e. signals that can be found in a low-voltage grid, should be measured without any problem by the static energy meter. This requirement of the MID is crucial as it poses a conformity assessment to which all products that are available on the market should conform. From the harmonized standards it is observed that there is a lack of civil standards in the frequency range from 2 kHz to 150 kHz and the test conditions are not representative for today's residential low-voltage grid, which combines many non-linearities. While the standards represent ideal sinusoidal voltages and currents, which today's realistic situation is clearly not [18]. As the low-voltage grid is typically low impedant. Furthermore, frequency-domain testing is used rather than time-domain, which can become problematic consid-

ering the non-linear and time variant behavior of the equipment that is present nowadays in a low-voltage system.

In the rest of this thesis those standards will be further investigated based on the research in the subsequent chapters. Chapter 3 will pinpoint several other cases of interference on static energy meters. Furthermore, several grid impedances are used to test the interference cases with different types of low-voltage grids, i.e. weak, strong, and conventional grids. Next, these interference cases will be analyzed based on the time-domain parameters in Chapter 5, which will show several non-linearities generated by the equipment that are not covered by the introduced static energy meter standards in this chapter. Besides, the typical emissions of equipment that is present in low-voltage systems will be analyzed in Chapter 6, followed by an overview of typical waveforms occurring at the meter connection point in Chapter 7. Both will address the issue that the common signals in a residential system are more harmful considering the non-linearities of the signals compared to the limits as addressed in the standards introduced in this chapter.

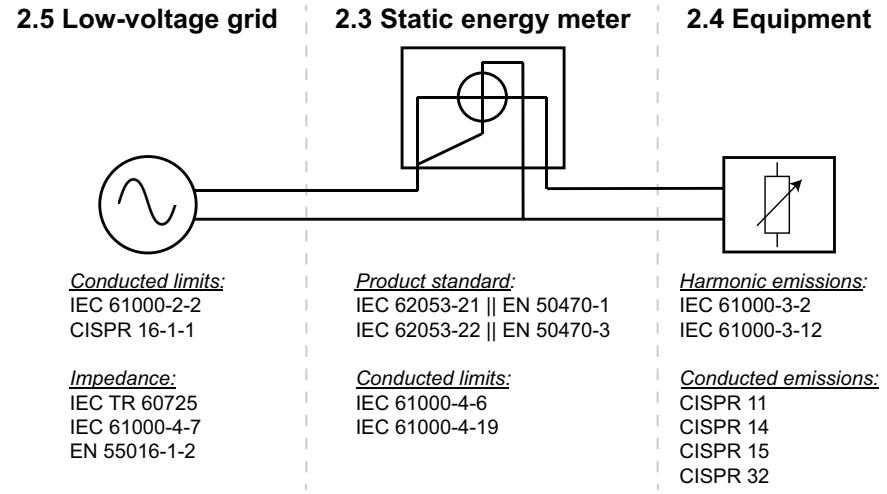

Figure 2.7. Summary of the relevant standards related to the EMI on static energy meters.

Chapter 3

Interference on static energy meters

The cases in which static energy meters give misreadings due to EMI, that are studied in regard of this thesis, are presented in this chapter. The content of this chapter comprises the research that was earlier published in [36], [37], [78]–[82].

3.1 Motivation

In the introduction of this thesis the EMI problems with static energy meters were already identified. One of the appliance causing these problems is dimmed lighting equipment as was evidenced in [31]. Of which the interfering current waveform was found to be of a pulsed nature and thus has a broad frequency spread, as shown in Figure 2.1. This results in an incorrect energy measurement on the static energy meter, which has a societal impact, as consumers might pay too much or too less for their energy consumption. In regard of this thesis, many possible interference cases are studied based on complaints of consumers about their energy bill. This chapter lists several interference problems on static energy meters that were identified. Furthermore, several variations on these experiments are performed to pinpoint the critical situations. This should help in the understanding of the waveforms that interfere with the static energy meter readings. And therefore, provides a solid basis for the understanding of the interference problem.

Conventional EMC analysis is done in the frequency domain. However, the analysis of the waveforms interfering with the static energy meters is (mainly) done in time-domain, as the equipment generating the EMI is non-linear and time-variant. Therefore, time-domain measurements and analysis are more valuable than their frequency-domain counterparts [17]. This was already demonstrated using several analysis methods and signal processing techniques to describe the necessary characteristics of the conducted interference [83].

This chapter is organized as follows: In Section 3.2 the measurement method that was used to measure the immunity of static energy meters in a laboratory situation is explained. Then, Section 3.3 describes several cases of conducted interference problems with static energy meters that are based on actual complaints from consumers about their energy bill. Afterwards, Section 3.4 describes a research case with inexplicable energy consumption that occurred with a correctly functioning meter. Finally, Section 3.5 discusses and concludes these findings.

3.2 Measurement method

This section describes the immunity measurement of static energy meters. The main purpose is to monitor the readings of the static energy meters in a controlled environment. And to test (combinations of) electrical loads after complaints of consumers, e.g. household appliances. Therefore, the energy consumption as measured by the static energy meters and a reference instrument was read out and compared. Furthermore, the voltage and current waveforms of the connected loads were captured.

A schematic overview of the measurement setup is visualized in Figure 3.1. During the laboratory measurements four different power supply settings were considered, which are listed below:

1. Standardized mains grid, to create an ideal standardized grid, such that the non-linearities of the power supply are not affecting the measurements. This supply voltage was generated by a four-quadrant Pacific Power Smart Source 140-TMX AC that was connected to a 50 µF line impedance stabilization network (LISN) creating an ideal grid at 50 Hz and 230 V_{rms}, and to provide a stable impedance to the power input of the static energy meters.

2. Low impedance grid, to create a grid in which the currents can flow easier. As Section 2.5 already addressed that the realistic on-site low-voltage grid is expected to be much lower than the impedances as specified in the standards. This grid was created using the same configuration as stated for the standardized mains grid, but by adding a 28.2 µF capacitor between phase and neutral.

3. High impedance grid, to represent a weak grid and to achieve the opposite of the low impedance grid. In this case it is harder for the currents to flow. Islanded or micro-grids are typical examples of weak grids. Again the same setup as the standardized mains grid was used, but now a 1.4 mH inductor was added in series on the lines.

4. Building's mains supply, to resemble a realistic low-voltage grid. The power was drawn directly from the power socket in the lab, which supplies a distorted sinusoidal voltage at 50 Hz and 230 V_{rms}.

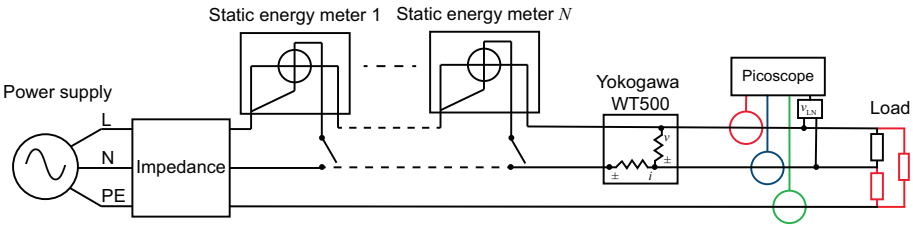

Figure 3.1. Schematic overview of the measurement setup.

After the power supply a series of static energy meters was connected. This can be seen in Figure 3.2, where 24 static energy meters are placed in series. For the measurement results presented in Section 3.3.1, 3.3.2 and 3.3.3 only ten specimen of static energy meters were monitored, while for Section 3.3.4, 24 static energy meters were measured, but the results of only four meters are shown as those did show erroneous results. The meters that were included in the test setup have different types of current sensors: current transformer, Hall effect-based current sensor, Rogowski coil, and shunt resistor. The meters include new and old models (i.e. before and after the publication of the IEC 61000-4-19 standard [29] in 2014) and represent the installed base of static energy meters in the Netherlands.

Figure 3.2. Picture of the 24 static energy meters placed in series in the setup.

To monitor the energy consumption readings of the static energy meter its S0-pulse interface was used. This is a blinking LED that blinks after a certain amount of energy consumption is measured, 0.5, 1, or 2 Wh depending on the specimen of the meter. An optical sensor was attached to this blinking LED,

that transduces the blinking into a digital voltage signal, so a 0 or 1 depending on whether the LED is turned on or off. This means that the number of pulses are counted, which corresponds to the energy consumption as measured by the static energy meter. Rather than counting the total number of pulses, it is also possible to measure the time between (one or a series of) consecutive pulses to obtain the power consumption of the connected load, as is visualized in Figure 3.3. The power is then calculated according to (3.1) and the difference in energy, ΔE, can be determined using (3.2). Where N_{pulse} is the number of pulses during the measurement interval Δt, and the factor f_{SM} is the number of times the static energy meter blinks per 1 Wh of energy consumption. This method allows for a much faster measurement, as only a couple of pulses are needed (ideally only two) to measure the power consumption of the connected load. As the static energy meters were placed in series, the first meter also measures the energy consumed by the second till last meter, which is maximum 2 W per meter according to the related standards IEC 62053-21 [58] and IEC 62053-22 [59]. Therefore, the energy consumption readings of the static energy meters were corrected with the consumed energy of the next static energy meters. This was done according to (3.3), where P_{cor} is the power correction because of the static energy meter's consumption and P_{SM} is the power measured by the static energy meter under test.

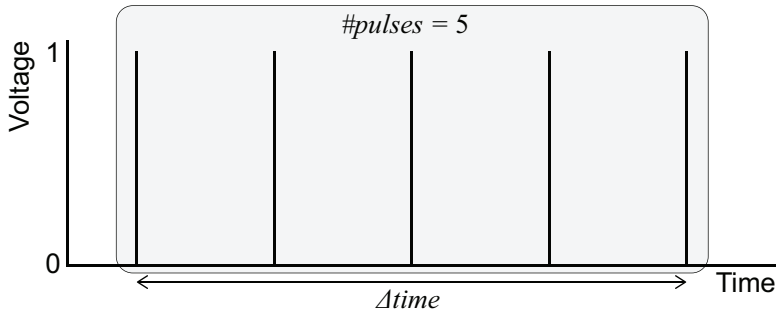

Figure 3.3. Digital voltage signal output of the optical sensor attached to monitor the energy and power consumption readings of the static energy meter.

$$P\,[\mathrm{W}] = \frac{\Delta E[\mathrm{Wh}]}{\Delta t[\mathrm{s}]} \cdot 3600 \tag{3.1}$$

$$\Delta E\,[\mathrm{Wh}] = (N_{\text{pulse}} - 1) f_{\text{SM}} \tag{3.2}$$

$$P_{\text{SM}}\,[\mathrm{W}] = P - P_{\text{cor}} \tag{3.3}$$

Subsequently, a Yokogawa WT500 power analyzer was added to act as a reference meter for the series of static energy meters. It has a basic power accuracy of 0.1% and a sampling rate of 100 kS/s, which should be adequate

for reference as we are focused on EMI, and not on metrology. In that sense, the deviations of the static energy meters under test with respect to the reference meter were calculated using,

$$\text{SM deviation}\,[\%] = \frac{P_{\text{SM}} - P_{\text{ref}}}{P_{\text{ref}}} \cdot 100\% \tag{3.4}$$

where P_{SM} is the power measured by the static energy meter under test and P_{ref} is the power of the reference.

Thereafter, the current and voltage waveform were measured using Pico Technology TA189 current probes that are within 0.5 dB accuracy in the frequency range up to 200 kHz, and a Pico Technology TA043 differential voltage probe with a frequency range up to 100 MHz. The currents on all lines (L, N, and PE) and the differential mode (L-N) voltage were measured. The probes were connected to a Pico Technology Picoscope 4824 pc-based oscilloscope. At least ten cycles at mains frequency were captured, which is equivalent to 200 ms, in accordance with the IEC 61000-4-30 [84]. A sampling frequency of 1 MS/s was used.

After this a connection point for the load under test was included. During various experiments a large selection of household appliances was tested, the next section provides a couple of examples that caused EMI problems with static energy meters. The specific loads used in those cases are introduced in the next section.

3.3 Conducted interference cases

This section addresses several conducted EMI problems resulting in incorrect energy consumption readings of static energy meters. The cases presented in this section are based on actual complaints from consumers about their energy bills in a residential situation.

3.3.1 Commercial off-the-shelf water pump

High energy consumption readings of a static energy meter were observed by a consumer when using a commercial off-the-shelf (COTS) water pump. This water pump, suitable for koi and fish ponds, has a remote unit to control the pump's capacity. The remote control can vary the capacity in ten levels between 8000 and 15000 liter per hour. The power consumption related to these levels is between 23 and 130 Watt, respectively, as specified by the manufacturer. By using this remote control with the pump, small pulsed currents are drawn. A picture of the water pump is shown in Figure 3.4.

During the measurements the water pump together with the remote control were connected as a load to the measurement setup. The remote control was varied between level 1 (lowest water pump speed) and level 10 (highest water pump speed), to observe the difference in drawn currents and created

Figure 3.4. Picture of the COTS water pump placed inside a circular container filled with water.

interference. Furthermore, the grid impedance was varied throughout the measurements to observe its effect on the interference of the static energy meter. This is done because Section 2.5 describes that the grid impedance in a realistic situation is much lower than the impedance described in the standards. In that sense, four different power supply settings were considered, as explained in Section 3.2, which are: standardized mains grid, low impedance grid, high impedance grid, and building's mains supply.

First, for the standardized mains grid the current waveforms associated with the corresponding water pump capacity levels can be seen in Figure 3.5. It is remarkable that an uni-polar pulsed current waveform was drawn by the water pump. Using this configuration the static energy meters show some deviations with respect to the reference meter, as can be seen in Figure 3.6. This figure

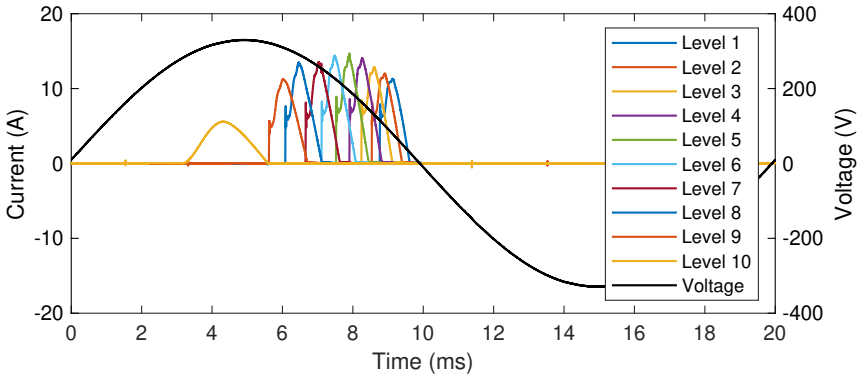

Figure 3.5. Measured waveforms for the ten different levels of the water pump's capacity, when using the ideal power supply with a standardized mains impedance.

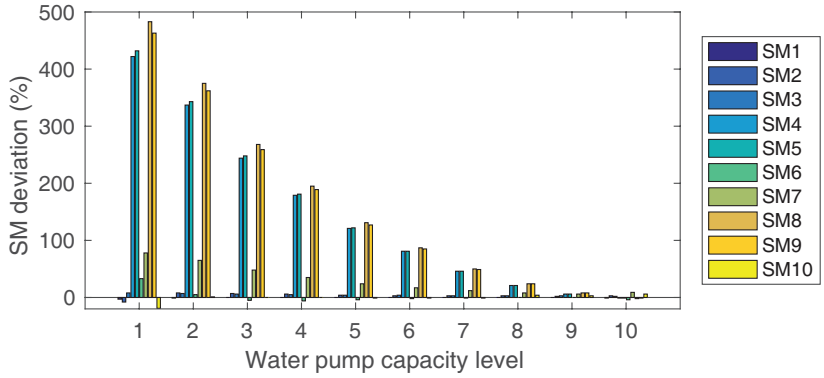

Figure 3.6. Deviations [%] between the static energy meters (SM) and reference when the setup is powered using the ideal power supply with a standardized mains impedance, for the ten different levels of the water pump's capacity.

shows the deviations of the static energy meters with respect to the reference meter, per level of the water pump's capacity, and deviations between -19% and +483% were found.

Second, the measurements were repeated and the impedance of the network is changed to a low impedance network. Figure 3.7 shows the results using this configuration, where deviations between -17% and +2114% were found and are plotted in the same configuration as before. Meaning that around 20 times more power was measured by the static energy meter compared to the reference meter. These deviations are significantly higher than in the first case with a standardized mains grid. The measured current waveform for the water pump at level 1 is made visible in Figure 3.8(b), a similar effect was visible for the other

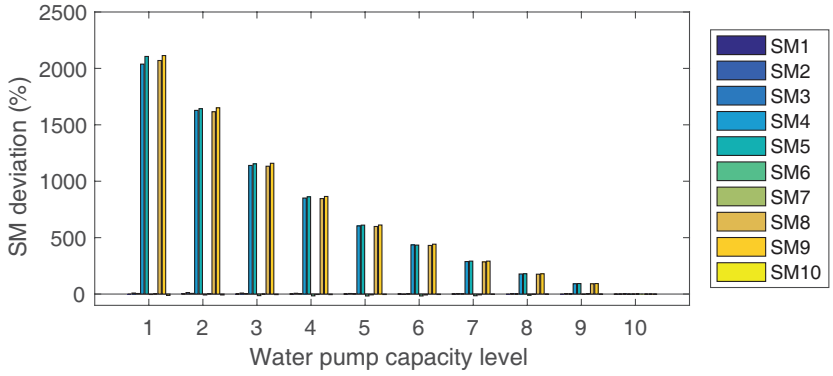

Figure 3.7. Deviations [%] between the static energy meters (SM) and reference when the setup is powered using the ideal power supply with a low impedance, for the ten different levels of the water pump's capacity.

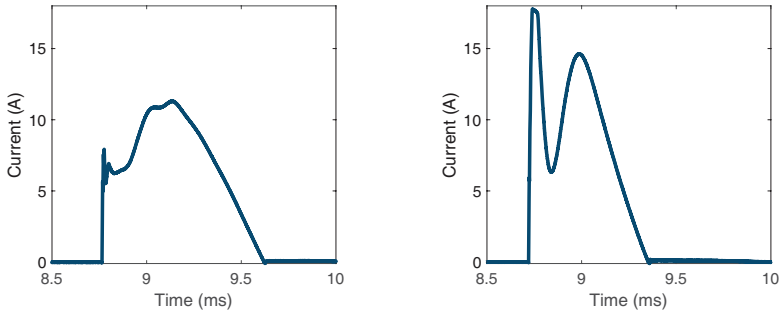

(a) Standardized mains grid

(b) Low impedance grid

(c) High impedance grid

(d) Building's mains supply

Figure 3.8. Measured current waveforms for different power supply settings of the water pump with remote control at level 1.

Table 3.1. Rise time, rising edge and slope of current spikes, for different grid impedances.

Grid impedance	**Rise time [µs]**	**Rising edge [A]**	**Slope [A/µs]**
Ideal	5.8	6.3	1.1
Low	13.8	14.1	1.0
High	5.4	6.3	1.2
Mains	18.8	13.7	0.7

capacity levels. Table 3.1 shows the 10%-90% rise time, rising edge, and slope for the different grid impedances. The 10%-90% rise times are used as it is a commonly used criteria for pulses [85]. It can be seen that the drawn current for the low impedance network has a peak value that is roughly two times higher compared to the current drawn in the standardized mains grid configuration in Figure 3.8(d). Due to the lower impedance of the grid the high frequency currents can flow more easily and the detrimental effect of the interference is amplified.

Thirdly, the measurements were repeated, but this time a high impedance network was used. Figure 3.9 shows the results using this configuration, where

deviations between -16% and +316% were found for the different static energy meters with respect to the reference meter, per level of the water pump's capacity. Figure 3.8(c) shows the measured current waveform for the water pump at level 1. Due to the high impedance of the mains, the current flows less easy, i.e. the peak value is lower and the pulse width is wider, and there is more ringing due to the inductive behavior of the mains. Consequently, the static energy meter errors are lower compared to the previous cases.

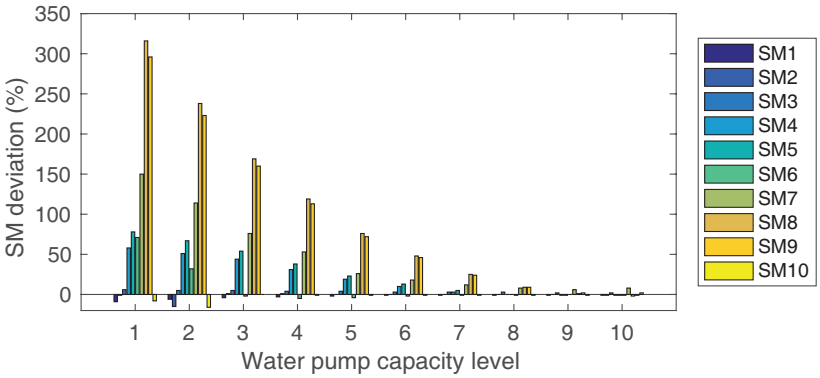

Figure 3.9. Deviations [%] between the static energy meters (SM) and reference when the setup is powered using the ideal power supply with a high impedance, for the ten different levels of the water pump's capacity.

Finally, the measurements with the building's mains supply were performed and the results can be found in Figure 3.10, which shows the deviations of the static energy meters with respect to the reference meter, per level of the water pump's capacity. Using the building's mains supply deviations between -61% and +2675% were found. This is significantly higher than all cases measured before. And could be explained by the current in Figure 3.8(d), which is the most extreme current pulse of all measurement cases.

From the experiments it is observed that when the water pump is set to a lower capacity level, the current waveform has a higher phase shift with respect to the voltage, as is visible in Figure 3.5. Which is decreasing the power consumption. For all measured situations higher deviations of the static energy meters are observed at these lower capacity levels (Figure 3.6-3.10). To analyze the characteristics of these pulses Table 3.2 shows the 10%-90% slope and charge, when the setup is supplied with the standardized mains grid for all different capacity levels. The slope and charge are relatively constant with varying capacity level, so the pulses are relatively similar. This means that it is more likely to have higher static energy meter interference if the current signal experiences more phase shift. Furthermore, it was evidenced that the impedance of the grid affects the interference of the static energy meter. As the low impedance grid allows high-frequency currents being drawn more easily, the time-domain pulsed current is more extreme, and consequently the interference

is higher. This is an important observation as a realistic residential grid has a lower impedance compared to the reference impedances of the standards as was shown in Section 2.5, based on the residential impedance measurements from [77].

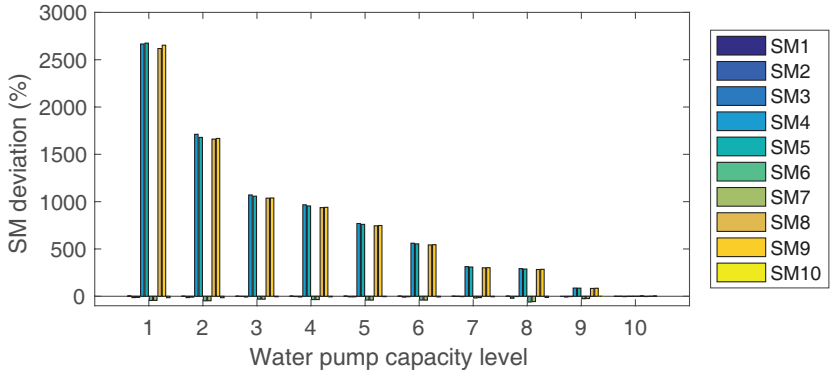

Figure 3.10. Deviations [%] between the static energy meters (SM) and reference when the setup is powered using the mains supply of the building, for the ten different levels of the water pump's capacity.

Table 3.2. Slope of current pulse rising and area under the current wave over one period, for remote control combined with water pump for different capacity levels.

Capacity level	**Slope [A/µs]**	**Charge [mC]**
1	1.1	6.3
2	1.1	6.8
3	1.2	7.2
4	1.2	8.0
5	1.1	8.2
6	1.1	8.6
7	1.1	8.2
8	1.0	8.5
9	0.8	7.8
10	0.01	7.8

3.3.2 Water pump with TRIAC regulators

In addition to the measurements presented in the previous section, also measurements were preformed with the water pump in conjunction with three regulators. The purpose of these tests is to elaborate on the previous findings, by testing different configurations of the water pump. Therefore, three similar power regulators, intended to be used with a water pump to change its

speed/power, were tested. To regulate the power these regulators use a triode for alternating current (TRIAC) that is controlled by a variable resistance. The regulators were sold by different manufacturers, but the inside and outside look exactly the same. Figure 3.11 shows the electric circuitry inside the regulator. The electrical components inside differ slightly in their values, probably due to the tolerances of the cheap components that are used. This could potential give slight variations in the currents drawn, e.g. different rise times. During the measurements the regulator was tuned to three different water pump capacity levels, respectively low, medium, and high speed/power.

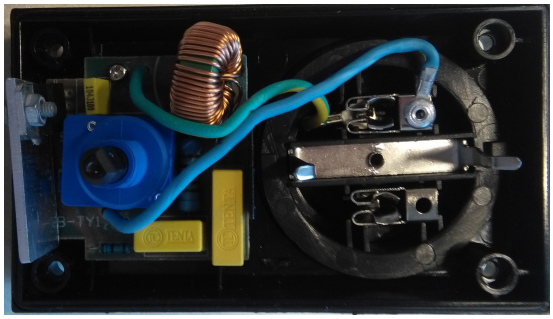

Figure 3.11. Electronics inside the power regulator.

The resulting measured deviations of the static energy meters are shown in Figure 3.12. Where R1, R2, and R3 correspond to the used regulator and L, M, and H to the speed/power that is either low, medium, or high. Deviations between -91% to +10%, -19% to +175%, and -90% to +16% are observed for regulator 1, 2, and 3, respectively. In Figure 3.13 the measured waveforms during the experiments are plotted. It shows the voltage waveform that is generated using the power supply without a load attached and the current waveforms generated in different load configurations. A lot of current spikes are present in the waveforms, even very narrow spikes that do not seem to have much power. The characteristics of the current spikes are shown in Table 3.3, showing the 10%-90% rise time, rising edges, and the related slopes. Since the waveforms show multiple spikes, the values in Table 3.3 indicate the maximum slopes found for a particular power level. When regulator 1 is used to create a low power level, the slope of the spike is 11 A/µs and deviations between -91% and +3% are observed. If the power level is changed to the medium level, resulting in a slope of 8.2 A/µs, the deviations are between -72% and +10%. So, lowering the slope and also lowering the deviations. When the power level is changed to high power, almost no deviations are observed. A similar effect can be seen for regulator 3, however in this case the deviation of static energy meter 4 and 5 are still very high in the case of the high power level. For regulator 2 the largest deviations can be seen for the medium power level, which can be explained by looking at Figure 3.13(b), which shows more current spikes in this situation compared to the low power level. So the superposition of the

spikes might increase the interference effect. Another observation is that in these experiments also negative deviations are observed, while in the previous subsection mostly positive deviations were shown to exist. Mainly negative deviations occur when using regulator 1 and 3, while the use of regulator 2 shows mostly positive deviations. This also shows that however the regulators include the same electrical components, a slight variation of these components can change the working conditions of it and thus create different EMI problems.

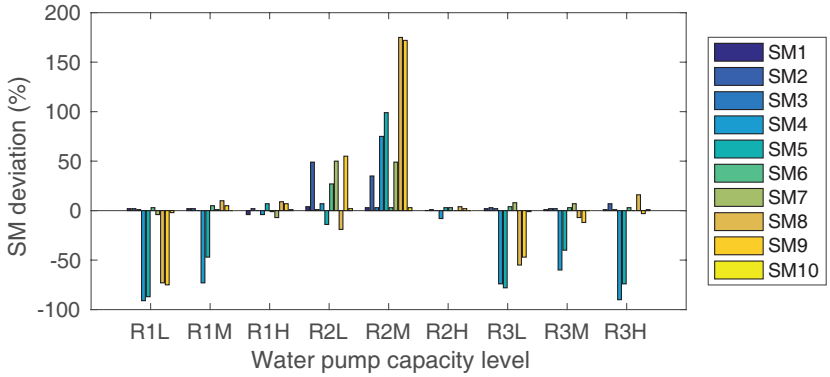

Figure 3.12. Deviations [%] between the 10 static energy meters (SM) and reference, for different combinations of the water pump and three regulator, respectively R1, R2, and R3, at different capacity levels, respectively low (L), medium (M), and high (H).

Table 3.3. Characteristics of the current waveforms from the water pump with different regulators (R1, R2, and R3) at different speed/power levels.

Speed level	**Rise time [µs]**	**Rising edge [A]**	**Slope [A/µs]**
R1 Low	1.5	16.0	10.7
R1 Medium	1.9	15.2	8.2
R1 High	2.1	4.2	2.0
R2 Low	1.1	12.2	11.6
R2 Medium	2.3	16.2	7.1
R2 High	2.8	3.9	1.4
R3 Low	1.5	15.0	10.3
R3 Medium	1.6	14.8	9.2
R3 High	2.0	12.6	6.4

3.3.3 Dimmed lighting equipment

Although it was shown that the slope of fast rising currents has an effect on static energy meter readings in the previous subsections, no direct correlation between them was shown. Therefore, additional measurements were performed

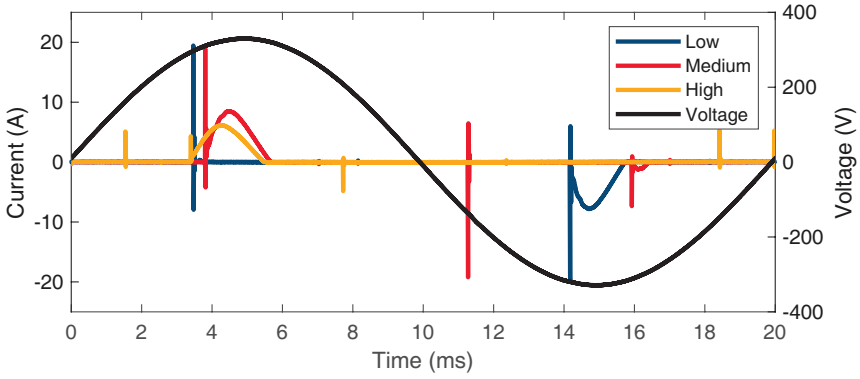

(a) Water pump with regulator 1.

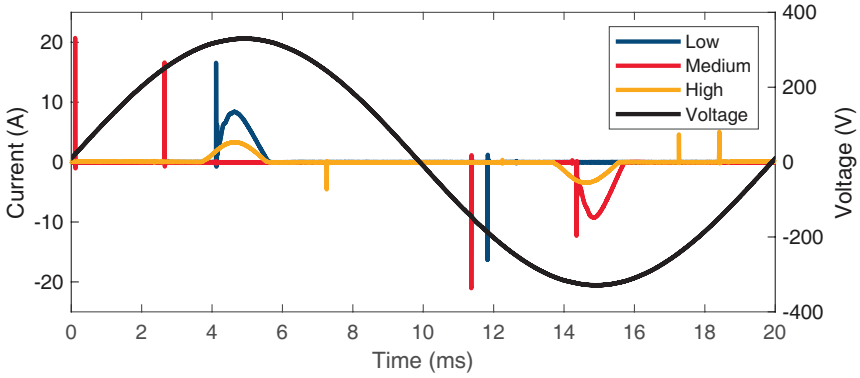

(b) Water pump with regulator 2.

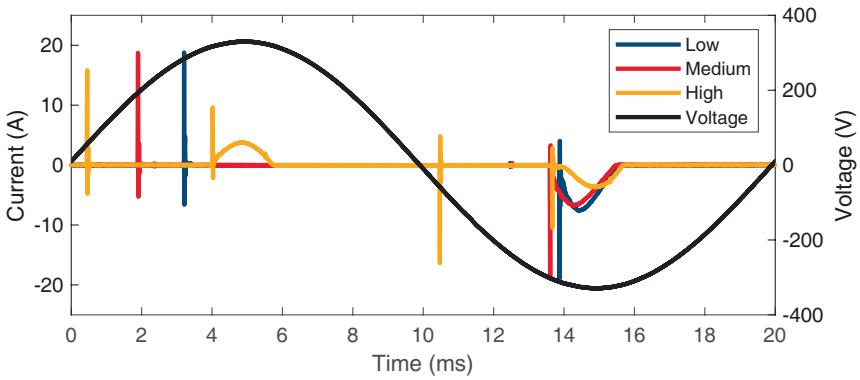

(c) Water pump with regulator 3.

Figure 3.13. Current waveforms generated during measurements for different loads, the voltage is the wave generated by the power supply without a load.

in which the slope was varied by inserting a line choke in series with the load, while keeping the other parameters constant. Increasing the value of this choke will create a higher impedance and will lower the slope of the current, i.e. limit the higher frequency components being drawn. As a starting situation the most severe interference case from [31] is used, where static energy meters are being interfered by dimmed lighting equipment of CFL and LED. The most severe situation corresponds to the lighting equipment being maximally dimmed, i.e. the dimmer is set to 135°. After the starting situation, where no line choke is added, chokes of the following inductance are added subsequently: 0.03, 0.08, 0.16, 0.24, 0.32, 0.7, and 1.4 mH. Creating a total of eight different test conditions. This has the same effect as changing the inductance of the line choke used as a filter inside the dimmer, as is done in [86] for the same purpose of changing the current slope. However, due to practical reasons it was chosen to add a line choke, i.e. there is no need to desoldering the printed circuit board of the dimmer every measurement.

The results of the measurements can be seen in Figure 3.14, where the deviations of the static energy meters with respect to the reference meter are shown, for the different line inductances. The corresponding waveforms can be seen in Figure 3.15. It shows the voltage waveform that is generated using the power supply without a load attached and the current waveforms generated with the different series inductance values. The corresponding characteristics of these waveforms can be seen in Table 3.4. Without a line inductance, static energy meter deviations between -4% and +342% are found, and the current slope was 5.6 A/µs. The addition of a line inductance decreases the current slope and decreases the static energy meter deviations. For example, the addition of a line inductance of 0.16 mH resulted in a less steep slope of 0.8 A/µs and static energy meter deviations between -6% and +212%. Reducing the slope even further to 0.02 A/µs, by adding a 1.4 mH line inductance,

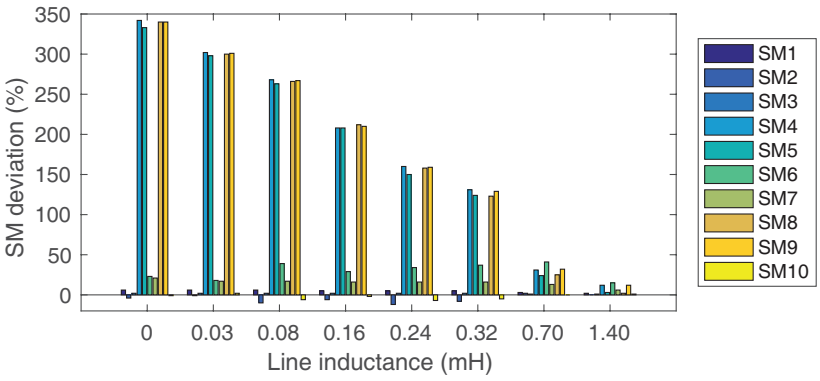

Figure 3.14. Deviations [%] between the static energy meters (SM) and reference, for different line inductances added.

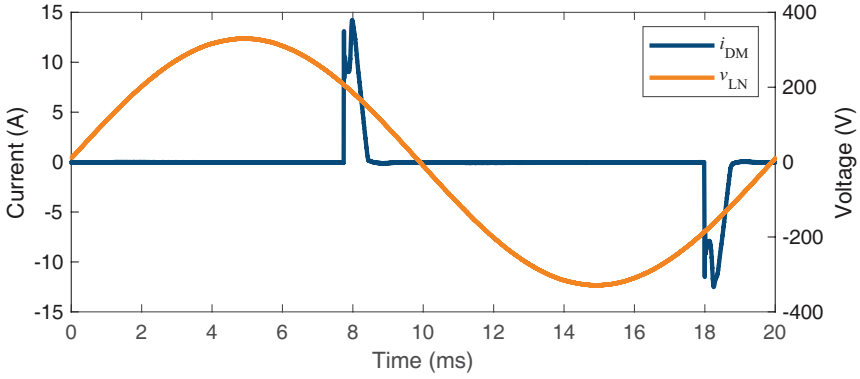

(a) No line inductance.

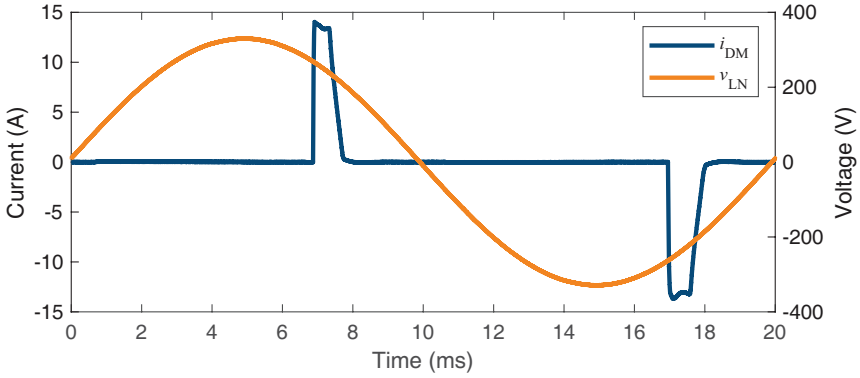

(b) 0.16 mH line inductance.

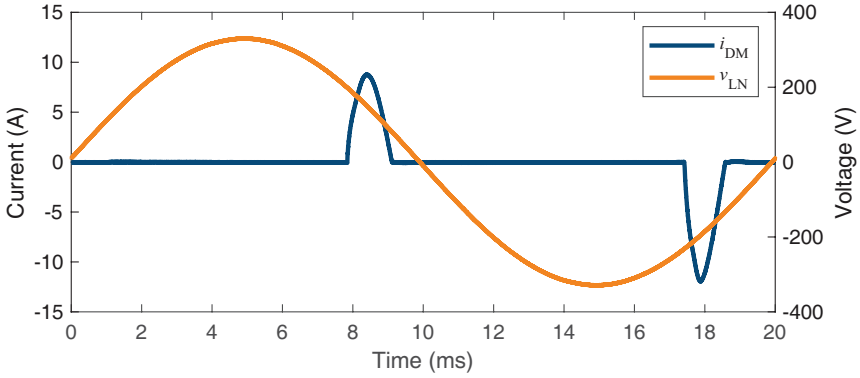

(c) 1.4 mH line inductance.

Figure 3.15. Current waveforms generated, inserted inductances given in mH, the voltage is the wave generated by the power supply without a load.

reduces the meter deviations below ±10%. In Figure 3.16 the maximum deviations for different static energy meters are plotted against the current slope. It shows higher interference if the current slope is larger.

Table 3.4. Rise time, rising edge and slope of current spikes, for different line inductances (ind.).

Line ind. [mH]	**Rise time [µs]**	**Rising edge [A]**	**Slope [A/µs]**
0	2.1	11.8	5.6
0.03	5.6	12.0	2.1
0.08	10.9	12.9	1.2
0.16	14.3	11.1	0.8
0.24	35.9	10.2	0.3
0.32	43.3	9.6	0.2
0.7	115	13.1	0.1
1.4	382	7.0	0.02

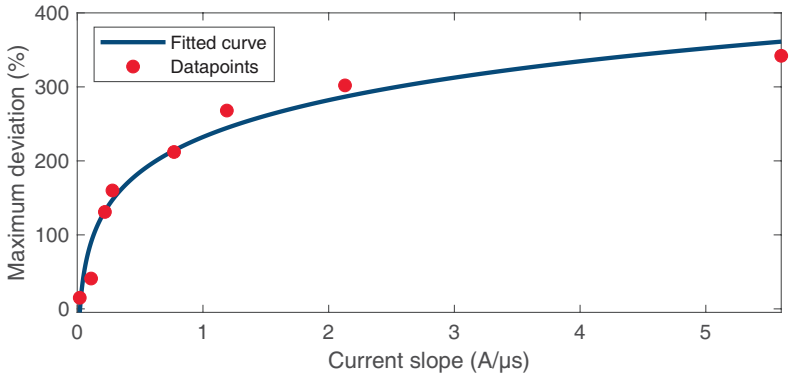

Figure 3.16. Correlation between the inclination of the current slope and the maximum static energy meter deviations.

3.3.4 Meters running backwards

After the interference cases as introduced in the preceding subsections, a consumer complaint was received about inconsistent energy readings of his static energy meter, after installing a COTS remote control for on/off switching of (connected) appliances. The COTS switch was connected to multimedia equipment (including a television), with the purpose of limiting the stand-by usage after using the equipment, by completely cutting off the power. This dropped the energy consumption as measured by the static energy meter and even resulting in a measured power generation, while no power generating device was connected. This behavior is visible in the consumption data of the static energy meter as is shown in Figure 3.17, where the black data corresponds to off-peak hours and the yellow data to peak hours. Figure 3.17(a) shows

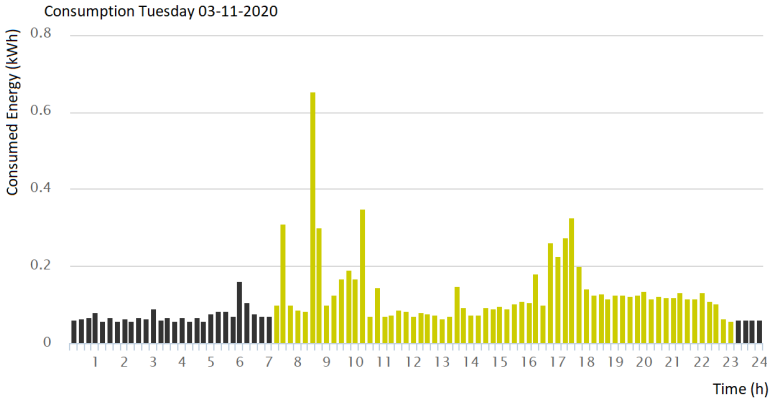

(a) Initial energy consumption.

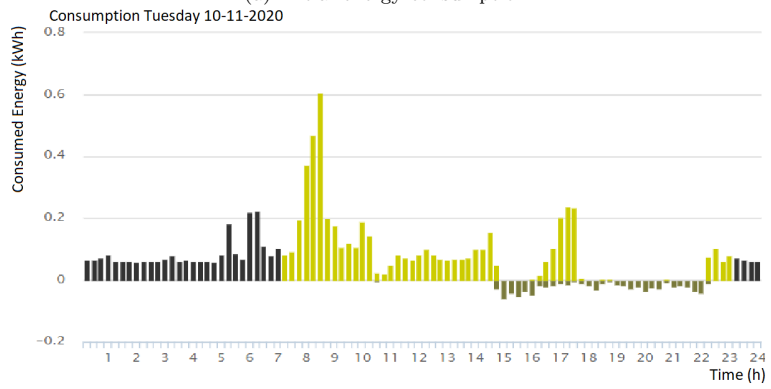

(b) Energy consumption after connecting the COTS switch.

Figure 3.17. Energy consumption data obtained from the installed static energy meter at the consumer's premise, where the black data corresponds to off peak hours and the yellow data to peak hours.

the initial consumption, and Figure 3.17(b) shows the consumption after connecting the COTS switch. It can be seen that the energy consumption drops significantly and even reaches negative values between 15:00 and 22:30. Which is strange as the household has no power generating equipment such as solar panels. The installed static energy meter was manufactured in 2017, and is thus compliant with the updated test standard IEC 61000-4-19 in 2014 [29]. This is unexpected as the test standard already covers the immunity of the meter.

This situation was reproduced in a laboratory situation to investigate the reason of this peculiar observation. After connecting the COTS switch it was directly found that it dims the connected equipment automatically. This is in contrast to the information the consumer gathered from his salesperson, who told him that the switch can be used for his intended purpose of limiting stand-by usage. When changing the dimming levels it turned out that phase firing angles between (approximately) 45° and 135° could be achieved. By default the dimming level was set to 45°. These waveforms are shown in Figure 3.18. For the measurements the minimum (45°), middle (90°), and maximum (135°) phase firing angles are used. The resulting measured powers by the static energy meters and the reference power analyzer are summarized in Table 3.5. For a phase firing angle of 45° the static energy meters measure a power generation, i.e. a negative consumption, while the reference meter shows that the power is consumed from the grid. Thus, the situation found in the household is properly reproduced. For the pulse with a phase firing angle of 90° no significant error is found. For a phase firing angle of 135° a much higher energy consumption was measured by the static energy meters. This shows that the phase firing angle of the pulse determines whether the interference results in a false generation of power, no significant error, or a higher power consumption.

Table 3.5. Static energy meter (SM) readings for the dimmed multimedia equipment at different phase firing angles.

#	**WT500**	**SM1**	**SM2**	**SM3**	**SM4**
45°	21 W	-297 W	-286 W	-350 W	-56 W
90°	22 W	35 W	32 W	42 W	37 W
135°	20 W	485 W	462 W	314 W	159 W

Afterwards, measurements with an AC controlled current load were performed, in order to have full control of the waveform parameters. This is not possible with a COTS appliance, as changing its setting may change multiple parameters at once. Using this load a triangular waveform was generated that has similar parameters such as the amplitude, phase firing angle, and slope as the dimmed multimedia equipment. The triangular current waveform was phase shifted with respect to the voltage, by keeping the triangular wave constant. The power error between the static energy meters (selected for this specific experiment) and the reference meter is visualized in Figure 3.19. No errors are observed for static energy meter 1. While for static energy meter 2

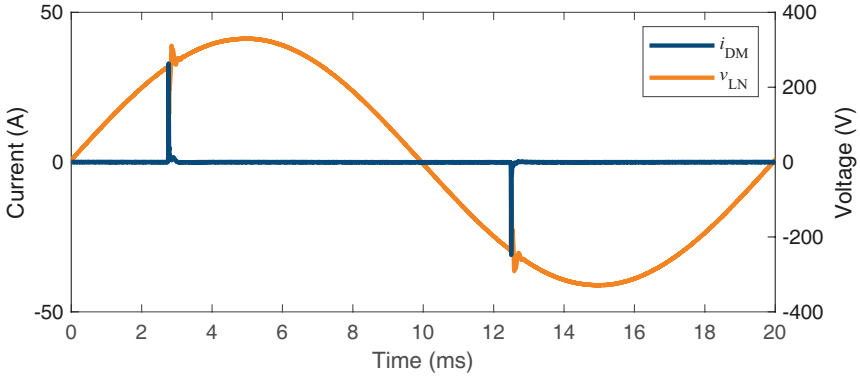

(a) Phase firing angle of 45°.

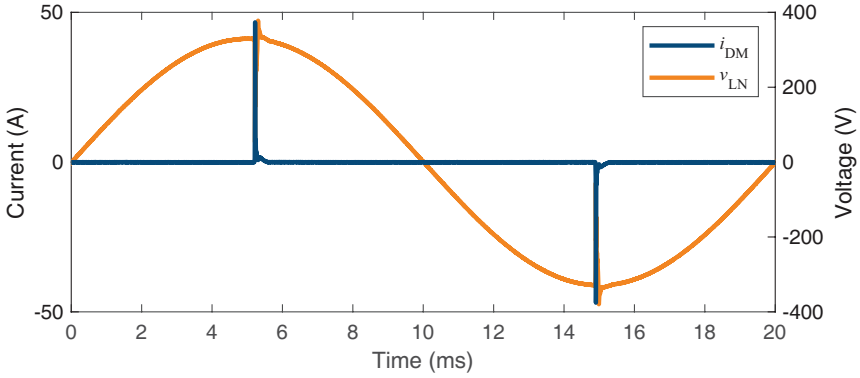

(b) Phase firing angle of 90°.

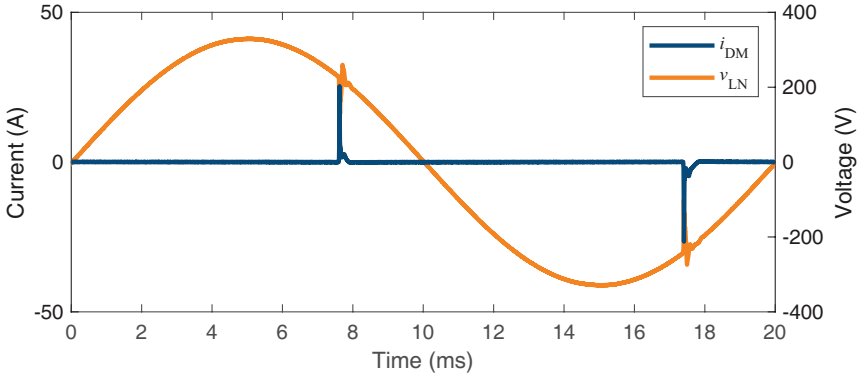

(c) Phase firing angle of 135°.

Figure 3.18. Measured current waveforms for the dimmed multimedia equipment at different phase firing angles.

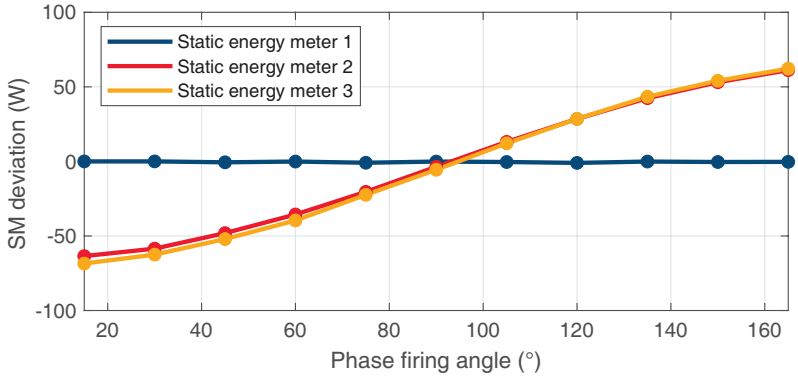

Figure 3.19. Static energy meter deviations for a triangular pulse with different phase firing angles.

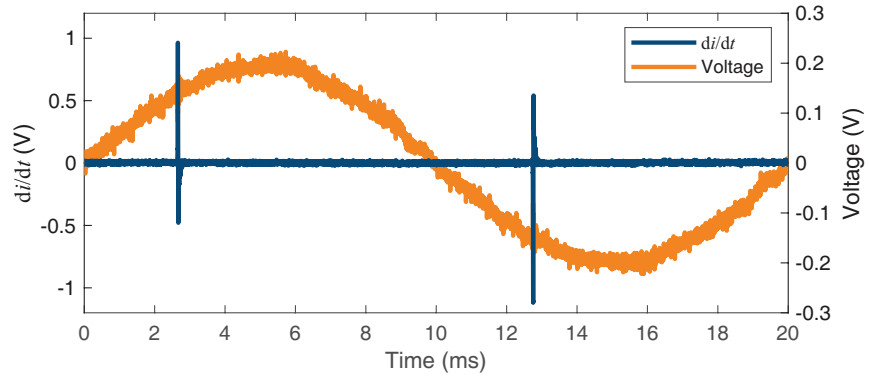

(a) Output of the Rogowski coil.

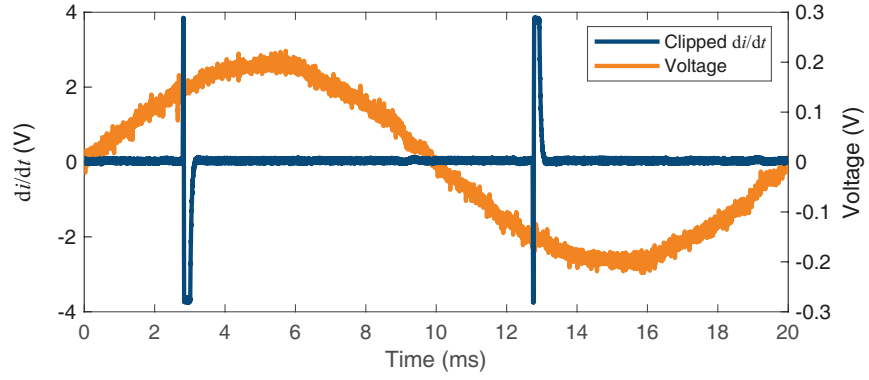

(b) Clipped output of the amplifier.

Figure 3.20. The measured output of the Rogowski coil inside the static energy meter and the clipped amplifier output, when measuring the pulsed current in Figure 3.18(a).

and 3, a phase firing angle lower than 90° resulted in an incorrect measured generation of power, and a phase firing angle higher than 90° resulted in an incorrect power consumption measurement.

Hereafter, measurement points were added inside the static energy meter to find the cause of these observations. Inside the static energy meter the current is measured by a Rogowski coil which differentiates the signal. Then, the output of the Rogowski coil is amplified and integrated to obtain the current waveform, according to the datasheet of the STPM01F energy meter IC [87], that is commonly embedded in meters placed in the Netherlands. A current waveform with a high $\mathrm{d}i/\mathrm{d}t$ will result in a relatively high amplitude at the output of the Rogowski coil. The output of the Rogowski coil inside the static energy meter can be seen in Figure 3.20(a), when measuring the pulsed current in Figure 3.18(a). The output of the Rogowski coil goes up to 1 V. This waveform is then amplified, however the maximum input voltage of the amplifier, as is shown in Table 3.6, is hereby exceeded. This results in clipping of the current signal at the output of the amplifier. Since the amplifier inside the static energy meter is incorporated inside the STPM01F chip, its output cannot be measured directly. To show the effect of clipping, an amplifier has been implemented with a maximum input voltage of 37 mV, closely relating to the worst case scenario for the amplifier in Table 3.6. The resulting clipped output can be seen in Figure 3.20(b). For such a maximum input voltage, both the rising edge and the falling edge of the pulse are clipped. However, the rising edge was faster, and a larger portion of the rising part is clipped. The clipping of the amplifier results in a distorted current waveform after integrating the output of the amplifier, due to the difference in steepness of the rising edge and falling edge. This effect is shown in Figure 3.21. Where it can be seen, by following the arrows, that when a triangular pulse with a faster rising than falling edge is measured by the Rogowski coil, the higher rising edge is clipped by the amplifier. Since the triangular pulse starts and ends at zero, the areas under the positive and negative slopes of the differentiated signal should be equal. However, this is not the case for the clipped signal, and the integrated signal will not return to zero and a mismatch is included. When multiplying this mismatch in the current, with the proper measured voltage, to obtain the power, an error will be introduced. When phase shifting this output current, including the mismatch, the error will be either positive or negative depending on the phase firing angle. This was already confirmed by the measurements in Figure 3.19.

3.4 Issues with a correctly functioning meter

Next to the interference cases presented in the previous section, also inexplicable energy consumptions can occur when the static energy meter is functioning correctly. Those are of interest to cover in this thesis from societal point of view, as it can impact the energy billing of the consumers directly. Furthermore, it can create awareness of consumers in their energy consumption. Several com-

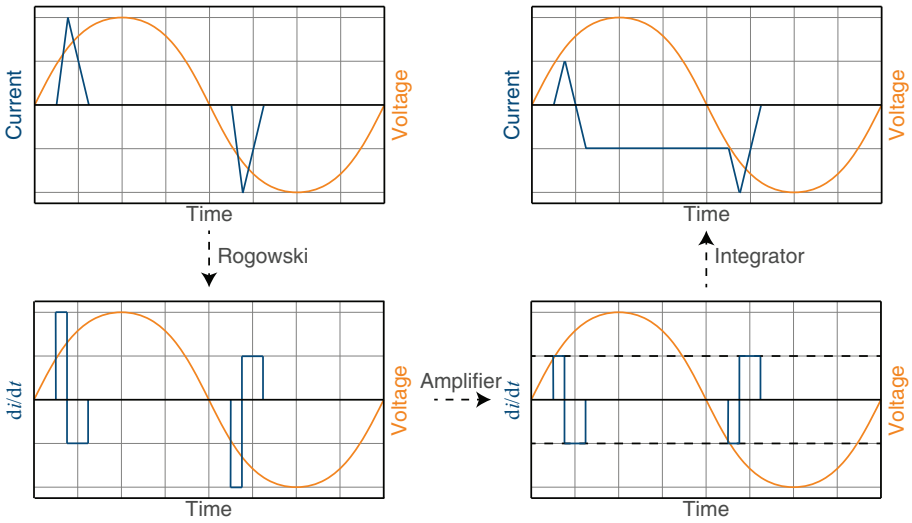

Figure 3.21. Schematic overview of the clipping of the differentiated current.

Table 3.6. Maximum input voltage of voltage and current channels of the amplifier inside the static energy meter [87].

Voltage channels		**Current channels**	
Gain	**Max input voltage (V)**	**Gain**	**Max input voltage (V)**
4	±0.30	8x	±0.15
		16x	±0.075
		24x	±0.05
		32x	±0.035

plaints were made by consumers about high energy consumptions that did not result from incorrect static energy meter readings. In most of the cases the consumers were not aware of the amount of energy produced by their appliances, for example, a microwave-oven that was used by the consumer quite frequent, or a large series of halogen lamp-spots. The introduction of energy consumption applications that receive the 15-minute consumption data from the static energy meter, e.g. an application via the utility company or via a third party, can help the consumers' awareness of their energy consumption. Furthermore, it can help researchers (or the utility company) to analyze inexplicable energy consumptions. The rest of this section will focus on two cases that impact the energy measurement (of a correctly functioning static energy meter). This is explained based on the Blondel theorem [88], that is used for measuring energy in a poly-phase system, e.g. the residential grid. Then, two contradiction cases to this theorem are discussed, that focus on a defective residual-current device (RCD) and the flow of leakage currents in non-linear appliances.

3.4.1 Blondel theorem

Measuring the energy in a poly-phase system is done according to the Blondel theorem [88]. This theorem states that in a system containing N current carrying conductors, N-1 current sensing elements are sufficient to measure the electrical energy consumption. This theorem is for instance used in low-voltage grids for determining the energy consumption [89], e.g. for billing purposes at residences by using the static energy meter.

In such energy meters, used in one-phase systems, the energy is determined using the line-neutral voltage and line current, so only one current sensing element is used. Whereas two elements are required if Blondel is followed correctly, as the system contains the line, neutral and protective-earth conductor. The use of fewer elements is done because of economical reasons [89]. This reduction is only valid if the system is balanced, and other parts in the system are working properly, such as an RCD, that opens the mains circuit because of safety issues when a leakage current exists [90]. Similarly, for a three-phase system also the protective-earth conductor is not taken into account. In this subsection the theoretical background behind the Blondel theorem is given, as was published first in [88] and will be summarized hereafter.

A system containing N conductors is considered, at any moment in time the currents and potentials on these conductors are given by i_n and v_n, for all conductors. Then at any moment in time, the algebraic sum of the currents on all the conductors is zero, (3.5).

$$\sum_{n=1}^{N} i_n = 0 \tag{3.5}$$

The instantaneous power is the current multiplied by the potential delivered to the system, (3.6).

$$p = \sum_{n=1}^{N} i_n v_n \tag{3.6}$$

By introducing a common point, M, with potential v_m, the instantaneous power can be calculated as a function of the potential difference between the N-th conductor and the common point as seen in (3.7).

$$p = \sum_{n=1}^{N} i_n (v_n - v_m) \tag{3.7}$$

Which is proven true since it is known from combining (3.5) and (3.6) that (3.8) holds.

$$\sum_{n=1}^{N} i_n v_m = v_m \sum_{n=1}^{N} i_n = 0 \tag{3.8}$$

Which can then be substituted into (3.6), resulting in (3.7). Furthermore, when dealing with alternating polyphase currents, the currents and potentials are periodical functions with period T, such that the average power can be written as (3.9).

$$P_m = \frac{1}{T}\int_0^T p\,\mathrm{d}t = \sum_{n=1}^{N} \frac{1}{T}\int_0^T i_n(v_n - v_m)\,\mathrm{d}t \tag{3.9}$$

For practical measurements all of the partial powers can be calculated and added algebraically. In these measurements the common point must be chosen such that the relative values of the potentials and the distribution of the currents does not change. This common point is generally the return conductor of the other N-1 conductors in the circuit. Lets assume the N-th conductor as common point, then (3.7) can be rewritten as (3.10), which shows that only N-1 current sensing elements are needed to measure the energy in polyphase systems.

$$p = \sum_{n=1}^{N} i_n(v_n - v_N) = \sum_{n=1}^{N-1} i_n(v_n - v_N) \tag{3.10}$$

In the rest of this section a one-phase low-voltage grid is considered. Such a system has three conductors: the line, neutral, and protective-earth. Figure 3.22 shows a schematic of such a system. According to the Blondel theorem,

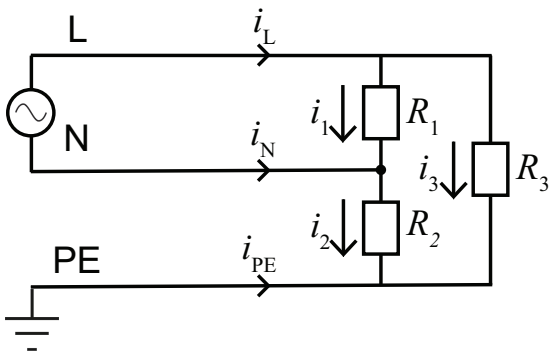

Figure 3.22. Schematic of a one-phase distribution system.

(3.10), and taking the neutral conductor as the common point, the power is determined using (3.11).

$$p = (v_{\mathrm{L}} - v_{\mathrm{N}})i_{\mathrm{L}} + (v_{\mathrm{PE}} - v_{\mathrm{N}})i_{\mathrm{PE}} \tag{3.11}$$

In residential energy metering only the first term involving the line-neutral voltage and line current is taken into account, because it is assumed that the system is earthed and no voltage potential exists between the neutral and protective-earth conductor, so no current can flow through the protective-earth. However, a voltage drop between the neutral and protective-earth conductor does exist, caused by an impedance due to the length of the cable between the residential system and the transformer were the neutral is earthed. Because of this voltage drop a current can flow in the protective-earth, thus making the aforementioned assumption incorrect, and in order to determine the total energy the second term in (3.11) should also be taken into account.

Hereafter, in Subsection 3.4.2 and 3.4.3, two cases are considered in which a protective-earth current exists and thus the energy metering is not performed correctly.

3.4.2 Defect residual-current device

In this subsection a case study is described in which a broken RCD resulted in a large current flow through the protective-earth in a residence. This came to light, because the consumer noted an abrupt increase of his energy bill, which could not be explained based on his connected appliances. After switching off (groups of) devices in the residence, it was found that the increased energy consumption resulted from the oven in stand-by mode. The current flowing through the line conductor is shown in Figure 3.23. It has an rms value of 6 A, and consequently a power of 1500 W was drawn. Which is strange as the oven was in stand-by and no parts of the oven were heated.

By coincidence the mains plug of the oven was inverted, so swapping the line and neutral conductor, and remarkably the large energy consumption was not measured anymore. From this observation a short circuit was found between the neutral and protective-earth conductor of the oven, and the unintended path had an impedance of 30 Ω. This meant that in the original case, with the mains plug inverted, there was a short circuit between the line and the protective-earth conductor of the oven, causing a large current to run through the protective-earth conductor. This problem was not thought of before, because this would normally open the mains circuit due to the RCD for such a high current running through the protective-earth. However, it turned out that the RCD was broken and did not function anymore, which made it possible for the leakage current to flow.

So, an current unbalance between the line and neutral conductor was observed. Inverting the mains plug of the oven, so swapping the line and neutral

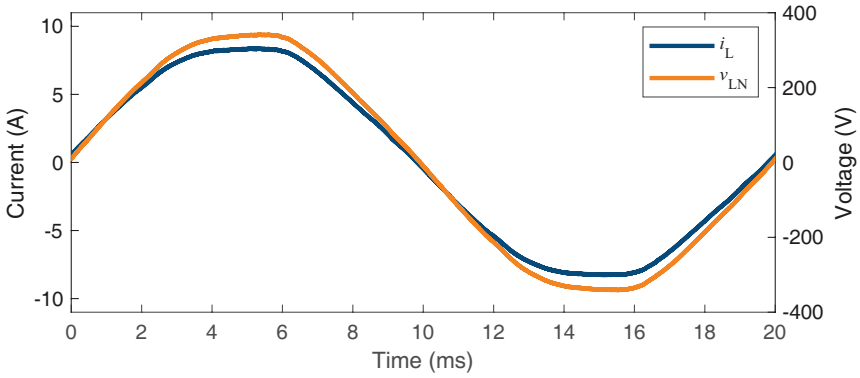

Figure 3.23. Measured line current and line-neutral voltage of the oven in stand-by.

conductor, will create a difference in current measurements. This issue is illustrated in Figure 3.24 using the electrical circuit and inserting a current element in the line and neutral conductor. In the first situation, the line current element measures the contribution of the load and short circuit, while the neutral current element only measures the current of the load, Figure 3.24(a). In the second situation, the current element in the neutral conductor measures only the current generated by the load, while the neutral current element is also affected by the leakage current, Figure 3.24(b). Meaning that a situation can occur in which the line and neutral currents are unequal, and thus the situation is non-compliant to the Blondel theorem. This has a large effect on the energy measurement used to determine the households consumption for billing purposes. Another thing that can be learned from this case study is that an RCD may not function because of wear, and one should check the functionality of the RCD regularly to overcome (potential) dangerous situations or over-billing of consumed energy.

3.4.3 Leakage currents in non-linear appliances

A second case study was performed to investigate the flow of leakage currents for non-linear appliances. Ideally the leakage current should be zero during normal operation, however in reality appliances produce a small leakage current due to filter capacitors (Y-capacitors). This can result in failures or malfunctions, e.g. unwanted tripping of RCDs [91]. As a non-linear load a COTS water pump combined with a dimmer was used, which already showed large EMI issues in Section 3.3. It was connected to the mains grid. The current and voltages on all lines were measured. One period of the recorded waveform is shown in Figure 3.25. This measurement shows a current flowing on the protective-earth conductor, and an unbalance between the current flowing through the line and neutral conductor. The leakage current shows a damped sine wave with a relatively high frequency compared to the mains frequency, for which a

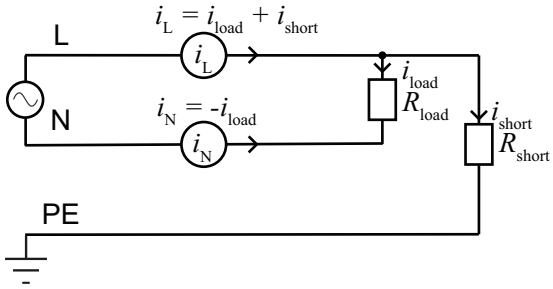

(a) Situation 1

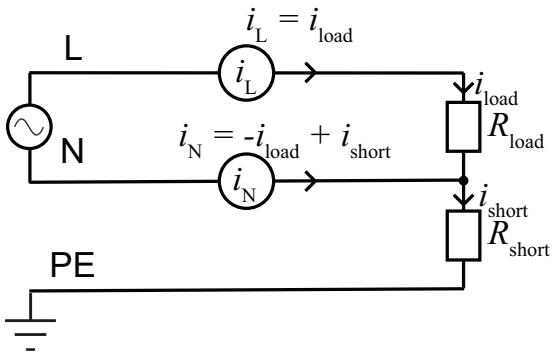

(b) Situation 2

Figure 3.24. Electrical circuits creating an unbalance between the line and neutral conductors, for two different situations.

zoomed in plot is shown in Figure 3.25(c).

When it is assumed that no voltage potential exists between the neutral and earth conductor, and measuring the energy according to Blondel, the current flowing through either the line or neutral conductor should be measured. As the current flowing through both conductors should be identical according to Blondel. The average power is calculated according to (3.12) and (3.13), which agree with the Blondel theorem, where K is the total number of samples.

$$P_{\mathrm{L}} = \frac{1}{K} \sum_{k=1}^{K} i_{\mathrm{L}}\,[k]\, v_{\mathrm{LN}}\,[k] \tag{3.12}$$

$$P_{\mathrm{N}} = \frac{1}{K} \sum_{k=1}^{K} i_{\mathrm{N}}\,[k]\, v_{\mathrm{LN}}\,[k] \tag{3.13}$$

The calculated power using the line current measurement is 29 W, whereas using the neutral current measurement the calculated power turns out to be 30 W. This shows a difference of 3% between the two measurements, which can

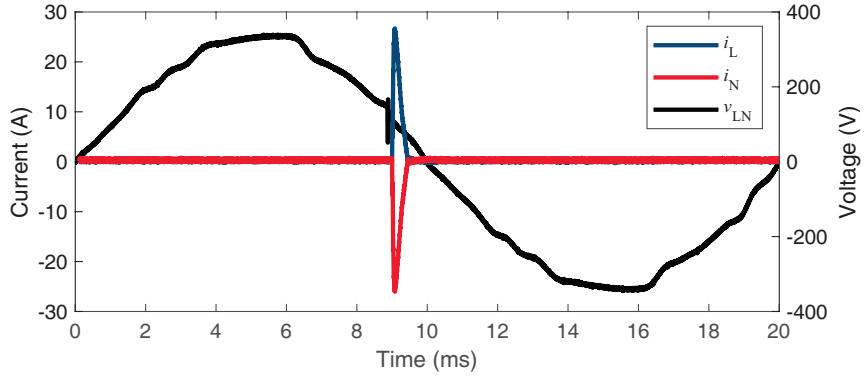

(a) Line and neutral currents

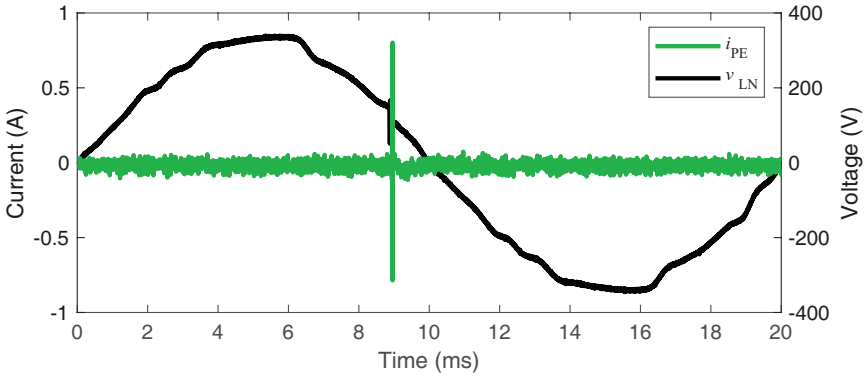

(b) Protective-earth current

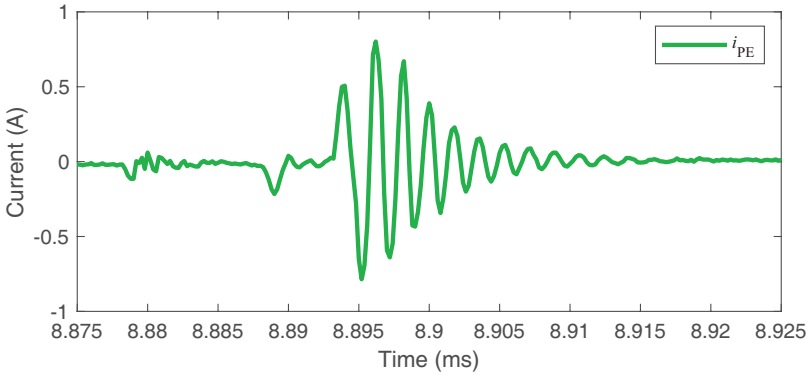

(c) Zoomed protective-earth current

Figure 3.25. Measured currents of the non-linear speed-controlled water pump.

be explained because the current unbalance resulting from a current flowing through the protective-earth. And shows a non-compliance with the Blondel theorem. For electricity metering, e.g. in static energy meters, this could result in incorrect readings and wrong billing. For example swapping the line and neutral conductor by mirroring the mains plug could be beneficial for consumers or utilities. As this case study uses a load with a low energy consumption, the billing effects will not be significantly, however with high power loads that behave non-linear this issue could become problematic.

A more extensive overview of leakage currents from non-linear appliances is given in [92]. It shows a significant leakage current for several non-linear appliances, so strengthening the previous observation. Furthermore, the distortion of the grid and the interactions between appliances can considerably affect the drawn leakage currents.

3.5 Discussion and conclusion

Several cases that resulted in interfered energy readings of the static energy meter are presented in this chapter. EMI issues were found due to a COTS speed-controlled water pump, dimmed light equipment of CFL and LED lighting, and multimedia equipment. This can result in under- or over-estimation of the energy consumption of the static energy meter. In all EMI cases the currents drawn represent non-LTI pulsed currents. These have rise times in the range between 2 µs and 150 µs, and current slopes larger than 0.1 A/µs. The interference was affected by the impedance of the grid, i.e. a lower impedance result in higher errors, due to the fact that high frequency currents are drawn easier in that case. Furthermore, also the slope of the pulsed current affected the interference, were a larger slope results in larger errors. Next to that, also the phase firing angle between the current pulse and the voltage can alter the errors. It is even found that, for a static energy meter utilizing a Rogowski coil as its current sensing element, the under-estimation is so large that the negative error can be higher than the actual consumption. This means that the static energy meter will report an incorrect power delivery back to the grid, while actually energy is being consumed by a load.

Furthermore, problems in energy metering was found due to a current unbalance between the line and neutral conductor, while the static energy meter was working correctly according to its specification. This occurred because energy measurements are performed according to the Blondel theorem that states that for a system containing N conductors, only N-1 current elements are needed. For the residential system it is assumed that the system is earthed and no current can flow on the protective-earth conductor. Therefore only N-2 current elements are used, i.e. in a one-phase system only the line current is measured. However, two cases are shown where a protective-earth current was flowing resulting in an unbalance between the line and neutral conductor and difference in energy measurement. This occurred for example in the case of to a broken RCD and in case of flowing leakage currents for non-linear appliances.

The broken RCD can create an unsafe and hazardous situation, so checking its proper working is highly recommended.

In the remainder of this thesis, Chapter 4 characterizes and determines the suitability of CTs that are used to measure pulsed currents in order to allow for a proper measurement. Thereafter, the measured waveforms contributing to interference on static energy meters are further analyzed in Chapter 5. This is done by analyzing the time-domain parameters of the interfering signals, to find out which parameters can be correlated to the metering errors. In that sense, the current slope, peak value, pulse width, charge, and crest factor of the waveforms are investigated. Subsequently, in Chapter 6 the critical parameters that were correlated to the metering errors based on the laboratory experiments as presented in this chapter, are compared to the emissions of equipment that is present in typical residential situations. And in Chapter 7 the critical parameters are compared with measured data of an on-site low-voltage grid, measured at the meter connection point.

Chapter 4

Current transducers for pulsed currents

This chapter describes a study on CTs for the measurement of pulsed currents in laboratory and on-site situations. The content of this chapter comprises the research that was earlier published in [93], [94].

4.1 Motivation

The previous chapter has shown several EMI cases involving static energy meters. The current waveforms associated with the interference are narrow pulses, with rise times in the range between 2 µs and 150 µs, and current slopes larger than 0.1 A/µs. In order to measure such impulsive currents in the time-domain, in laboratory or on-site situations, accurate CT elements are needed. Because of the fast rise times, these CTs should have a very wide instantaneous frequency range without any phase shifts.

Conventional techniques to determine the electrical response of CTs are performed in the frequency-domain, such as the IEEE Std C57.13 [95]. And use sinusoidal CW currents which are swept in frequency and amplitude. This determines the operating ranges of the CTs, but without measuring the phase the effect of wide-band signals can be overlooked. The necessity of time-domain testing was already addressed in Chapter 2, because systems behave non-linear and/or time-variant. Therefore, the systems response to the superposition of CW currents of multiple frequencies is not equal to an impulsive current, and time-domain testing is needed. The use of signal processing on the time-domain data was already shown to provide the necessary characteristics of a time-variant system in [83]. And the use of time-domain characterization methods is not a new idea, as [96] already proposed to use wide-band pulses to characterize responses in linear systems. From this time-domain response also the frequency-domain response of the system can be determined using a Fourier transform. The characterization of CTs in the presence of harmonic

distortion is discussed in [97], where it is proposed to excite the CTs by a fundamental and harmonic frequency, because this test is closer to the actual working conditions of the CTs. Experimental results using this method show differences with the traditional frequency response tests [98], but these occur only when the air gap of the core is also changed. In [99] research on time-domain calibration of CTs is discussed, using a Rogowski coil intended to be the used with pulsed currents. However, the resulting response is not quantified using time-domain parameters. Other time-domain analysis measurements are shown in [100], in which the time-domain responses of CTs that use a current transformer, Rogowski coil, Hall element, and shunt resistor are investigated. Small differences in the time-domain parameters, as the rise time and peak value, of the tested CTs are observed.

The purpose of this chapter is to analyze the electrical response of CTs using impulsive currents that are representative to the currents found in household situations, and compare those results with conventional CW test methods. Time-domain parameters are extracted to verify if the short rise times and steep inclining slopes of pulsed currents are measured correctly by the CTs in the time-domain. Furthermore, the frequency-domain response of these impulsive signals is determined using fast Fourier transform (FFT), and is compared to conventional methods that use CW signals. Additionally, the measurement of energy and power is considered when the current waveforms represent non-linear signals.

The rest of this chapter is organized as follows: Section 4.2 describes a set of time-domain parameters that is relevant for the analysis of pulsed currents. Then, Section 4.3 describes the measurement method used to characterize the CTs using a time, and a frequency-domain approach. The results of the time-domain characterization is shown in Section 4.4. And Section 4.5 shows the frequency-domain results. Then, in Section 4.6 the measurement of energy with pulsed currents is considered. Finally, Section 4.7 discusses and concludes the findings on the test methods for CTs when measuring pulsed current waveforms.

4.2 Time-domain analysis

A set of time-domain parameters is composed for the analysis of the impulsive test signals used to characterize the CTs in this chapter. In order to quantitatively describe the time-domain responses of the CTs under test and to compare them with respect the reference device. These parameters are an extension of the parameters that were already introduced in Chapter 3. Again the 10%-90% rise/fall times are used as this is a common criteria for describing pulses [85]. To resemble the pulsed currents that cause EMI on static energy meters as showed in Chapter 3, a square-wave signal is used as a test signal. In contrast to the triangular shaped test signals as used in Section 3.3.4, the square-wave signals also considers the on-state that is present in the interfering waveforms in Section 3.3.1. When lowering the duty-cycle, the square-wave signal will transit into a triangular signal. Due to the distortion caused by

the parasitic components in the system, the considered square-wave signal has a certain overshoot and ringing before it stabilizes to its steady state value. This current signal and the domain parameters are shown in Figure 4.1, these parameters are explained one-by-one hereafter:

- 100% value (i_{100}): the steady state value of the current.
- Peak (i_{pk}): the peak value of the current, which could be higher than the 100% value of the current due to overshoot.
- Signal edge ($\mathrm{d}i$): the difference between the 10% and 90% value of the current.
- Rise time ($\mathrm{d}t_{\mathrm{rise}}$): the time the current needs to rise from 10% to 90% of the steady state value.
- Rising slope ($\mathrm{d}i/\mathrm{d}t_{\mathrm{rise}}$): the ratio between the signal edge ($\mathrm{d}i$) and rise time ($\mathrm{d}t_{\mathrm{rise}}$).
- Fall time ($\mathrm{d}t_{\mathrm{fall}}$): the time the current needs to fall from 90% to 10% of the steady state value.
- Falling slope ($\mathrm{d}i/\mathrm{d}t_{\mathrm{fall}}$): the ratio between the signal edge ($\mathrm{d}i$) and fall time ($\mathrm{d}t_{\mathrm{fall}}$).
- Pulse width (t_{width}): the time the current needs in-between its rise to 50% and its fall to 50% of the current value.
- Charge (q): is determined using (4.1), where N is the total number of samples (and should at least cover one cycle), i is the current, and Δt is the time between two samples. When comparing two currents the ratio between N and Δt of both currents should be equal.

$$q\,[C] = \sum_{n=1}^{N} i(n) \cdot \Delta t \tag{4.1}$$

4.3 Method

Two methods to test the response of CTs were used. The first method used impulsive signals, and the second was a conventional test method that used CW signals.

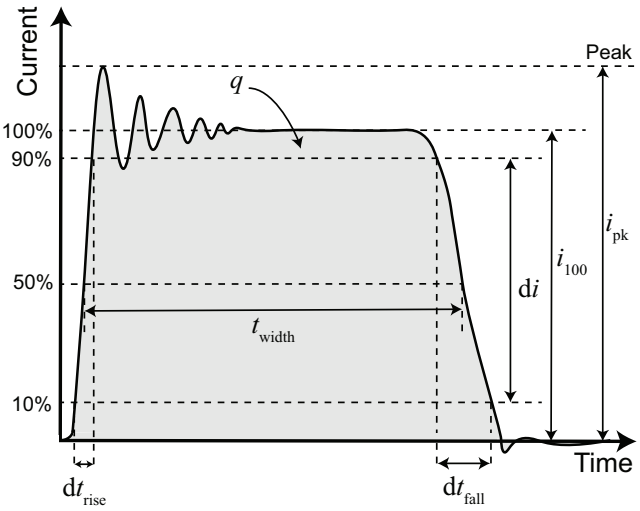

Figure 4.1. Visualization of the time-domain parameters used to describe the response of CTs when measuring pulsed currents.

4.3.1 Response using impulsive signals

The impulsive signals were supplied using a gallium-nitride (GaN) half bridge that generated a pulse width modulation (PWM) signal. The half bridge consists of a GS665EVBMB motherboard and a GS66508/16T daughter board. The half bridge was operated via a schmitt trigger which was controlled using a function generator model 3314A from HP. The carrier frequency and dc-offset of the function generator controls the repetition frequency, f_{r}, and duty-cycle (so the pulse width) of the generated impulse. The motherboard was powered by a voltage of 12 V, that was supplied by a dc power supply model 72-2720 manufactured by TENMA. The half bridge was connected to a dc power supply model E36234A manufactured by Keysight, generating V_{supply}, on the supply side, and to a 2.4 Ω 300 W power resistive load on the load side. The resistor is verified from 10 Hz up to 200 kHz using an LCR bridge, model HM8118 manufactured by Rohde and Schwarz. On the load side, line inductance can be added, using additional cable length, to increase the rise and fall time of the PWM pulse. Depending on the load, a current, I_{supply}, will flow through the conductor which is then measured by the CTs under test. Three different commercially available CTs were used: model TA189 from Pico Technology, model SEN-11005 from SparkFun Electronics, and model AM 503 from Tektronix. These are referred to as: CT1, CT2, and CT3. These transducers measure the current non-invasively, using the current transformer method, and all have a similar measurement range according to the manufacturer specifications. The CTs were placed in a calibration fixture, which is shown in Figure 4.2. A differential voltage probe model TA043 manufactured by Pico Technology measures the voltage over the resistor, acting as a shunt resistor used as a reference. The

CTs under test and reference were connected to a 5444B Picoscope digitizer manufactured by Pico Technology, this is a pc-based oscilloscope. The digitizer captures ten cycles of the response of the CTs and reference at frequency f_r using a sampling rate of 40 MHz. Some setup elements are from the same manufacturer, however all are calibrated independently. Table 4.1 shows the bandwidth limitations of the used setup elements as they were specified. The schematic of the test setup is shown in Figure 4.3.

The generated PWM signal, Figure 4.4, was varied throughout the experiments to verify the response of the CTs in different scenarios that resemble the interference cases in Chapter 3. The tested CTs are intended to measure non-linear currents that occur in low-voltage distribution networks at mains frequency. The non-linear current waveforms of interest have critical rise times between 2 µs and 150 µs, this corresponds to frequency components between 1 kHz and 500 kHz, as was evidenced to result in static energy metering errors in the previous chapter. Therefore, repetition frequencies, f_r, of 50 Hz, mains frequency, and 10 kHz, with lower harmonics around the critical rise times, were used. The current amplitude, I_{supply}, was varied between 2 A and 10 A, by varying V_{supply} between 5 V and 20 V. The current slope was varied by inserting additional wire length, which is referred to as line inductance in Figure 4.3. This was done to resemble the waveforms of interest related to interference on static energy meters as presented in Chapter 3, in which a correlation between the inclining slope and EMI issues is shown.

The results obtained using this method were further processed. The time-domain parameters as introduced in Section 4.2 were determined, and the frequency-domain behavior was determined using an FFT. For the frequency-domain, the gain of the CTs was determined with respect to the reference. Frequency components other than the harmonics of the fundamental frequency were removed, as those are considered as noise. Harmonics with an amplitude lower than the CTs resolution are considered as noise and were also filtered out. Both responses are then compared with the reference.

4.3.2 Response using CW signals

To compare the results to conventional test methods, a characterization using CW signals was also performed. This was done by using a CW signal with an amplitude of 1 A, of which the frequency is swept from 10 Hz to 1 MHz, using 100 steps per decade. The signal was generated using a 5444B Picoscope digitizer manufactured by Pico Technology. This generated signal was then amplified by an audio amplifier model 6552-1A manufactured by Solar Electronics for frequencies from 10 Hz to 100 kHz, and a wideband RF amplifier model 110C manufactured by Kalmus for frequencies from 100 kHz to 1 MHz. The generated CW signal was applied to the 2.4 Ω resistor. The CTs, reference, and digitizer were connected in the same manner as before.

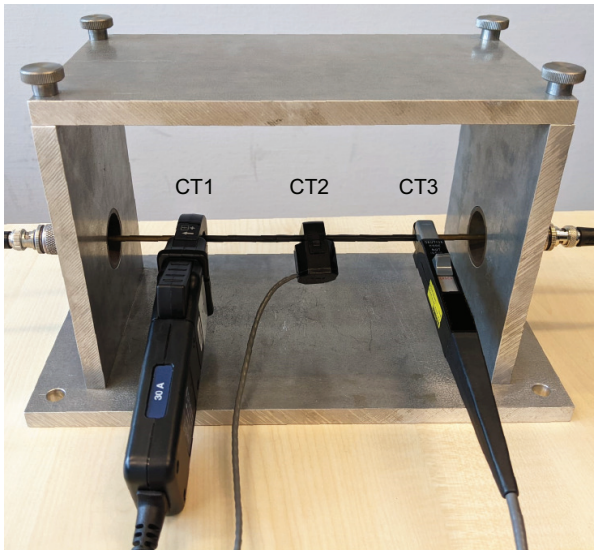

Figure 4.2. Calibration fixture to which the CTs under test were mounted.

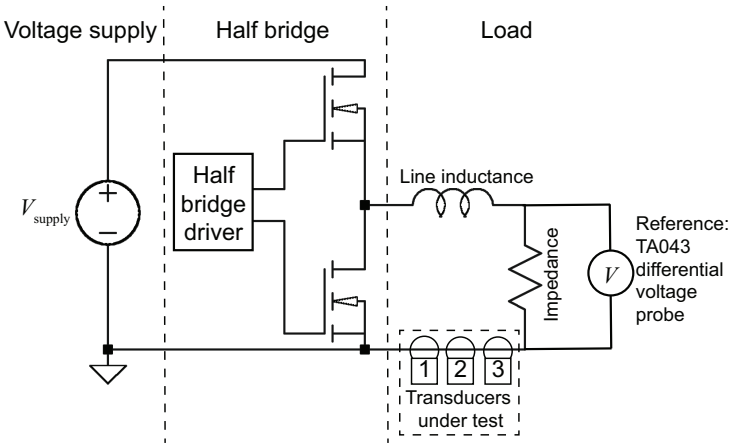

Figure 4.3. Schematic of the test setup generating impulsive signals.

Table 4.1. Bandwidth limitations of the setup elements.

Setup element	**Bandwidth**
Half bridge	0-10 MHz
Load: 2.4 Ω	10-200 kHz
Digitizer: 5444B Picoscope	0-200 MHz
Reference: TA043	0-100 MHz
CT1: TA189	0-100 kHz
CT2: SEN-11005	0-75 kHz
CT3: AM 503	0-200 kHz

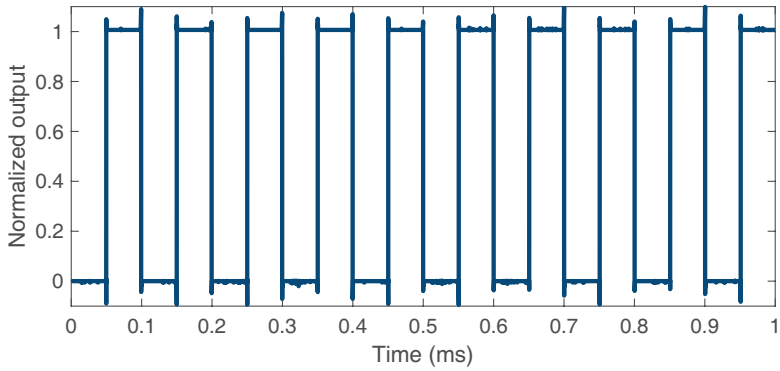

Figure 4.4. Normalized 10 kHz PWM signal, with duty-cycle of 50%.

4.4 Time-domain results

4.4.1 Initial setup settings

The time-domain responses of the CTs using the impulsive test are shown in Figure 4.5, and in Figure 4.6 the time-domain parameters of each CT can be seen with the relative errors with respect to the reference, also the absolute value of the reference is shown. There is a slight difference in the 100% current for all CTs compared to the reference. The peak current of CT1 is higher than the reference, resulting from overshoot before the current falls towards zero. Also the other CTs have a difference in peak current. For CT2 a slower rising slope compared to the reference is observed, i.e. it has a smaller frequency bandwidth than the reference. Also the other CTs experience a difference in the fall time. The width and charge are nearly identical.

4.4.2 Varying setup settings

Changes in the setup settings were made and the effect of this on the CTs is tested. Figure 4.7(a) shows the effect of lowering the current amplitude. In this case the effect is shown on CT1, because it has the largest error in peak current based on the initial settings. It shows that the deviation of the peak value increases when lowering the amplitude, although the absolute deviation remains nearly identical. This is remarkable as the absolute overshoot is expected to be lower at lower amplitudes. When increasing the rise time by adding inductance, it is clear from Figure 4.7(b) that a lower rise time will result in higher deviations for CT2. A similar effect can be seen for the fall time. As a square wave signal with higher rise or fall times correspond to the inclusion of less frequency components, consequently the frequency limit of the CT is not reached, and thus the differences are less. Changing the repetition frequency from 10 kHz to 50 Hz does not have a big influence on the time-domain pa-

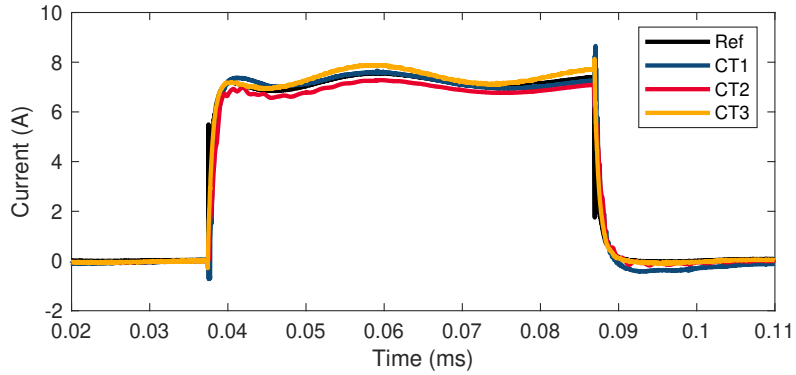

(a) Time-domain response

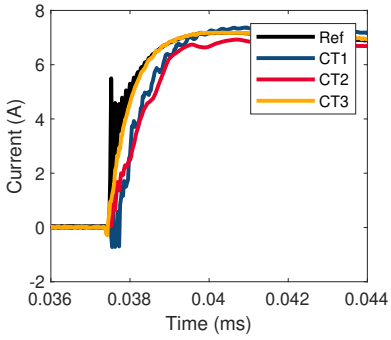

(b) Rising edge

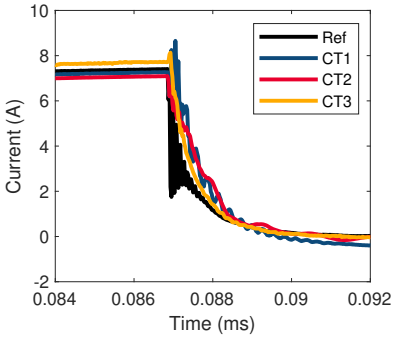

(c) Falling edge

Figure 4.5. Time-domain response of CTs and reference (Ref), when using an impulsive signal.

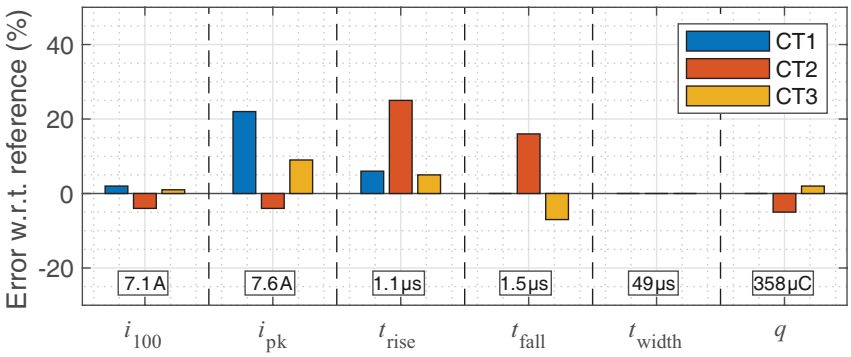

Figure 4.6. Time-domain parameters of the CTs with respect to the reference, for: f_r=10 kHz and I_{supply}=7 A.

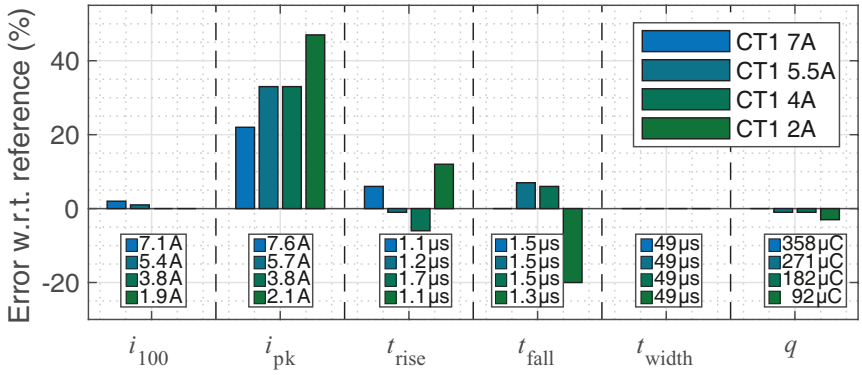

(a) Varying the amplitude; I_{supply} is 7 A, 5.5 A, 4 A, and 2 A.

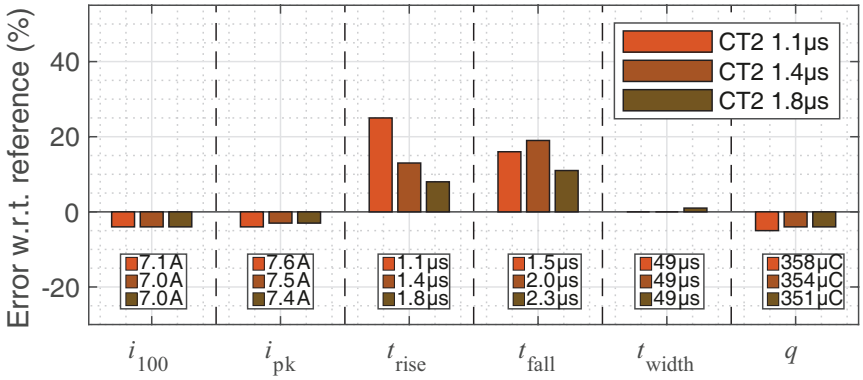

(b) Varying the rise time; t_{rise} is 1.1 µs, 1.4 µs, and 1.8 µs.

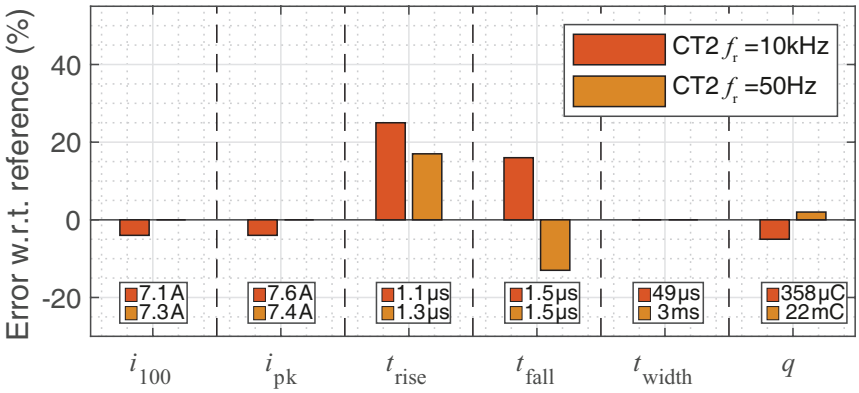

(c) Varying the repetition frequency; f_{r} is 10 kHz, and 50 Hz.

Figure 4.7. Time-domain parameters of the CTs with respect to the reference, when varying different setup settings.

rameters, as Figure 4.7(c) shows the effect on CT2. The deviation of the rise time is slightly lower, but the total rise time increased, so this follows from the previous variation.

4.5 Frequency-domain results

The frequency-domain responses of the CTs with respect to the reference can be seen in Figure 4.8, it shows the results of the CW test and the FFT of the impulsive test. The results obtained using CW signals show a flat response in the bandwidth of the CT and are in accordance with the specifications of the manufacturers. The orange and yellow dots obtained via the FFT of the impulsive test indicate the response with respect to the reference at the fundamental and harmonic frequencies of the impulse. The responses from both tests are comparable, and the points obtained using impulsive test are within the rated 1 dB accuracy in the manufacturers specifications.

4.6 Measurement of energy

Alternatively, the response of CTs, when those are used to measure the energy consumption, were analyzed when exposed to the realistic on-site interference currents presented in Chapter 3. This is done using a different measurement setup and CTs as before. Seven different load situations were tested, which cover three linear loads and four non-linear loads. These represent standard (linear) test signals of different amplitudes and non-linear signals known to cause errors in static energy meter readings, respectively. Linear signals as generated by a heater of 190, 800, and 1800 W (R190, R800, and R1800, respectively) are used. And non-linear signals as generated by a water pump at dimming level 1, 4, and 9 (WP1, WP4, and WP9, respectively) are used. Additionally, non-linear signals from a dimmed heater at 190 W and a phase firing dimmer at 145 degrees (R190D145) are used, so to resemble a chopped sine-wave. The characteristics of these test signals are depicted in Table 4.2. The current was measured using a current sensor model SCS-075-0050A:0.333V manufactured by Power Standards Lab (CT4), which is a current transformer. The voltage was measured using a differential voltage probe model TA043 from Pico Technology. The responses of the CTs and the voltage were measured synchronously using a Picoscope 5444D pc-based oscilloscope. The average power over 10 cycles resulting from the product between the voltage and current was determined, and was compared to the same reference as used in Chapter 3. The schematic of this experiment is depicted in Figure 4.9. Then, the deviation in measured energy was compared to the reference instrument using,

$$\text{SM deviation}\,(\%) = \frac{E_{\text{dut}} - E_{\text{ref}}}{E_{\text{ref}}} \cdot 100\% \tag{4.2}$$

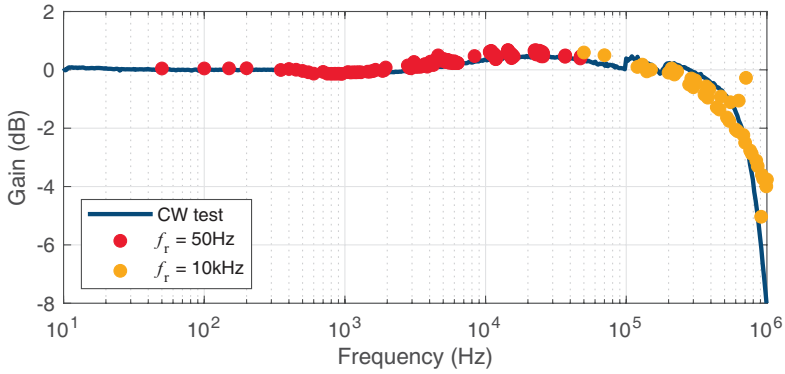

(a) Frequency response of CT1.

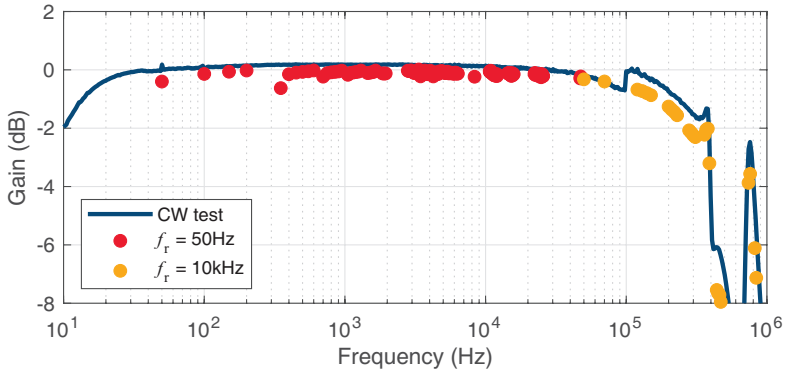

(b) Frequency response of CT2.

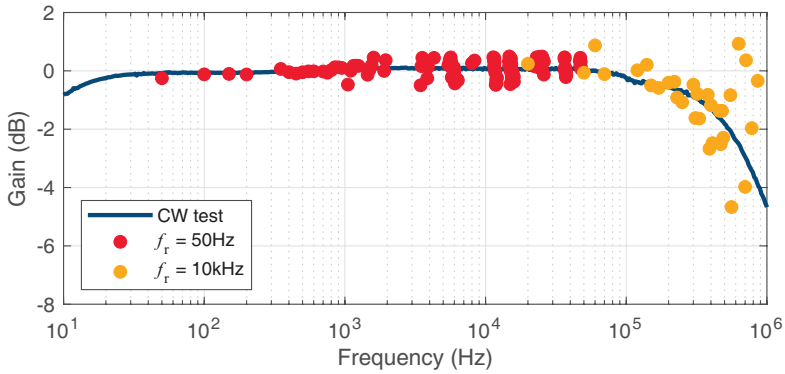

(c) Frequency response of CT3.

Figure 4.8. Frequency response of tested CTs, plot contains the CW test, and test using impulsive signal of 50 Hz and 10 kHz.

Table 4.2. Time-domain parameters of the test signals.

Test signal	Charge (mC)	Crest factor	Peak value (A)	Pulse width (ms)	Slope (A/µs)
R190	16.9	1.4	1.3	20	$3.5{\cdot}10^{-4}$
R800	66.4	1.4	5.2	20	$1.3{\cdot}10^{-3}$
R1800	149	1.4	11.7	20	$3.0{\cdot}10^{-3}$
WP1	4.8	9.1	17.2	0.4	2.8
WP4	6.6	8.5	17.2	0.8	2.2
WP9	7.1	8.0	17.1	0.7	2.0
R190D145	0.3	9.9	0.8	1.2	0.3

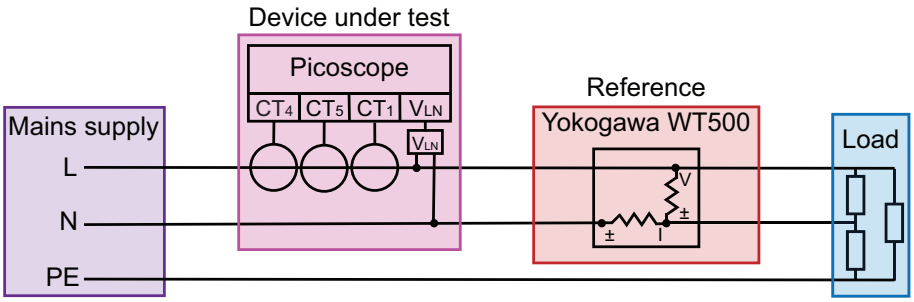

Figure 4.9. Schematic of the measurements with three different CTs.

where E_{dut} is the measured energy of the device under test, which is the tested CT, and E_{ref} is the energy measured by the reference instrument. This method is similar to the method used to test the readings of static energy meters in Chapter 3.

The results are summarized in Table 4.3. Here, in red the deviations exceeding the maximum permissible limits for electricity meters in Europe with approval of the European MID according to the European standard EN 50470-3:2006 [62], as introduced in Chapter 2, are highlighted. The results show that for WP1 and WP4 deviations above the permissible limits occur, while the other test signals cause no deviations exceeding the permissible limits.

In order to find the root-cause of the deviations in the measured energy consumption, the most critical situation was analyzed in more detail, i.e. when it is loaded with WP1. Therefore, this specific measurement was repeated with three CTs that have a different current measurement technique, namely: model SCS-075-0050A:0.333V manufactured by Power Standards Lab (CT4), model CWT3 from Power Electronic Measurements (CT5), and model TA189 from Pico Technology (CT1). Where CT4 is a current transformer, CT5 is a Rogowski coil, and CT1 is a Hall sensor. A photograph of these CTs is depicted in Figure 4.10. Using an FFT, the power over frequency was determined and then accumulated over the frequency ranges of interest.

(a) CT4 (b) CT5 (c) CT1

Figure 4.10. Photograph of the used CTs.

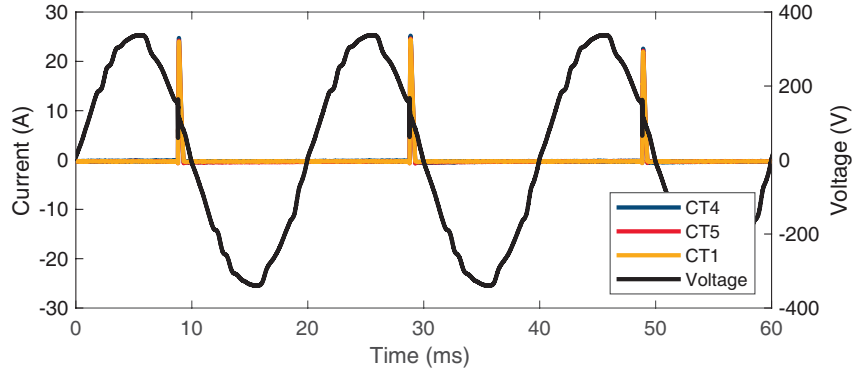

(a) Complete response

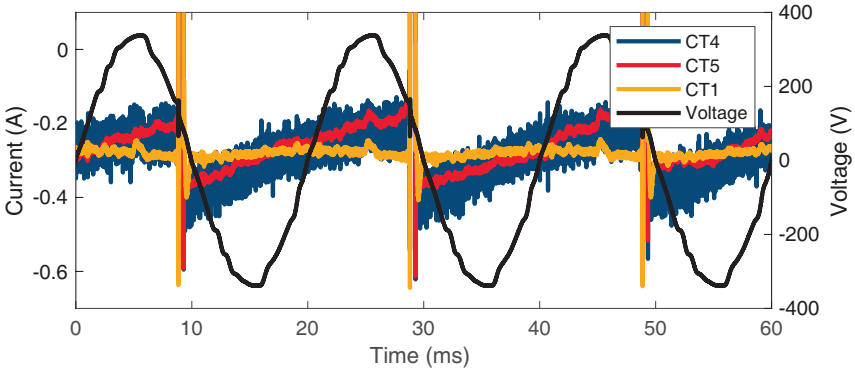

(b) Zoomed response

Figure 4.11. Response of the CTs measuring load WP1.

Table 4.3. Energy measurement results using different test signals, when using CT4.

Test signal	$E_{\mathbf{dut}}$ **(Wh)**	$E_{\mathbf{ref}}$ **(Wh)**	**SM deviation (%)**
R190	3.4	3.5	-2
R800	21.7	22.9	-2
R1800	27.1	27.4	-1
WP1	2.9	2.1	38
WP4	3.0	2.5	18
WP9	4.3	4.4	-1
R190D145	14.1	14.3	-2

Table 4.4. Power readings per frequency.

Frequency (Hz)	**CT4**	**CT5**	**CT1**
<50	0.0 W	0.0 W	0.0 W
50	41.3 W	42.5 W	31.9 W
>50-1000	0.8 W	0.7 W	0.7 W
>1000-10000	-2.0 W	-2.0 W	-2.0 W
>10000	0.0 W	0.0 W	0.0 W
Total	**40.1 W**	**41.2 W**	**30.6 W**
Deviation	31 %	35 %	0 %

The results are presented in Figure 4.11 and Table 4.4. For both CT4 and CT5 in the time period in which no pulse is present, and the signal should have a zero value, however a saw-tooth in the zoomed response is present. The presence of this saw-tooth is likely to produce the observed energy deviation. For CT4 and CT5 power deviations of 31% and 35% are measured, respectively. From the power per frequency it is clear that the saw-tooth, which is repeating with the fundamental frequency of 50 Hz, is resulting in a higher measured power at the fundamental, as this is the only frequency where differences between the CTs are observed.

Next, it is verified whether the measured pulsed part is similar and the difference between the responses of the different CTs is due to the existence of the saw-tooth only. Therefore, the pulses were extracted from the original measured response and the time-domain parameters were determined using the parametric waveform model that will be presented in Chapter 5. The resulting parameters are presented in Table 4.5. Here, it is shown that all parameters are similar and the difference between the measured powers originates most likely due to the saw-tooth behavior of CT4 and CT5. The product of the saw-tooth and the voltage results in an additional power of approximately 10 W.

Table 4.5. Time-domain parameters of responses CTs.

Parameter	CT4	CT5	CT1
Charge (mC)	5.6	5.4	5.5
Crest factor	10.8	10.8	10.7
Peak value (A)	23.5	23.0	22.8
Pulse duration (ms)	$4.8{\cdot}10^{-1}$	$4.6{\cdot}10^{-1}$	$4.9{\cdot}10^{-1}$
Slope (A/µs)	1.2	1.6	1.7

4.7 Discussion and conclusion

In this chapter, it is shown that the impulsive test method using a half bridge to characterize wide-band CTs provides a good alternative to conventional CW testing. However, the time-domain response of the impulsive tests suggest initially errors, the frequency-domain shows that these errors occur because the corresponding frequencies are outside the bandwidth of the CTs. These can thus also be filtered out of the time-domain response data. The repetition frequencies used try to resemble currents at mains frequency (50 Hz), and at critical frequencies based on previous research (10 kHz), however the combination of both generate 35% fewer measurement points compared to the CW test in the bandwidth up to 1 MHz. Furthermore, the repetition frequency of the impulses should be optimized to avoid overlap of the harmonics and to create a better spreading of the frequency points, thus better coverage in this bandwidth. Still, the impulses allow to test multiple frequency points at once compared to CW testing, so less test signals are needed and testing can be more time-efficient. Eventually, increasing the square-wave signals was done in [101], and shows that a fairly good spread of frequency points can be achieved using this test method. Also, it shows that the square-wave signals generated have a certain distortion, i.e. over-voltage/current and ringing, similar to the response in Figure 4.5, due to the parasitics in the circuit. However, the frequency components added because of this could also be beneficial as it adds more frequency points, but to have consistent and reproducible results it should be avoided. Furthermore, according to the manufacture's specifications the GaN half bridge allows to test up to 30 A with a bandwidth of 10 MHz. In comparison the CW test would require the use of a high power wide-band amplifier to achieve these high currents in a wide bandwidth, and is thus a more expensive solution.

Next to that, when the CTs are used to measure pulsed currents from typical household appliances, discrepancies in the current response are observed. Where the response slightly varies when no pulse and thus current is present in the measured signal, and an additional saw-tooth is present in the response. The product of the voltage and the saw-tooth in the current response, results in a measured energy in addition to the energy of the pulse. Which leads to the occurrence of energy measurement errors outside the permissible limits for electricity meters in Europe [62]. While for linear sinusoidal currents as used

in immunity tests, no issues for the energy measurement system are observed. This shows the need of immunity tests using pulsed currents to test the limits of energy metering systems, and thus signals with a combination of frequencies. Instead of using frequency-domain tests as is done in the IEC 61000-4-19 standard [29]. Because pulsed test methods show the errors in the energy measurement due to the current droop, while single-tone currents do not show this problem.

Based on the response of CTs as characterized based on the method as shown in this chapter, CTs are selected for the measurement of on-site currents in the next chapters. That is, in Chapter 6 proper CTs are selected for the measurement of currents generated by typical household equipment. And for the measurement of currents that occur at the meter connection point in Chapter 7.

Chapter 5

Waveform model for time-domain interference

In this chapter, a parametric waveform model to analyze current waveforms that result in static energy meter interference is defined. The content of this chapter comprises the research that was earlier published in [102]–[104].

5.1 Motivation

In Chapter 3, several cases are found that indicate EMI on static energy meters. These cases were analyzed in more detail in a laboratory environment.Issues were found due to modern appliances that are behaving non-linear, e.g. a COTS water pump, dimmed light equipment of CFL and LED lighting and multimedia equipment. The critical waveforms drawn using the non-linear appliances show impulsive currents with a high peak value and low rms value, i.e. a high crest factor. A fast rising slope was found to be critical, which was above 0.1 A/µs, the corresponding critical rise times were between 2 µs and 150 µs. Furthermore, the existence of more household appliances related to metering errors were reported in [38].

Next to these laboratory experiments as described in Chapter 3, it is of interest to survey the signals occurring at meter connection points. The existence of current waveforms with fast increasing slopes that occur in low-voltage customer terminals is shown in [105]. Furthermore, in the framework of the MeterEMI project [43] surveys were performed in modern low-voltage distribution networks. Preliminary results are shown that include networks with EV charging stations [106], and PV installations [107]. This resulted in a vast repository of data sets comprising of on-site current waveform measurements, which will be described in more detail in Chapter 6 and 7.

However, a parametric definition of such critical waveform, that enables their identification in real scenarios, remains an unsolved technical challenge, because of the inherent complexity and diversity of the current waveforms found

on-site. Therefore, simple time-domain analysis algorithms that assume bi-level pulses do not work. Collaterally, the absence of the referred parametric definition hinders the possibility of establishing new testing standards concerning the immunity of the static energy meter with respect to EMI problems.

To produce such a set of standardized artificial test signals is one of the goals of the MeterEMI project [43]. In this regard, this work aims at defining and validating a parametric model for the current waveforms that result in significant errors in static energy meter readings. This model must provide a simplified, yet accurate, mathematical description of the current waveforms, such that it is easy to standardize into test waveforms. Therefore, it is intended to reproduce the features that have been found to be highly correlated to the errors in the static energy meter readings. Then, the data collected in previously performed laboratory experiments, as described in Chapter 3, is fitted into the waveform model to obtain parametric versions of such current waveforms, and to evidence the important parameters to be used in future immunity test signals. Here we focus only on the parameters that could be extracted from the modelled current waveform, however it should be noted that the phase firing angle between the voltage and the current pulse has an influence on the error, as was already pinpointed in Chapter 3 and in [23], [86]. Even though this is not investigated in this chapter because it is not a characteristic that is related to the modelled waveform, it should be noted that the static energy meter errors might be amplified because of the phase firing angle.

The rest of this chapter is organized as follows: Section 5.1 describes the waveforms that have been linked to significant errors in static energy meters. Section 5.3 presents the waveform modelling approach and it is followed by the analysis of the key waveform parameters that can be extracted from the model in Section 5.4. Section 5.5 discusses the critical waveform parameters related to static energy meter errors. Section 5.6 investigates the use of the modelled waveforms as artificial test signals for future standardization. Section 5.7 discusses the use of wavelet-based signal representations as an alternative method for type testing. Finally, Section 5.8 closes with the conclusions of this chapter.

5.2 Waveforms resulting in significant errors of static energy meters

The current waveforms resulting in errors on static energy meter readings do not follow the voltage and are non-linear. These currents are resulting from a single appliance. Two examples, representative for the waveforms resulting in static energy meter errors as shown before in Chapter 3, are shown in Figure 5.1 and they will be referred to as pulse 1 and 2. In the waveforms a clear current pulse is visible, and one period consists of one pulse as these waveforms are unsymmetrical/uni-polar, i.e. there is no current pulse in the second half of the sine wave. It is also possible that the waveform has multiple pulses for

a symmetrical/bi-polar waveform or a superposition of multiple pulses, e.g. when using multiple appliances. Pulse 1 is supplied by the voltage of a buildings mains supply, while pulse 2 uses the voltage supplied by a 4-quadrant amplifier, and a LISN to provide a stable impedance. This higher impedance compared to the buildings mains supply is resulting in a larger voltage dip. The two current waveforms shown are slightly different, pulse 1 rises to its peak value in one go, Figure 5.1(a), while pulse 2 can be considered as a superposition of two trapezoidal pulses, it increases very fast to a first peak value of approximately 8 A, declines and then it increases further to the peak value, Figure 5.1(b). Both pulses have a high peak value compared to a low rms value of approximately 1.5 A, and therefore a high crest factor of 10. The pulses increase very fast to their peak values, the time to rise from 10% to 90% of the pulse peak value is 20 µs and 3 µs for pulse 1 and 2 respectively. Typical values are between 2 µs and 150 µs for waveforms resulting in static energy meter errors. And the corresponding critical rising slopes are above 0.1 A/µs.

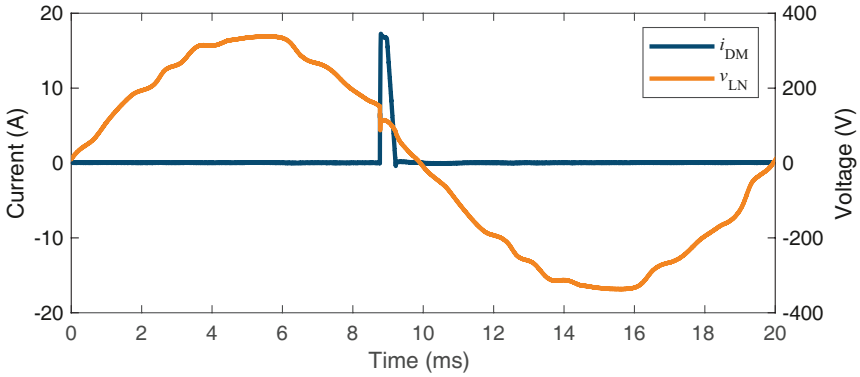

(a) Pulse 1

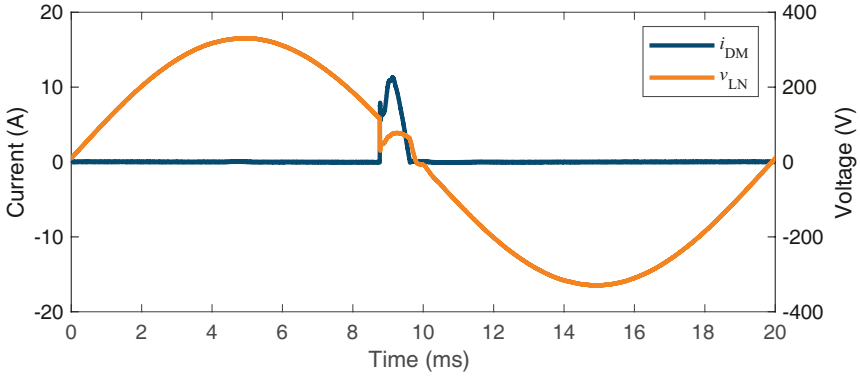

(b) Pulse 2

Figure 5.1. The two different signal types considered.

A parametric model is composed, based on a set of 60 current waveforms and resulting static energy meter deviations during lab measurements which were reported in Chapter 3. The model is explained based on the waveforms presented in Figure 5.1, which are representative for the set of waveforms.

5.3 Modelled waveform

From the interfering pulses a modelled waveform is composed. This modelled waveform is intended to be a simplified version of the actual current waveform while still representing all its relevant features, to make it useful for future test standards. In particular, it is proposed to approximate the interfering waveforms, $p(t)$, through a combination of piece-wise linear functions, $y_i(t)$, that is, a superposition of linear fitted segments given by,

$$p(t) = \sum_{i=1}^{k+1} y_i(t), \tag{5.1}$$

where $y_i(t)$ is the equation of a straight line defined between a pair of k change-points occurring at the discrete instants τ_{i-1} and τ_i, in other words,

$$y_i(t) = \begin{cases} a_i t + b_i & \text{for } \tau_{i-1} < t \leq \tau_i \\ 0 & \text{for } t \leq \tau_{i-1} \vee t > \tau_i \end{cases} . \tag{5.2}$$

The piece-wise linear segments can be estimated through segmented regression if the change-points instants are known. Several computational methods for this purpose are described in [108]. Here, the underlying optimization problem is to find the optimal change-points, which means, the extreme points of each linear segment that allow an accurate representation of the measured waveform through the proposed model.

For this purpose, a three step algorithm has been designed. First, the current pulses are extracted from the measurements and then they are aligned and combined for the different occurrences of the same pulse. Second, the change-point detection is implemented through the pruned exact linear time (PELT) method [109]. Third, the redundant change-points are removed to create an even more simplified representation of the interfering impulse. The details of the algorithm's steps are provided in the following subsections. The waveform model is then validated by comparing its fit to the original measured waveform.

5.3.1 Pulse extraction

The interfering current pulse is only present in the waveform during a short time interval in each period, Figure 5.1, and in the rest of the waveform the signal has a value of zero. To analyze the pulse more thoroughly it is extracted from the original waveform, using the process described below:

1. The time-domain records obtained from the experiments comprise several periods of the mains frequency. The data is segmented per period resulting in n frames. It might be possible that multiple pulses occur within one period, e.g. when the waveform is bi-polar. In that case the sign of the negative pulse is reversed, as a result the frequency of pulse occurrence is doubled.

2. The peak amplitude of the pulses observed during each cycle is extracted. The interfering pulses are treated as bi-level waveforms. Consequently, the state levels are calculated according to the histogram method [85].

3. The transition instants between state levels in the rising and falling edges are detected for a mid reference level equivalent to the 10% of the difference between the high and low state levels. This is consistent with the commonly applied criteria of 10%-90% - 90%-10% used for the measurement of the rise and fall times, respectively [85].

4. The state level tolerance, Tol, is defined considering the variation between the extremes values of the pulses peak amplitudes according to,

$$Tol\,(\%) = \pm 100 \times \frac{\max(A_{peak}) - \min(A_{peak})}{2\ \mathrm{mean}(A_{peak})}, \tag{5.3}$$

   where the max(·), min(·) and, mean(·) operators calculate the maximum, minimum and average values of the pulses' peak amplitudes.

5. Finally, the pulses are extracted from each frame. For that purpose the duration of the extracted waveforms is calculated as twice the maximum pulse width among the different pulse occurrences. The extracted pulses are then aligned with respect to the first rising edge and a time margin of 50% of the pulse width is allowed before and after the transition instants.

The result of the pulse extraction process is plotted in Figure 5.2. Among the ten occurrences of the pulse (displayed in different colors), from pulse 2, Figure 5.2(b), it is evidenced that waveform characteristics such as the peak amplitude and duration vary significantly from cycle to cycle even if the shape of the pulse remains similar.

5.3.2 Change-points detection

The change-point analysis is the identification of points within a data set where certain statistical properties change. For instance the standard deviation, the rms level, the mean value or even the slope.

Provided that each interfering pulse extracted in the previous step is represented by an ordered sequence of sampled data points $P_{1:n} = \{p_1, p_2, ..., p_n\}$ each point corresponding to the instants $t_{1:n} = \{t_1, t_2, ..., t_n\}$ and that it is of interest to fit $(t_{1:n}; P_{1:n})$ according to the model in (5.1) and (5.2) for a number of $k + 1$ piece-wise linear segments, then a number of k optimal change-points,

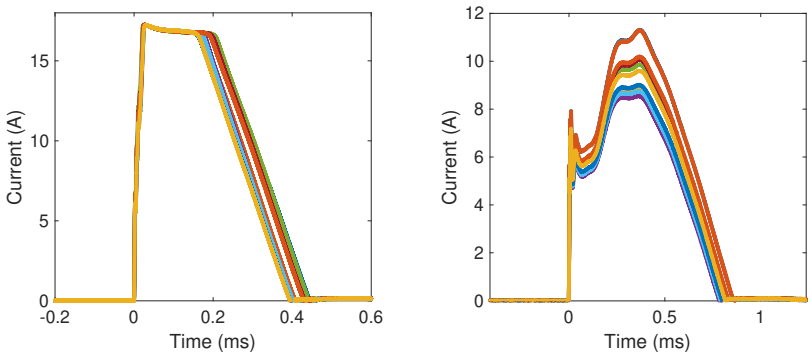

(a) Pulse 1 (b) Pulse 2

Figure 5.2. Result of the pulse extraction process applied to ten cycles at mains frequency.

$cp_{1:k}$, must be calculated for segmenting the data set according to abrupt changes in the waveform's mean value and slope. Those change-points occur in discrete time instants $\tau_{1:k} = \{\tau_1, \tau_2, ..., \tau_k\}$. Each change-point discrete instant corresponds to a vector position that is an integer between 1 and $n-1$ inclusive.

We define $\tau_0 = t_1$ and $\tau_{k+1} = t_n$ and assume that the change-points are ordered such that $\tau_i < \tau_j$ if, and only if, $i < j$. Consequently, the k change-points will split the data set into $k+1$ segments, with the i-th segment containing $P_{(\tau_{i-1}):\tau_i}$.

One commonly used approach to identify multiple change-points is to minimize (5.4),

$$\sum_{i=1}^{k+1} \left[C_i \left(P_{(\tau_{i-1}):\tau_i} \right) \right] + \beta f\left(k\right), \tag{5.4}$$

where $C_i(\cdot)$ is the cost function for the i-th segment and $\beta f(k)$ is a penalty to guard against over fitting. For linear cost functions, the PELT method is computationally efficient for finding the change-points. More about the PELT method and other algorithms for solving the previous equation are reviewed in [109].

With regards to the cost function in (5.4), a suitable choice is the sum of squared errors, SSE, since it is a measure of the goodness of fit that is meaningful for regression models. The SSE of the i-th segment is given by,

$$SSE_i = \sum_{j=1}^{m} \left(p_{j,i} - y_i(t_{j,i})\right)^2, \tag{5.5}$$

where $(t_{j,i}; p_{j,i})$ is the time-amplitude coordinate of the j-th waveform point of the i-th segment with that segment containing a number of m samples. A small SSE indicates a tight fit of the model to the data.

Then, the best linear fit of the subset of m waveform points in the i-th segment $P_{(\tau_{i-1}):\tau_i}$ is obtained through the least squares regression, that is,

$$a_i = \frac{\sum_{j=1}^{m} (\bar{p}_i - p_{j,i})(\bar{t}_i - t_{j,i})}{\sum_{j=1}^{m} (\bar{t}_i - t_{j,i})^2}, \tag{5.6}$$

$$b_i = \bar{p}_i - a_i \bar{t}_i, \tag{5.7}$$

where a_i and b_i are the slope coefficient and the intercept of the i-th segment in (5.2) respectively and $\bar{p}_i$ and $\bar{t}_i$ are the mean values of the waveform amplitudes and of their corresponding time instants, respectively.

5.3.3 Change-points selection

Next the most suitable number of change-points is determined and it is decided whether or not the detected change-points are relevant to construct the model waveform. First, the appropriate number of change-points are determined. The two pulses in Figure 5.1 can be described in the most simple manner by one (pulse 1) or a superposition of two pulse(s) (pulse 2). This will result in four and six change-points, for pulse 1 and 2 respectively. However, the slope of the rising part is not constant, and to retain the relevant information of the pulse, splitting (for example) the rising part in different segments allows us to retain the information about the steepest part of the slope, instead of modelling the slope as a single segment. Therefore, without making the modelled waveform too extensive, ten change-points in between the beginning and the end point of the pulse are used, so a total of twelve. The resulting modelled waveform is plotted in Figure 5.3.

Second, the redundant information created by the addition of extra change-points is removed. The slopes of the consecutive linear piece-wise segments are compared and when those are similar the middle change-point is removed. It was found that when the difference between consecutive slopes is lower than 0.6% of the maximum absolute slope of the signal, the middle change-point could be removed. As in that case the consecutive slopes are nearly identical, and it did not add information considering the parametric description in the next section. This simplification results in an optimized version of the model waveform that represents all the features of the original measured waveform. The redundant change-points are indicated in Figure 5.3, and two and one change-points are removed for pulse 1 and 2 respectively.

5.3.4 Modelled waveform validation

Validation of the model is done through comparison with the actual measured result. Figure 5.4 presents a comparison between the average measured waveform and its modelled representation with each change-point indicated through

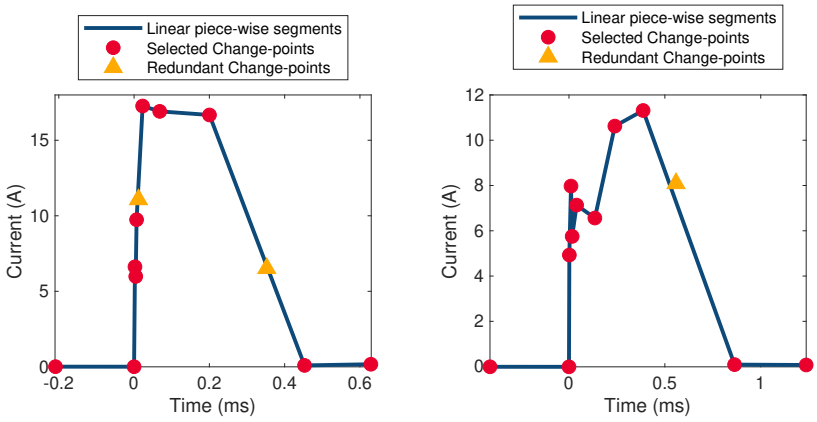

(a) Pulse 1 (b) Pulse 2

Figure 5.3. Fitted modelled waveform using twelve change-points, which are either selected or provide redundant information and are removed in step 2.

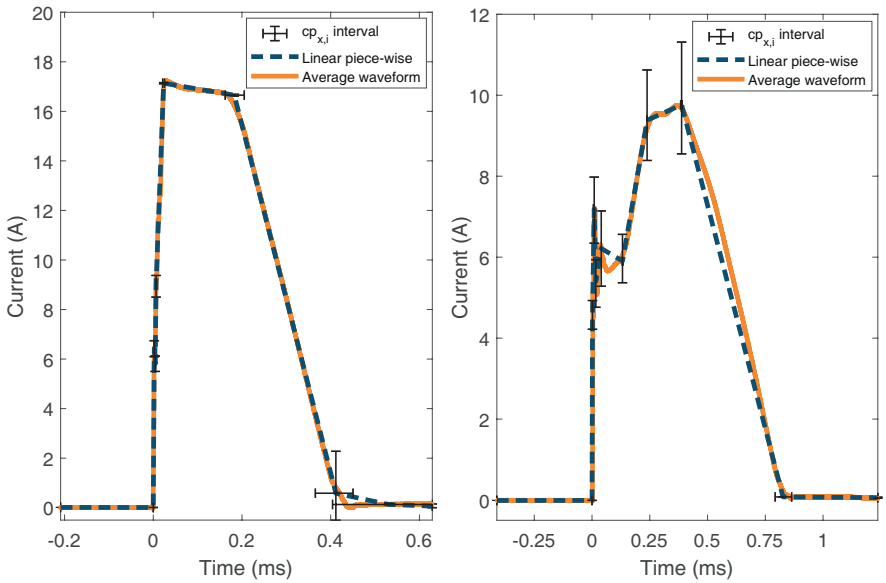

(a) Pulse 1 (b) Pulse 2

Figure 5.4. Comparison between the average measured waveform and its modelled representation.

its expected value and its confidence interval for the horizontal and vertical coordinates. In that sense, individual occurrences of the pulse contained between the change-points intervals are considered to be representative of the same waveform model. It is interesting to notice that the variability in the time instants of the change-points is, in general, lower than the variability in their amplitude.

As for the goodness of fit, the mean squared error (MSE) between the average waveform (reference value) and the linear piece-wise model (estimated-value) was used because it provides a scalar value that is easy to calculate, compare and interpret. For pulse 1, $\text{MSE}_1 = 7.3 \times 10^{-4}$ A^2 and for pulse 2, $\text{MSE}_2 = 2.8 \times 10^{-3}$ A^2. In both cases the MSE is very low, which confirms the excellent fit observed between experimental data and the modelled waveform.

Likewise, the power spectrum of the measured and modelled waveforms is also in excellent agreement as is shown in Figure 5.5. It evidences that no significant distortion is added to the modelled waveform and the same bandwidth is ensured. For both, pulse 1 and pulse 2, the spectrum was calculated up to 1 MHz with a frequency resolution of 200 Hz. For this purpose, the pulse repetition frequency was the mains frequency (50 Hz) and the sampling rate used was 20 MHz.

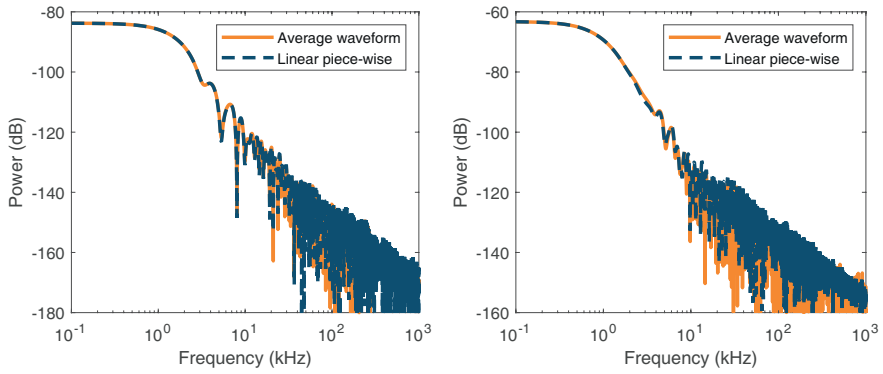

(a) Pulse 1 (b) Pulse 2

Figure 5.5. Spectrum comparison between the average measured waveform and its modelled representation.

5.4 Parametric model

In order to reduce the complexity in the description of the interfering current pulses, the modelled waveforms are characterized through a set of scalar parameters. Such that these parameters could be easily implemented in future standardized test signals. In this respect, the waveform parameters are determined for the modelled waveform, $p(t)$, and can be determined by the set $\mathbf{M}$

of k change-points, $cp_{1:k}$,

$$\mathbf{M} = \{cp_x\{t_{x,i}\ ;\ y_i(t_{x,i})\} : x = 1, ..., k\}. \tag{5.8}$$

The extracted parameters are visualized in Figure 5.6, and are explained one-by-one hereafter:

- Slope ($\Delta i/\Delta t$): the slope between two consecutive change-points, i.e. the ratio between the amplitude and time difference between consecutive change-points,

$$\frac{\Delta i_x}{\Delta t_x} = \frac{y_i(t_{x+1,i}) - y_i(t_{x,i})}{t_{x+1,i} - t_{x,i}}. \tag{5.9}$$

  A single pulse consists of multiple segments, and thus multiple slopes. By taking the maximum or minimum value, the maximum rising or falling slope respectively, could be determined. This is different from the commonly used 10%-90% - 90%-10% criteria [85], especially for pulse 2. Where we see in Figure 5.3(b) that the 90% value of the rising part is located between change-point 7 and 8, while the fastest rising part is between change-point 2 and 4. As it is expected that the fast changing edges, and thus steep absolute slopes will contribute to misinterpretation of the measured signals in energy metering, this definition of maximum rising and falling slope is a better indication for the fast changing slopes.

- Peak value (i_{pk}): represents the peak value of the pulse, meaning the change-point with the highest amplitude,

$$i_{\text{pk}} = \max(\{y_i(t_{x,i}) : x = 1, ..., k\}). \tag{5.10}$$

- Pulse width (t_{width}): the time required to rise to 50% and fall to 50% of the peak value (i_{pk}), where the time instances are linearly interpolated on the segments, this is consistent with the commonly used criteria for pulse width [85].

- Charge (q): the area circumferenced by the pulse and the zero current line, to calculate this the area between consecutive change-points and the zero current line is determined and summed. This is a combination of a triangle with height ΔI_x and a square with height $\min(y_i(t_{x,i}), y_i(t_{x+1,i}))$, both have width Δt_x,

$$q = \sum_{x=1}^{k} \left(\frac{1}{2}\Delta i_x + \min\left(y_x(t_{x,i}), y_x(t_{x+1,i})\right) \right) \cdot \Delta t_x. \tag{5.11}$$

- Crest factor (CF): the ratio between the peak value (i_{pk}) and the rms value (i_{rms}) of the pulse over one cycle at mains frequency, this indicates

how extreme the peak value of the pulse is in comparison with the rest of the signal is,

$$CF = \frac{i_{\mathrm{pk}}}{i_{\mathrm{rms}}}. \tag{5.12}$$

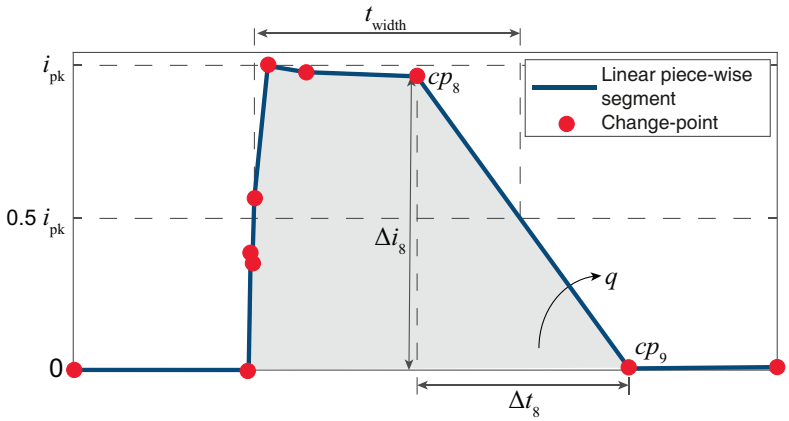

Figure 5.6. Representation of the parametric description as extracted from the modelled waveform.

5.5 Critical waveform parameters resulting in metering errors

Considering the model that accurately represents and describes the interfering current waveforms, it is of interest to identify which, if any, of those parameters are correlated to the static energy meters errors. In order to evidence which parameters are of importance to consider in future immunity tests for EMI on static energy meters. However, this problem is not trivial because most parameters defined in the previous section are not independent from each other, that is, there are cross correlations and interactions between them.

From the static energy meter data in Chapter 3, it is known that not all static energy meters result in the same maximum errors, as shown in Figure 5.7. Therefore, the static energy meters are subdivided in classes, these different classes might also relate to different critical parameters. This division could also be related to the current sensing element in the static energy meter (SM):

- SM class A: Large errors, the maximum errors of the static energy meters above 200%, the static energy meters measure the current using the Rogowski coil principle.

- SM class B: Medium errors, the maximum errors are between 50% and 200%, the static energy meters measure the current using the current transformer principle.
- SM class C: Small errors, the maximum errors are below 50%, the static energy meters measure the current using either a shunt resistor or Hall effect sensor.

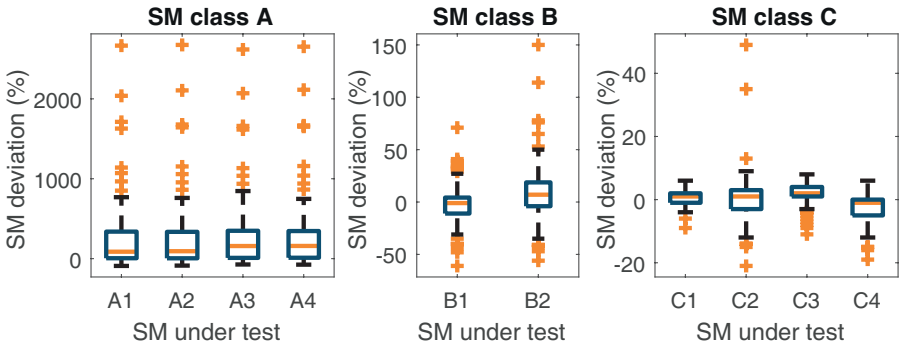

Figure 5.7. Difference in the distribution of the maximum errors in static energy meters (SM) by class and specimen.

The deviations are calculated using,

$$\text{SM deviation}\,[\%] = \frac{P_{\text{SM}} - P_{\text{ref}}}{P_{\text{ref}}} \cdot 100\% \tag{5.13}$$

where P_{SM} is the power measured by the static energy meter under test and P_{ref} is the power of the reference, according to the measurement procedure explained in Chapter 3.

Now we will have a look at the correlation between the parameters and the errors for the different classes of static energy meters indicated, considering the meters in SM class A. First, the relation between the crest factor and static energy meter errors is plotted in Figure 5.8, it is visible that when the crest factor increases the errors also increase. When the crest factor exceeds 5, errors start to occur. The crest factor provides a valuable first selector, because it already differentiates between linear and non-linear waveforms, and will only select the pulsating waveforms. Although this correlation is clear, it is not univocal, as there are also situations where a crest factor higher than 5 is present, but no high error was found, so more parameters need to be considered.

Second, the correlation between the pulse width and the errors is plotted in Figure 5.9. When the pulses become narrower than 1 ms the static energy meter errors tend to increase. However, this correlation is also not univocal, and within this graph three segments are identified in which the errors increase when the pulse width decreases. From segment 1 to 3 the pulses peak value

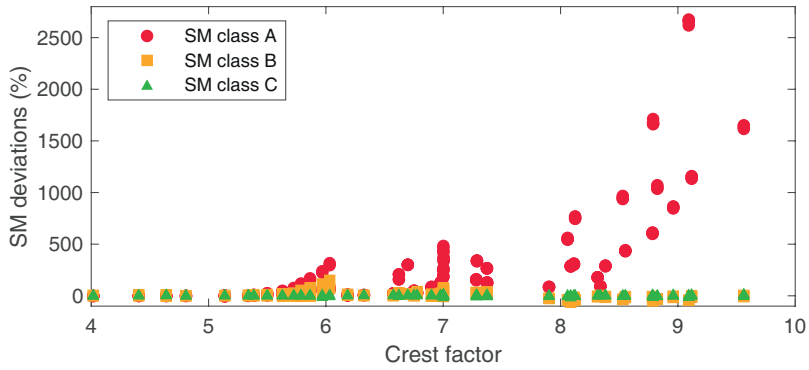

Figure 5.8. Correlation between the crest factor and the static energy meter (SM) deviations.

reduces while the pulse contains the same range of charge. As a result, when the pulses become narrower, also the amount of charge decreases, Figure 5.10, and the errors tend to increase as is visible in all three segments. It should be noted that for one static energy meter specimen the errors in segment 3 increase to higher values compared to the other specimen.

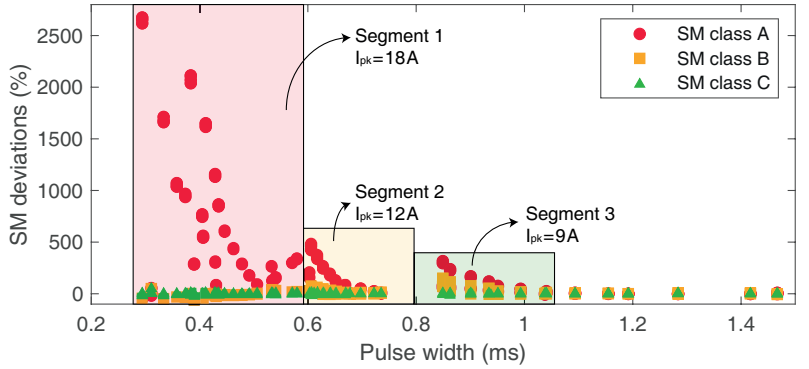

Figure 5.9. Correlation between the pulse width and the static energy meter (SM) deviations.

Third, as already noticed, when the segments indicated before are compressed, i.e. the pulse width becomes narrower, the peak value increases and higher errors are occurring, as visible in Figure 5.9. For example, the pulses in segment 1 have the highest peak value and the highest errors, but the pulse width also changes. In that sense, higher peak values are more likely to produce higher errors, but it is more complicated than that due to inter parameter dependencies.

Fourth, when the amount of charge of the pulse is decreasing the errors tend to increase, Figure 5.10, but, as we saw with the segments, the extremity

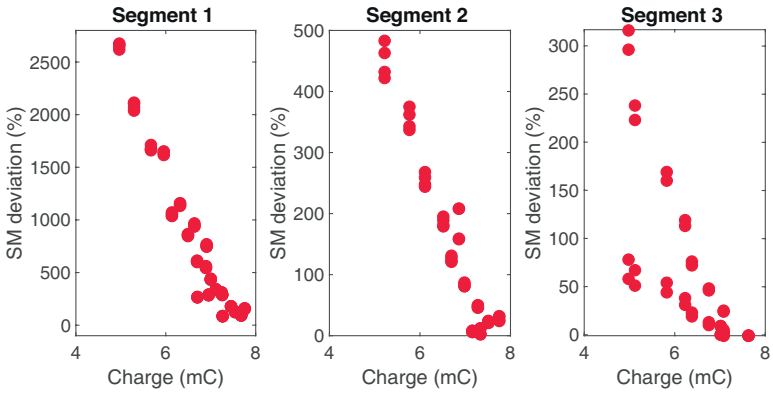

Figure 5.10. Correlation between the charge and the static energy meter (SM) deviations per segment, for SM class A.

of the error is then more dependent on the width of the pulse.

Fifth, the maximum slope in the rising part of the pulse is correlated to the errors in Figure 5.11. In this plot two curves are visible in which the errors increase with an increasing rising slope, and a part is visible containing outliers that do not seem to have a correlation with the maximum slope. For the outliers the maximum slope is very large, however the pulse width is really wide, in fact the pulse width is outside the limits of the plot in Figure 5.9. The points in segment 2 and 3 are all on curve 2, while the points in segment 1 are divided between curve 1 and 2. For the points in segment 1 the pulse width is really low, and the errors are more correlated to the decrease in charge rather than the slope, however we still see an increase in errors with the slope in curve 1 and 2 for these points.

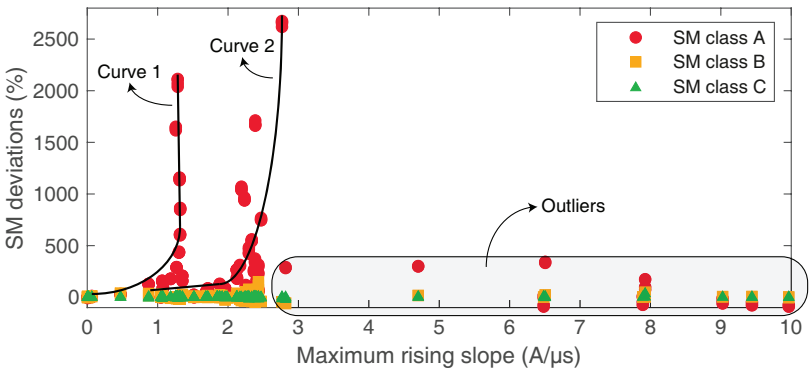

Figure 5.11. Correlation between the maximum rising slope and the static energy meter (SM) deviations.

Sixth, for the maximum falling slope, so minimum slope of the pulse, no clear relationship with the errors was found, because all the pulses had similar falling slopes.

The previously noted correlations are clearly visible for SM class A in the provided plots, and they also hold for SM class B and C. In that sense the same pulses, and thus parameters, are resulting in errors in the static energy meter readings. But depending on the SM class, and thus the current measuring element, the severity of the error is altered. However, for the meters in SM class B the static energy meter errors are mostly negative when the pulses are in segment 1, and for SM class C in all segments the errors are for the most part negative. But still the error's absolute value increases, or becomes more negative, based on the same correlated parameters discussed before.

5.6 Modelled waveform as artificial test waveform

The waveform model as described in Section 5.3 forms a simplified representation of the actual interfering current pulses as shown before in Chapter 3. The reduction of complexity is intended to minimize waveform features that are not correlated to the metering error while preserving the parameters that are relevant for estimating the impact of such interference. Here it is of interest to investigate if the modelled waveform result in similar static energy meter errors as the original waveforms, that is, to validate how well the modeled waveform represents the original waveform from the perspective of their interfering effect. In this way it can be determined whether the simplified artificial test waveforms can be included in future test standards easily.

For that purpose, the interference on static energy meters resulting from the original and modelled waveform are tested on a test-bed, that is described in more detail in [103]. Therefore, the original waveforms that are representative for the set of interfering waveforms, as visualized in Figure 5.1, are tested as well as its modelled waveforms representations in Figure 5.3. Furthermore, also an even further simplified version of the waveform is used, by reducing the number of change-points to a minimum while still preserving its trapezoidal shape. That is, for pulse 1 and 2 the change-points are reduced to four and six, respectively. This simplification is visualized in Figure 5.12. The static energy meter errors resulting from these interfering pulses are determined using (5.13). And the results are presented in Table 5.1. The artificial waveforms seem to cause static energy meter errors that are similar to the errors obtained when using the original real-world waveform themselves. This proves that the simplifications made for obtaining the modelled waveform still contain the relevant critical features of the original waveform. And makes the modelled (as well as the trapezoidal) waveforms suitable for use in future test procedures.

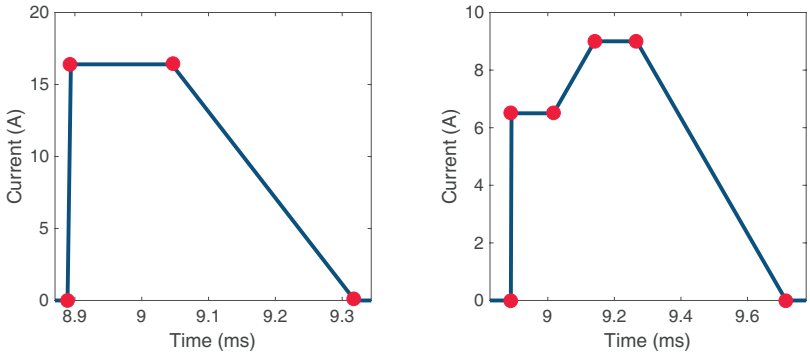

(a) Pulse 1 (b) Pulse 2

Figure 5.12. Simplified trapezoidal waveforms that are used as artificial waveforms for static energy meters, as obtained from Figure 5.3 by reducing the number of change-points.

Table 5.1. Static energy meter (SM) errors for the artificial waveforms.

Signal	**Type**	$\mathbf{P}_{\mathrm{ref}}$	**SM1**	**SM2**	**SM3**	**SM4**
Pulse 1	Original	29 W	6 %	2527 %	1 %	1961 %
Pulse 1	Modelled	28 W	6 %	2565 %	2 %	1998 %
Pulse 1	Trapezoidal	23 W	5 %	3234 %	3 %	2520 %
Pulse 2	Original	28 W	8 %	968 %	1 %	334 %
Pulse 2	Modelled	27 W	8 %	974 %	1 %	342 %
Pulse 2	Trapezoidal	19 W	6 %	1377 %	3 %	525 %

5.7 Wavelet-based representation of waveforms for type-testing

Research in Chapter 3 has shown that the EMI on static energy meters is caused by pulsed current waveforms. And in Section 5.1 it was observed that the interference signals can be described using a trapezoidal pulse. Therefore, the waveform model as presented in this chapter is based on that ascertainment. However, the modelled waveform is quite limited to this type of trapezoidal waveform. Therefore, an alternative method was also considered for the description of the interference waveforms that is based on a wavelet-based representation. In that sense, such wavelet-based representations are more suitable when also other non-trapezoidal pulses are considered. Still, the aim of this alternative method is to describe the pulsed waveforms that resulted in static energy meter errors using a frequency-domain approach that only requires a few coefficients.

Many frequency-domain and hybrid time-frequency-domain techniques have been used in the literature to analyse power systems signals, including short-time Fourier transform [110], S-transform [111], and wavelet packet transform

[112]. However, for our purpose, the waveform's information should be handled in an easy and compact fashion, rather than to provide a useful analysis or insight into the signals. The work in [113] presents a comprehensive review of the state of the art of compression techniques for electric signals. One clear trend is that electric signals are mainly composed by a steady-state sinusoidal part and transients impulses (or high frequency oscillations). The former are well described by discrete Fourier transform methods, while the latter are not. The great suitability of wavelet transforms for compressing transients and pulses is well recognised, thanks to their good localisation in frequency and time, and to the capability of concentrating a great share of the signal information in very few coefficients [114]. Therefore, following up on the study performed in [115] the discrete wavelet transform (DWT) is chosen for the present application, proving to be effective and efficient for the task.

The theoretical background and implementation of a wavelet-based algorithm for describing the interference signals is described in detail in [104]. A DWT is based on a basic function (mother wavelet) that determines the characteristics of the transform, i.e. the basic function can be regarded as the impulse response. In order to select a suitable configuration of mother wavelet and number of decomposition levels, an extensive study has been carried out, considering the reconstruction performance of several wavelet configurations. The Daubechies wavelet with two vanishing moments ($db2$) and 7 levels of decomposition is selected. Furthermore, it was already proven to be suitable for describing impulsive waveforms resulting in static energy meter interference in [116].

In order to validate the wavelet-based representation, it is tested experimentally on the same testbed as was used in the previous section, and is described in more detail in [103]. This is done by verifying that the reconstructed waveforms can effectively reproduce the same level of static energy meter error as the original ones, i.e. they preserve the error-inducing features. And similar to the previous measurements the static energy meter errors resulting from these interfering pulses are determined using (5.13). Four test waveforms are selected from the interfering cases in Chapter 3. Waveform 1 to 4 represent the water pump at level 1 from Section 3.3.1, that use the standardized mains grid, low impedance grid, high impedance grid, and the building's mains supply, respectively. For each test waveform, four wavelet-based representations have been used in the validation in order to test the sensitivity of the static energy meter error to different compression ratios resulting from reconstruction using 100, 50, 20 and 10 coefficients. A static energy meter of which it was known that it is not immune to the interfering pulsed waveforms was selected for the validation. Table 5.2 shows the resulting static energy meter errors for the different compression ratios used. It can be observed that the waveforms reconstructed using only 10 coefficients are not always sufficiently accurate to preserve the error-inducing features. This is the case for waveform 3, where the error reduces from 259% to -6%. However, all the performed tests indicate that a reconstruction with 20 coefficients (i.e. 0.1% of the total number of

coefficients) can produce waveforms that reproduce the error-inducing features with sufficient accuracy.

Table 5.2. Static energy meter errors for the wavelet-based waveforms for different compression ratios, i.e. different wavelet coefficients.

Wavelet coefficients	**Waveforms**			
	1	**2**	**3**	**4**
Original	409 %	2190 %	259 %	2279 %
100	398 %	2182 %	256 %	2265 %
50	411 %	2230 %	262 %	2283 %
20	420 %	2249 %	251 %	2307 %
10	380 %	2048 %	-6 %	2388 %

5.8 Discussion and conclusion

In this chapter a parametric waveform model is shown which provides a simplified description of complex non-linear waveforms. And it allows to describe the interference waveform by a limited amount of data-points instead of a highly sampled complex waveform. The identification of critical parameters has shown that erroneous waveforms are in general narrow, fast rising, pulses, where, on average, higher crest factor, narrower pulse width, higher peak amplitude, less charge, and higher slopes, will contribute to an increase in the metering error. The critical ranges of these time-domain parameters are shown in Table 5.3.

Table 5.3. Critical ranges of time-domain parameters found to result in interference of static energy meters.

Parameter	**Critical range**
Charge	4-8 mC
Crest factor	> 5
Pulse width	0.2-1.2 ms
Rising slope	> 0.1 A/µs

Furthermore, it was found that the maximum value of the static energy meter errors is related to the current metering element. In that sense, the Rogowski coil contributes to the highest errors, followed by the current transformer principle, while using a shunt resistor or Hall effect sensor result in most cases in lower energy reading of the static energy meter.

The use of the modelled waveform for future standards is validated in an arbitrary-waveform testbed, and this showed meter reading errors similar to those caused by the original real-life waveforms. When reducing the complexity even further, by removing change-points to get a trapezoidal waveform, still similar errors are found. This shows that these simplified artificial waveforms

are suitable candidates for improved standardization of static energy meter testing.

Alternatively, also the wavelet-based representation has shown to be an useful method for representing the original interference waveforms in a simplified fashion for type-testing. A laboratory experiment using a real static energy meter has validated the technique, showing that a reduction from thousands of coefficients to only few tens is sufficient to reproduce the error levels observed in static energy meters with good accordance to the errors produced by the original error-inducing waveforms. Still, understanding the interference waveforms is way easier and straightforward using the waveform modelling approach in time-domain compared with the wavelet-based representation. For which the correct understanding of the test waveforms requires the knowledge of the underlying mathematical theory. Also, this makes it harder to tweak or change certain parameters of such wavelet-based test signal by an engineer. Whereas, changing the slope of a modelled pulsed representation to find the limits of a certain system (e.g. the static energy meter) is more straightforward.

Following up on the waveform model as shown in this chapter, the parameters that found to be critical in relation to the static energy meters, as shown in Table 5.3, are compared to the emissions of equipment that is present in typical residential situations in Chapter 6. Next to that, in Chapter 7 the critical parameters are compared with measured data at the meter connection point of a couple of test sites, so covering realistic on-site waveforms from the low-voltage grid.

Chapter 6

Emissions of equipment in low-voltage networks

This chapter presents a survey of the time-domain emissions generated by equipment that is present in residential low-voltage networks. The content of this chapter comprises the research that was earlier published in [117], [118].

6.1 Motivation

In low-voltage networks there is an increased use of equipment with a non-linear behavior compared to traditional linear equipment, which resulted in several conducted EMI cases [9]. For example, EMI cases involving static energy meters are presented in Chapter 3, that resulted from pulsed currents. The critical parameter ranges of those critical currents are obtained in Chapter 5, and are shown in Table 5.3. Other EMI problems may arise in PLC [119], where the current pulse duration affects the communication [15]. Therefore, it is useful to research the emissions generated by equipment that is present in residential low-voltage networks. And focus explicitly on the analysis of those waveforms in the time-domain, as extreme time-domain parameters correlated to the metering errors before.

A study of the harmonics generated by household appliances is provided in [120], which focuses on the harmonics until 2.5 kHz (50th harmonic), instead of the frequency range till 150 kHz, which is of interest for conducted EMI problems, as there is a lack of civil standards in this frequency range, as is clear from Chapter 2.

Next to the emissions from household appliances in general, the EMI from lighting equipment is of particular relevance to investigate, as 15% of the global energy consumption is generated by lighting equipment [121]. And those emissions are one of the major causes of EMI on static energy meters [31]. Previous research on the high emissions of lighting equipment focuses on the harmonic emissions instead of the time-domain EMI [122]. Furthermore, it was shown

that grid impedance affects these emissions [123]. Next to the introduction of LED technology that allows energy efficient lighting, dimmers can alter the ambience to a desired level and reduce the consumed energy even more. Dimmers are of interest as there is a lack of applicable emission limits for dimmers in the IEC 61000-3-2 [44].

In this chapter, the extent of EMI to which static energy meters are exposed to is investigated by the analysis of an extensive survey of current waveforms drawn by typical household equipment. Furthermore, a special focus is put on the emissions from dimmed lighting equipment in various realistic on-site situations. In this way, the existence of equipment with critical time-domain parameters related to the interference of static energy meters is researched. This is done using a time-domain EMI approach [124], capable of synchronous multi-channel measurements [125]. These waveforms are analyzed in the time-domain using a parametric model as described in the previous chapter. And a statistical overview is presented dividing equipment per category according to the IEC 61000-3-2 [44]. In the end the results are compared to critical waveforms that resulted in static energy meter interference.

This chapter is organized as follows: First, Section 6.2 covers the measurement method that is used to measure the emissions of the surveyed equipment in time-domain. Second, Section 6.3 shows the emissions obtained from dimmed lighting equipment using different technologies. Third, in Section 6.4 a survey of the emissions from equipment in low-voltage networks is presented in time-domain. Finally, Section 6.5 concludes this chapter.

6.2 Method

This section covers the method that was used for obtaining the emissions of different equipment. First, the measurement setup is explained. Second, the post-processing algorithms are explained.

6.2.1 Measurement setup

To cover a large variety of equipment, measurements were performed at different residential locations. The survey on the dimmed lighting equipment in Section 6.3 was performed using the buildings mains supply of the laboratory. And the survey on the emissions of different equipment in Section 6.4 covers several different locations: an office environment, a hardware store, several residential premises, and at a boiler manufacturer, all throughout The Netherlands. During the measurements the mains supply of the test location was used. These might differ slightly from each other, which portrays the realistic on-site environment where the static energy meter is located and is therefore not a problem. After the mains plug a breakout box was connected, such that the currents and voltage can be measured safely according to Figure 6.1, followed by a connection point for the measured equipment, Figure 6.2. The voltage and currents are measured synchronously using a multi-channel time-domain

EMI approach [125]. Pico Technology current probes TA189 within 0.5 dB in the frequency range up to 200 kHz, calibrated according to the time-domain method in Chapter 4, and a Pico Technology TA043 differential voltage probe with a frequency range up to 100 MHz, are used and these were connected to a Picoscope pc-based oscilloscope. At least ten cycles at mains frequency were captured, which is equivalent to 200 ms, in accordance with IEC 61000-4-30 [84], and a sampling frequency of at least 1 MS/s was used.

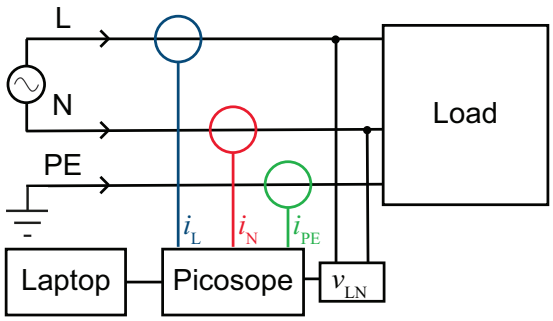

Figure 6.1. Schematic overview of the measurement setup.

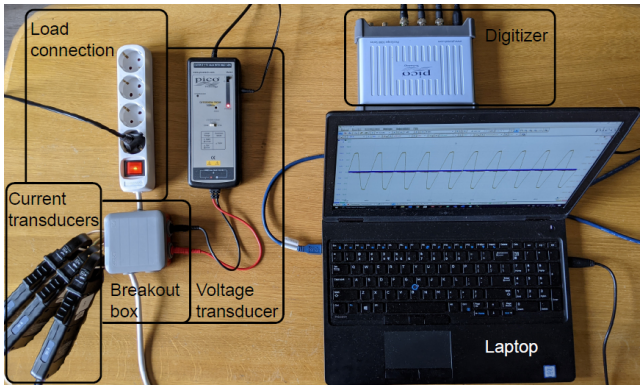

Figure 6.2. Measurement setup.

6.2.2 Post-processing

The captured waveforms were post-processed to obtain the time-domain parameters: charge, crest factor, peak value, pulse duration and rising slope, using the parametric model as described in Chapter 5. Also the active power of the waveform was determined. Furthermore, the frequency-domain representation was determined using a FFT, to visualize the time and frequency-domain simultaneously [126]. For the results in Section 6.4, the parameters are presented

statistically using the Turkey's boxplot method [127], which visually summarizes the data using the following components: the median (Q2), the lower (Q1) and upper (Q3) quartile, the minimum (min), and maximum (max). Points that have a value of 1.5 times the interquartile range from the median are marked as outliers and are visible with a dot in the presented graphs. In this way the survey will provide a statistical overview of currents from equipment used under real operating conditions.

6.3 Dimmed lighting equipment

This section shows the emissions of different dimming principles combined with different light equipment, including linear and non-linear luminaries, and discusses them.

6.3.1 Description of the loads

Lighting equipment of different technologies is used: a halogen lamp, a dimmable LED, and a non-dimmable LED. By using both the dimmable and non-dimmable LED the dimmers are tested inside and outside its intended use. The associated waveforms and characteristics of these luminaries are shown in Figure 6.3 and Table 6.1, respectively. It is remarkable to notice that the non-dimmable LED produces a uni-polar waveform. Furthermore, the dimmable LED has a lower peak value, longer pulse duration, and slower inclining slope compared to the non-dimmable LED. Then, two COTS dimmers are used to control the intensity of the connected lamps. One uses the TRIAC principle for dimming and is a rising edge dimmer, and the other uses a metal-oxide-semiconductor field-effect transistor (MOSFET) for switching, and can be set to rising or falling edge dimming manually. This means that a total of three dimming situations is realized by these dimmers.

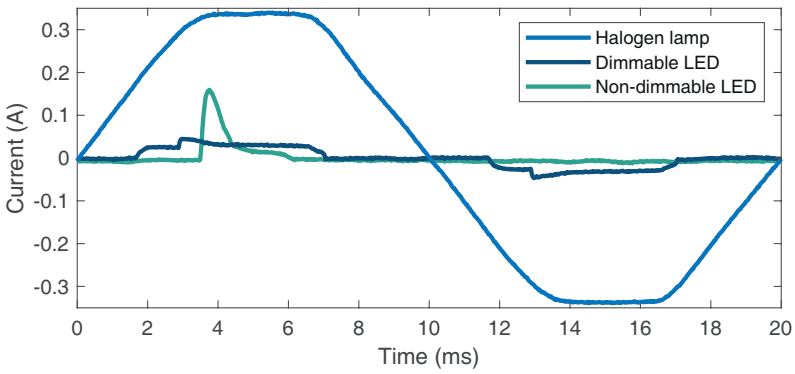

Figure 6.3. Time-domain emissions of the (undimmed) lighting equipment.

Table 6.1. Time-domain parameters of the lighting equipment in combination with dimming equipment.

Lighting equipment	**Number of luminaries**	**Dimming equipment**	**Type of dimming**	**Power (W)**	**Charge (mC)**	**Crest factor**	**Peak value (A)**	**Pulse duration (ms)**	**Slope (A/ms)**
Halogen	1	-	-	57.5	2.1	1.4	0.34	10	0.1
Dimmable LED	1	-	-	4.7	0.2	2.9	0.05	7.1	0.4
Non-dimmable LED	1	-	-	2.2	0.2	5.6	0.16	2.5	1.1
Halogen	1	TRIAC	Rising edge	11.2	0.6	6.1	0.62	3.0	14.8
Halogen	1	MOSFET	Rising edge	11.6	0.7	4.6	0.46	2.9	8.1
Halogen	1	MOSFET	Falling edge	10.5	0.6	4.6	0.44	3.1	5.6
Dimmable LED	10	TRIAC	Rising edge	8.3	0.4	11.5	1.64	0.5	19.9
Non-dimmable LED	10	TRIAC	Rising edge	18.0	7.1	8.9	15.22	1.8	243.8
Dimmable LED	10	MOSFET	Rising edge	8.7	0.4	11.2	1.48	0.5	21.5
Non-dimmable LED	10	MOSFET	Rising edge	24.8	2.3	8.5	6.17	0.8	31.5
Dimmable LED	10	MOSFET	Falling edge	7.1	0.4	6.3	0.42	1.7	4.4
Non-dimmable LED	10	MOSFET	Falling edge	19.1	1.6	7.0	3.16	0.9	20.7

6.3.2 Dimming principles with linear load

First, the basic functioning principles of the dimmers are exemplified using the linear halogen lamp. The rising edge dimming, using either the TRIAC or MOSFET based dimmer, cuts out the first part of the sine wave, as is shown in Figure 6.4(a) and Figure 6.4(b). It can be seen that the TRIAC dimmer results in an overshoot when the halogen lamp starts drawing current. Alternatively, the falling edge dimming cuts out the second part of the sine wave, as is shown in Figure 6.4(c). In all dimming situations the dimmer is set to the most dimmed setting. The time-domain parameters of the dimmed halogen lamp are shown in Table 6.1. The overshoot of the TRIAC based dimmer results in a larger peak value and consequently a larger maximum slope. This shows that the MOSFET based dimmer reduces the noise and EMI compared to the TRIAC dimmer. For the MOSFET based dimmer comparable parameters are found for the rising and falling edge dimming principle, although the absolute slope is slightly higher when using rising edge dimming. So the MOSFET based falling edge dimmer reduces the EMI even further.

6.3.3 TRIAC based rising edge dimmer with non-linear load

Second, the TRIAC based rising edge dimmer is used with the non-linear LEDs. Here ten luminaries are used to operate the dimmer inside its advised operating power range. The time-domain emissions are plotted in Figure 6.5, and the corresponding parameters are shown in Table 6.1. The non-dimmable LED has a significant larger peak value, pulse duration, and slope compared to the dimmable LED. For the non-dimmable LED almost no light intensity change was observed when dimming the lamp. The switch mode power supply of the non-dimmable LED uses a large capacitor, in the small time interval allowed by the dimmer to draw current, the capacitor is charging fast and provides enough charge to light up the lamp. This explains the resulting extreme pulsed current drawn by the non-dimmable LED. It is remarkable that the emissions from the dimmable and non-dimmable LED have a different phase firing angle. For the dimmable LED the intensity of the lamp is decreasing and consequently less power and charge is drawn. Still, when dimming the lamp a more pulsed current is drawn, as the crest factor and peak value increase, whereas the pulse duration decreases compared with the undimmed lamp.

6.3.4 MOSFET based rising edge dimmer with non-linear load

Third, the emissions of the non-linear LEDs in combination with the MOSFET based rising edge dimmer are measured. Again ten luminaries are used to operate the dimmer inside its advised operating power range. The waveforms are shown in Figure 6.6 and the time-domain parameters are shown in Table 6.1. In this case the pulsed currents of both LEDs have a similar phase firing angle. For the dimmable LED comparable time-domain parameters are found, although the slope is slightly higher. This is remarkable as the MOSFET

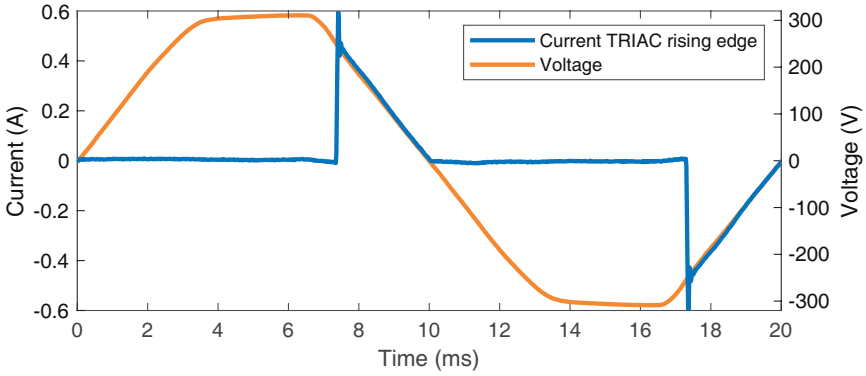

(a) TRIAC

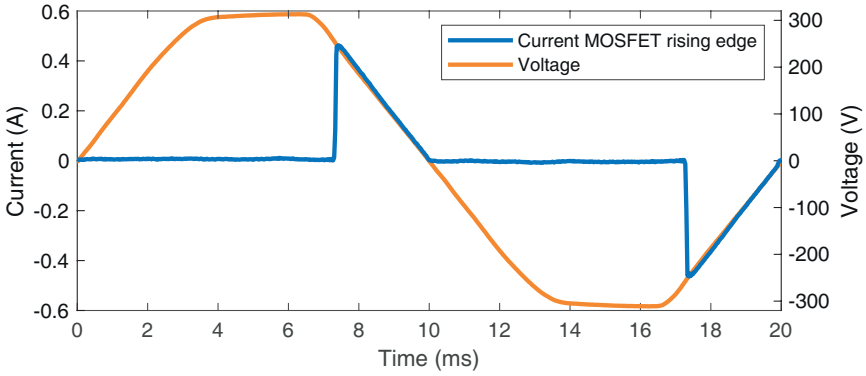

(b) Rising edge

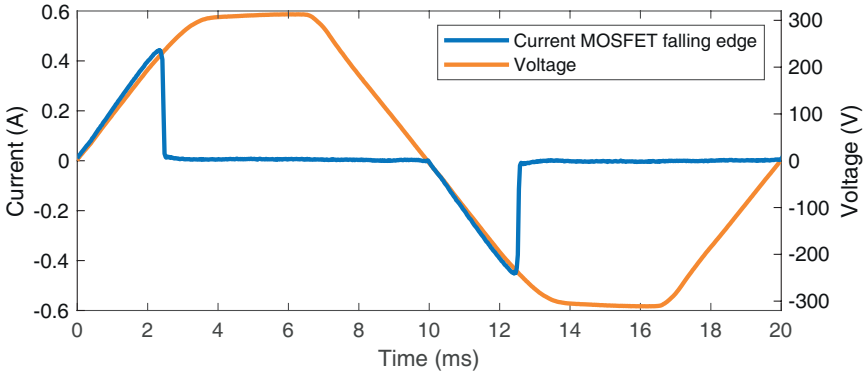

(c) Falling edge

Figure 6.4. Dimming principles exemplified with a (linear) halogen lamp.

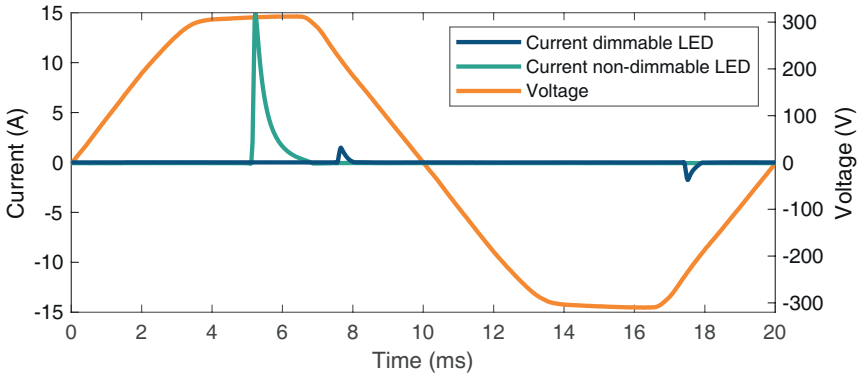

Figure 6.5. Time-domain emissions of the TRIAC based rising edge dimmer.

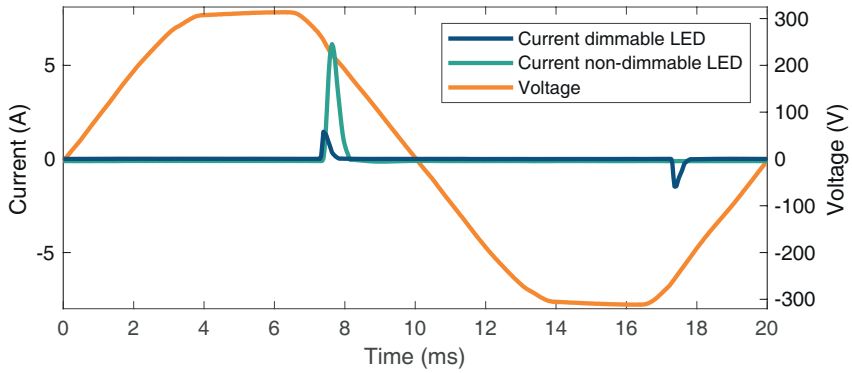

Figure 6.6. Time-domain emissions of the MOSFET based rising edge dimmer.

based dimmer did reduce the time-domain parameters and thus the emissions for the halogen lamp. For the non-dimmable LED the peak value decreased drastically, but also in this case the slope was higher compared to the TRIAC based rising edge dimmer. This shows that the non-linear LEDs are affected differently compared to the halogen lamp.

6.3.5 MOSFET based falling edge dimmer with non-linear load

Fourth, the MOSFET dimmer is set to operate as falling edge dimmer and is combined with the non-linear LEDs. Once more, ten luminaries are used to operate the dimmer inside its advised operating power range. In Figure 6.7 and Table 6.1 the waveforms and parameters are shown, respectively. For the dimmable LED the pulse duration is significantly larger compared to the previous situations, also the peak value and slope are reduced. As a result the

crest factor is also lower, while the power and charge are still comparable. For the non-dimmable LED also the peak value is reduced, still the pulse duration is comparable. The slope did reduce slightly compared to the previous situations. The steepest absolute slopes were measured in the falling part of the pulse, this shows that the fast charging of the capacitor in the LED driver is less of an issue when using the falling edge dimming principle. For both LEDs the emissions did reduce significantly for the MOSFET based falling edge dimmer. So the MOSFET based falling edge dimmer can be considered as the best dimming principle in terms of conducted EMI.

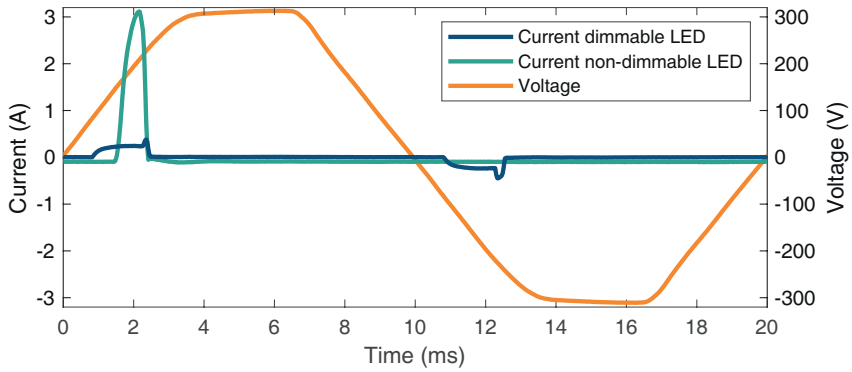

Figure 6.7. Time-domain emissions of the MOSFET based falling edge dimmer.

6.3.6 Frequency-domain analysis

Fifth, the frequency-domain representation of the dimmable LED combined with the rising and falling edge MOSFET based dimmer is shown in Figure 6.8. The TRIAC based dimmer is not shown as the time-domain analysis showed a similar result compared to the rising edge MOSFET based dimmer. As was already observed in the time-domain analysis, the emissions are lower when the falling edge dimmer is used. Because the active power is lower than 25 W and a plug-in dimmer is added, no emission limits apply for this lighting equipment according to the IEC 61000-3-2 [44], however the harmonic frequency content is significantly large. This is exemplified by a comparison with the limits of a 25 W luminary, which has a significantly higher 50 Hz component of 0.1 A. However the harmonic frequency components of the dimmable LED exceed these limits, as is visible in Figure 6.8. This shows that a dimmed LED has significant harmonic emissions that might cause interference problems in low-voltage grids.

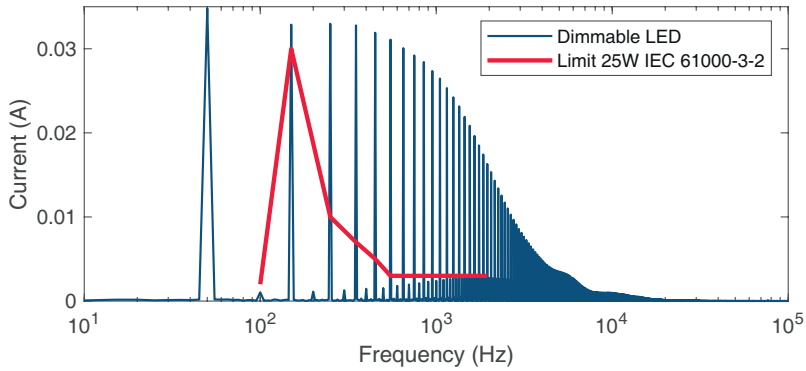

(a) Rising edge

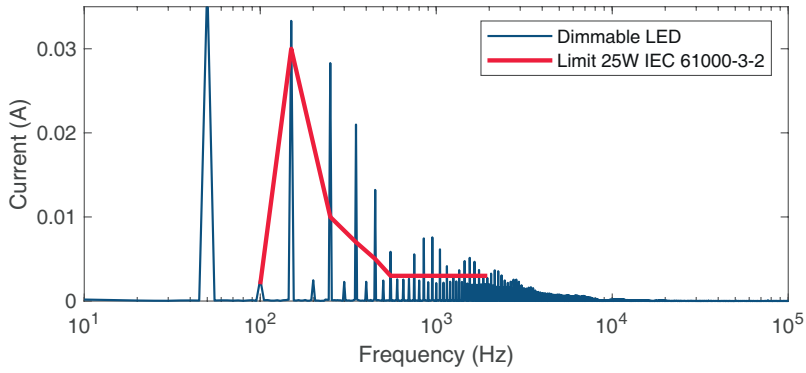

(b) Falling edge

Figure 6.8. Frequency-domain plot of dimmable LED with MOSFET based dimmer.

6.4 Statistical equipment survey

Next, in this section a survey is performed on the time-domain emissions of a large variety of typical household equipment. To investigate to what extend the observed critical non-linear waveform parameters, as found in Chapter 5, are present in the currents in realistic on-site equipment.

6.4.1 Different categories of equipment

The variety of equipment surveyed is subdivided into different categories according to the IEC 61000-3-2 [44]. This standard specifies the limitations of harmonic currents injected into the public low-voltage network for equipment with a rated current up to 16 A. The four categories have different emission limits, and are listed below:

- Class A: normal usage:

  - Household appliances.
- Class B: very short usage:
  - Portable tools.
- Class C: continuous usage:
  - Lighting equipment.
- Class D: normal usage, but special current waveform:
  - E.g. personal computers, monitors and receivers.

For equipment with a rated power of 75 W or less, other than lighting equipment, no emission limits apply. This equipment is of particular interest, because the waveforms that result in metering errors also have a low power consumption. This equipment is treated as Class A, B, C, or D depending on its usage. In addition, when combining a plug-in dimmer with (a series) of lighting equipment no emission limits are applicable, and a combination could generate highly distorted currents, that might result in metering errors [31]. Such combinations are treated as Class C equipment when found in a real-world situation. Further, the performance of equipment that is used (or installed) for a longer period may reduce because of ageing of electrical components [14], this might effect the current emissions. For example, ageing of the built-in electrolytic capacitors for voltage smoothing due to its non-linear behavior [128]. Therefore, we focus on installed equipment rather than brand new equipment, which also corresponds to its use in an everyday household situation.

6.4.2 Results

During the survey a total of 484 different equipment situations are measured, where Table 6.2 provides an overview of the surveyed equipment per category, and the number of appliances with critical parameters according to Table 5.3. A statistical overview of the charge, crest factor, and peak value is given in Table 6.3, the parameters inside the critical ranges are highlighted in red. A detailed visualization of the pulse duration and rising slope is given in Figure 6.9, as those parameters are found to be more critical in Chapter 5, the critical range is indicated in red. And 43% of the equipment contains critical parameters. For the slope especially, several outliers, with a high slope in the critical range, are found in all categories.

For the equipment surveyed in Class A (normal usage household appliances) 29% was linear equipment, where in some of these cases the current was phase shifted with respect to the voltage, which will contribute to the reactive power in the circuit. All this linear equipment did not include critical parameters. For the non-linear equipment in Class A, in a couple of cases the slope is higher than 0.1 A/µs, which resulted from a phone charger, washing machine and speed controlled water pump. For the phone charger the other parameters

Table 6.2. Overview of different surveyed equipment and equipment containing critical parameters, per category according to IEC 61000-3-2[44].

Category	**Surveyed equipment**	**Critical equipment**
Class A	300	124
Class B	81	9
Class C	68	57
Class D	35	16

Table 6.3. Statistical overview of the charge, crest factor, and peak value of the surveyed equipment.

#	**Charge (mC)**				
	Min	Q1	Q2	Q3	Max
A	$2.4{\cdot}10^{-4}$	$6.2{\cdot}10^{-2}$	$2.0{\cdot}10^{-1}$	$5.1{\cdot}10^{-1}$	34.6
B	$3.8{\cdot}10^{-5}$	$6.4{\cdot}10^{-1}$	1.6	3.4	24.2
C	$4.8{\cdot}10^{-5}$	$2.3{\cdot}10^{-2}$	$6.0{\cdot}10^{-2}$	$2.0{\cdot}10^{-1}$	2.6
D	$1.4{\cdot}10^{-3}$	$3.6{\cdot}10^{-2}$	$1.4{\cdot}10^{-1}$	$2.7{\cdot}10^{-1}$	$6.6{\cdot}10^{-1}$

#	**Crest factor**				
	Min	Q1	Q2	Q3	Max
A	1.7	3.1	4.2	6.2	52.5
B	1.7	2.2	3.1	3.4	21.7
C	2.6	5.4	6.5	9.6	37.7
D	2.8	3.6	4.7	6.5	38.0

#	**Crest factor**				
	Min	Q1	Q2	Q3	Max
A	$2.3{\cdot}10^{-3}$	$9.3{\cdot}10^{-2}$	$4.6{\cdot}10^{-1}$	$9.1{\cdot}10^{-1}$	17.5
B	$6.4{\cdot}10^{-3}$	$4.4{\cdot}10^{-1}$	$8.2{\cdot}10^{-1}$	2.7	11.0
C	$5.3{\cdot}10^{-3}$	$9.5{\cdot}10^{-2}$	$1.9{\cdot}10^{-1}$	$8.5{\cdot}10^{-1}$	13.3
D	$3.6{\cdot}10^{-2}$	$1.2{\cdot}10^{-1}$	$2.0{\cdot}10^{-1}$	$3.8{\cdot}10^{-1}$	1.2

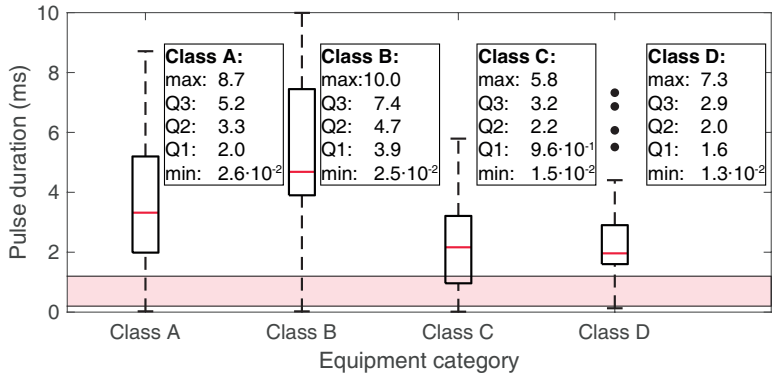

(a) Pulse duration

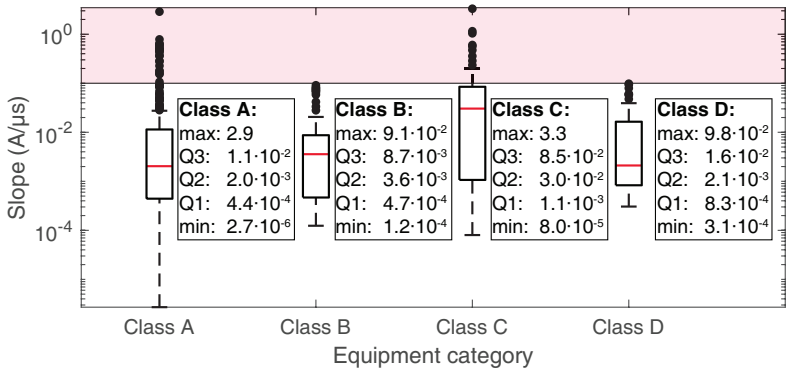

(b) Rising slope

Figure 6.9. Statistical overview of the pulse duration and rising slope of the surveyed equipment.

were far outside the critical ranges, as the pulse had a low peak value and charge. The pulse of the washing machine was quite significant, Figure 6.10, and the crest factor and slope are inside the critical range related to known static energy meter interference. The extremity of the time-domain emission of the water pump and the resulting existence of static energy meter interference was already shown in Chapter 3.

The waveforms generated by portable tools in Class B contain a lot of charge compared to the other categories, and as a result consume more power. Consequently, the median peak value is higher and the pulses are usually wider in comparison with the other categories. Due to this higher pulse duration, the crest factor of these waveforms is lower. Also no slopes in the critical region were found.

The lighting equipment in Class C has slopes inside the critical range which mostly occur in combinations with dimmers. Cases with narrow pulses with a

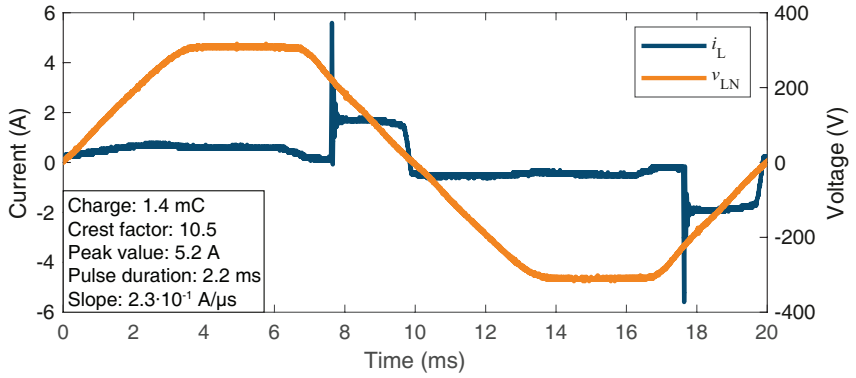

Figure 6.10. Waveforms resulting from a washing machine.

peak value above 1 A and a comparable wave-shape to the waveforms resulting in static energy meter interference in [31] were found. Furthermore, a case occurred in which transient pulses occur in dimmed lighting equipment, these have a very short pulse width and high slope, Figure 6.11. The peak value and therefore also the charge however are low, making their influence on the meter readings questionable. However, Chapter 3 has also shown the existence of transients in dimmed lighting equipment resulting in static energy meter interference, but those transients had a 50 times higher peak value.

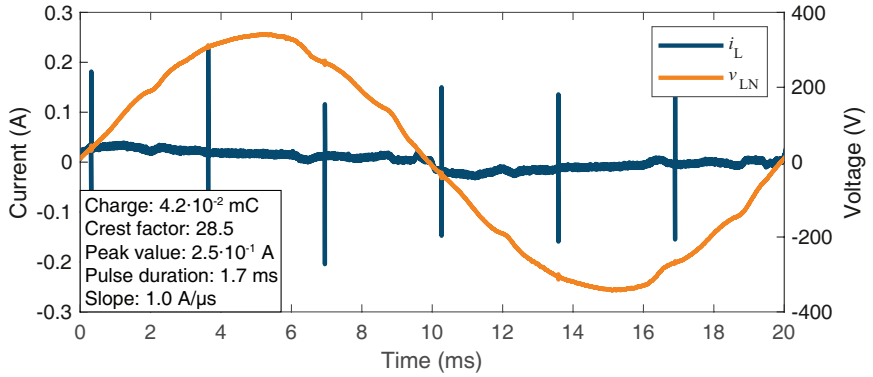

Figure 6.11. Waveforms resulting from dimmed light equipment.

For the equipment in Class D the crest factor indicates the existence of highly non-linear waveforms. However, this equipment has a lower power consumption, indicated by a low charge value, and also the max peak values are low compared to the other categories. Furthermore, no extreme slopes in the critical range are found.

The presented survey evidences the existence of equipment with a non-linear

behavior including parameters that could be critical in relation to static energy meter interference. Therefore, a realistic system that is combining these non-linearities could exceed the test signals immunity standards as the IEC 61000-4-19 [29] envisions. Such tests are only valid if the system can be considered as LTI, however as the results show, this is clearly not the case, this issue was already pointed out in Chapter 2.

6.5 Discussion and conclusion

The study on the emissions of (household) equipment, as presented in this chapter, has shown that many of the current waveforms are non-linear and contain time-domain parameters similar to the interference cases. First, the emissions of three different dimmer technologies combined with lighting equipment are analyzed. Both time- and frequency-domain analysis show the presence of pulsed currents with extreme emissions that could cause EMI problems in low-voltage grids. It was found that the MOSFET based falling edge dimmer has the lowest conducted emissions. As the time-domain parameters of the drawn waveforms were significant lower compared to rising edge dimmers that used the TRIAC or MOSFET for switching. For the TRIAC a large overshoot was observed with a linear halogen lamp which was not occurring with the MOSFET. However, for the non-linear dimmable LED similar emissions were found for the TRIAC and MOSFET when those are set to rising edge dimming.

The emissions generated by dimming equipment could result in serious EMC problems in residential (and also industrial) premises. As no regulations are applicable for dimmers, as was already shown in Chapter 2, which is explicitly true for plug-in dimmers that are sold independently from the luminaries. As in that case it is a stand alone product to which (almost) no standards apply. The types of luminaries to be used in conjunction with the dimmer is (mostly) specified or advised by the manufacturer, however it is not possible to control the situation a consumer uses the dimmer with in practice. Either due to lack of knowledge or laziness of the consumer/seller. As the lamp might work, i.e. gives light, but consequently creating a pulsed current that might harm other equipment (which could be the static energy meter).

Second, the equipment survey has shown that 43% of the equipment has parameters inside the critical range related to possible static energy meter interference. Where the critical parameters are based on the analysis of waveforms interfering with static energy meters in Chapter 5. In the majority of cases, that were surveyed, the equipment is non-linear. This indicates the wide variety of non-linear waveforms that are present in a residential environment where the static energy meter is placed in. And shows the large extent of the metering problem. Thus a realistic system that uses a static energy meter is combining these non-linearities and could exceed the test limits immunity standards such as the IEC 61000-4-19 poses, as were earlier mentioned in Chapter 2. Thus the present test standards are not representative for the realistic on-site situation.

The survey showed waveforms with fast inclining slopes above 0.1 A/µs,

which resulted from a phone charger, lighting equipment with dimmers, a washing machine and a speed controlled water pump. Both the washing machine and speed controlled water pump showed several parameters inside the critical range related to static energy meter interference. The power consumption of the charger however was low, resulting in low peak values compared to the others. For the lighting equipment both waveforms with fast rising narrow pulses and high peak values, as well as waveforms including small transients with low charge and peak values were observed. Equipment categorized as portable tools in Class B consume in general more power, which results in a higher peak value and wider pulse compared to other equipment. Monitors and computer equipment in Class D on the other hand have a low power consumption, resulting in a low charge and peak value.

In the remainder of this thesis, the study on real-world waveforms to which the static energy meters are exposed is extended. This is done by measuring the waveforms at the meter connection point in Chapter 7. So looking at the complete residential system, rather than the emissions of individual household equipment.

Chapter 7

Waveforms at the meter connection point

A study on the current waveforms that are typically occurring at meter connection points, and thus featuring an on-site situation where the static energy meter is installed, is presented in this chapter. The content of this chapter comprises the research that was earlier published in [107], [129].

7.1 Motivation

The extent of the interference cases involving static energy meters is unknown, because there is limited information about the waveforms drawn in household situations. Therefore, it is of interest to indicate the occurrence of pulsed waveforms resulting in interference in real situations, that are similar to the interference waveforms in Chapter 3. Which are narrow, fast rising current pulses, where a higher crest factor, narrower pulse width, less charge, and a higher slope, are the factors that contribute most to an increase in the interference, as was evidenced in Chapter 5. And the critical ranges of these time-domain parameters are shown in Table 5.3. The existence of non-linearities that are occurring in low-voltage grids was shown in [52]. It shows, among others, short-duration spikes, oscillations related to the switching frequency of the power electronics, and voltage distortion. In [105], the existence of current waveforms with fast inclining slopes that occur in low-voltage customer terminals are shown. Moreover, within the framework of the MeterEMI project [43] surveys are performed in modern low-voltage networks, including networks with EV charging stations [106], and PV installations [107]. To cover the emissions of modern equipment that includes power electronic converters and that are increasingly used in nowadays low-voltage network. It was found that the on-site surveyed waveforms are typically a superposition of the fundamental frequency, other frequency components including pulses and low amplitude random noise. This makes it complex to analyze the parameters of the pulses included in such

signals, and to correlate them to static energy meter interference.

This chapter aims to detect the critical current waveforms in relation to interference of static energy meters that occur in a large set of on-site surveyed data. This is achieved by comparing the on-site waveforms with a reference data set including the parameters that were found to be critical in laboratory experiments. For this purpose, the on-site waveforms with an unknown metering error are processed to extract their relevant waveform parameters, and then, the error is estimated using an interpolation function. This provides a tool for objectively and automatically selecting those on-site waveforms with similar time-domain characteristics as those from the reference data set. Considering that similar critical waveforms result in comparable mean errors, this approach is expected to effectively identify which of such surveyed waveforms could induce static energy meter interference.

The rest of this article is organized as follows: Section 7.2 describes the parametric waveform model for the characterization of pulses in on-site waveforms. Section 7.3 describes and validates the approach to estimate the interference. Section 7.4 describes the measurement method used to survey on-site current waveforms. In Section 7.5, the results of the survey are presented, showing a statistical overview of the parameters encountered at the on-site, and the estimated static energy meter errors of such waveforms based on the introduced estimator. Finally, Section 7.6 discusses and concludes these findings.

7.2 Parametric waveform model for the characterization of pulses in on-site waveforms

The waveforms measured in on-site situations are a superposition of different signals consisting of a combination of linear (resistive) and non-linear loads, and noise. The aim of this model is to characterize the pulsed part of such waveforms in a simplified manner, as the pulsed parts are correlated to static energy meter interference in Chapter 5. Therefore, in post-processing, the pulsed and linear parts are separated using a mains frequency filter, after which the time-domain characteristics are determined using the parametric waveform model introduced in Chapter 5. The filter makes the model more robust to noise as well as to the presence of non-impulsive current components.

7.2.1 Filtering out the mains frequency

The mains (fundamental) frequency is removed from the measured signal, because it does not cause metering errors and it simplifies the waveform by retaining the pulsed part that could be correlated to the interference. Furthermore, conventional tools for determining time-domain parameters use 10-90% state levels [85] which will also take the fundamental frequency into account. The spectrum of the waveform is calculated using an FFT, after which the frequency contents between 40 Hz and 60 Hz are removed (considering a fundamental fre-

quency of 50 Hz), such that higher order harmonics remain unchanged. This is important, because otherwise we might be able to extract the pulse, but then the pulse has an amplitude offset when it is super-positioned with a highly linear waveform. Figure 7.1 shows an example of a test wave that consists of a harmonic distorted sine-wave super-positioned with a pulse. After applying the mains frequency filter, the pulse is separated from the fundamental frequency.

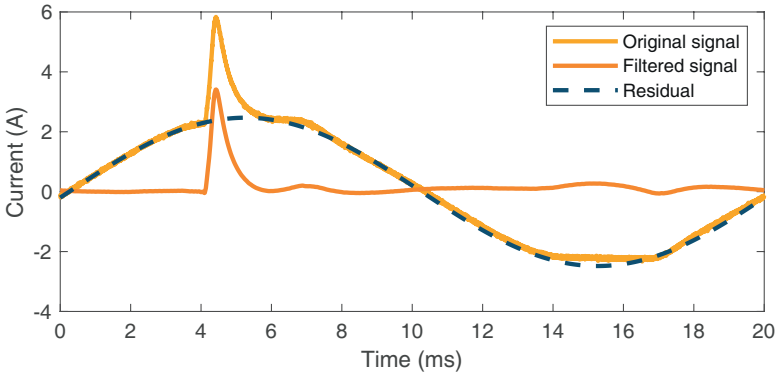

Figure 7.1. Mains frequency filter separating the pulsed part from the fundamental frequency of a measured signal.

7.2.2 Parametric waveform model

The parametric waveform model in Chapter 5, which describes the time-domain characteristics of a pulsed waveform, can now be applied. It indicates change-points at the extreme points of the waveform where the statistical properties change and fits linear piece-wise segments in between. An optimal number of ten change-points was found in Chapter 5 that preserves the shape of the original waveform while reducing its complexity. Consequently, noise will not be treated as a statistical change, as the limited number of change-points makes sure that the noise is not the most significant change of the waveform compared to the changes of the complete waveform. So the model is robust against low amplitude random noise present in the waveform. The filtered signal in Figure 7.1 is modelled using this approach resulting in Figure 7.2, which forms a fair representation of the original pulse. The use of this model is needed, because conventional tools determine time-domain parameters based on bi-level pulses, which is not the case for the waveforms encountered on-site. For example, Figure 7.3 shows a pulse with more than two levels, due to oscillations in realistic waveforms.

Then a set of scalar parameters are obtained to describe the pulsed part of the waveform in the time-domain. Instead of using the pulse width (t_{width}), defined as the time the signal needs in-between its rise to 50% and its fall to 50% of the peak value [85], another metric is used for the duration of a pulse.

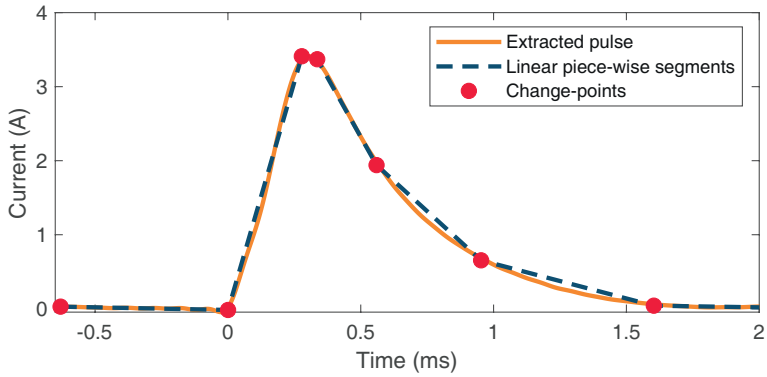

Figure 7.2. Extracted pulse and modelled waveform resulting from a pulsed time-domain current.

Because waveforms are encountered which are a superposition of two consecutive pulses where the first pulse has a relatively large amplitude compared to the second one, as it is exemplified in Figure 7.3. The pulse width will only relate to the first part of the pulse, because the amplitude of the second part is lower than the 50% reference threshold. Choosing a different threshold level for measuring the pulse width would not work either due to the slow decaying feature of the later part of the waveform. Therefore, pulse duration is defined as the time between the start and end instants of the pulse, which could easily be determined using the modelled pulse, as a change-point is provided at the start and end of the pulse. The modelled pulse is described by the following set of scalar parameters, that are exemplified in Figure 7.3 and explained in more detail in Chapter 5:

- Charge (q): the area circumferenced by the pulse and the zero current line.
- Crest factor (CF): the ratio between the peak value (i_{pk}) and the rms value (i_{rms}) of the pulse.
- Maximum slope ($\Delta i/\Delta t$): the maximum slope between two consecutive change-points.
- Peak value (i_{pk}): represents the peak value of the pulse.
- Pulse duration (t_{duration}): the time between the start and end instant of the modelled pulse.

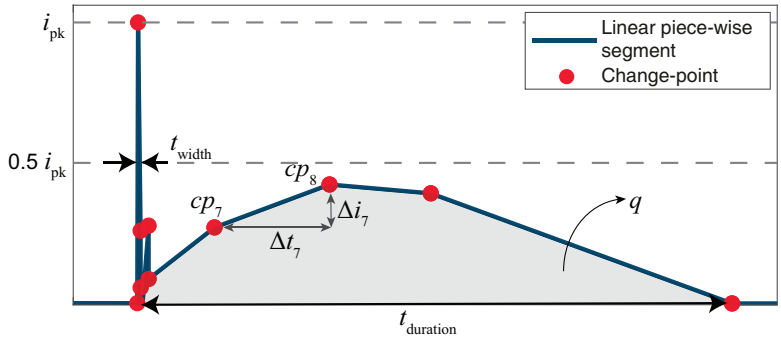

Figure 7.3. Parametric description of a modelled waveform.

7.3 Estimation of the static energy meter errors

An estimator is created to select critical waveforms from a large set of waveforms recorded on-site. The estimator is based on a reference data set of laboratory experiments of which the static energy meter errors are known. The waveforms included in the data set are characterized using the scalar parameters described in Section 7.2. Then for on-site recorded waveforms, of which the static energy meter deviations are unknown, the scalar parameters are determined and interpolated to this data set using an inverse distance weighting (IDW) function resulting in an estimated error.

7.3.1 Description of the reference data set

The data set contains 138 laboratory experiments of which the static energy meter deviations are known. It consists of 60 experiments that were presented earlier in Chapter 3 and 24 experiments with sightly varied measurement conditions. In most of these, in total 84 experiments, static energy meter errors were observed. Furthermore, the data set comprises 54 experiments that did not induce metering errors. These include mostly linear waveforms or pulses with less extreme parameters. All of these 138 waveforms, $p_n(t)$, have a set of parameters, $\mathbf{S}_n$. Inter parameter dependencies are shown in Chapter 5, i.e. different parameters show similar correlations with static energy meter errors, therefore the peak value and charge are not included in this model to avoid redundancy. The data set is described by,

$$\mathbf{S}_n = \left\{ CF_n; \frac{\Delta i_n}{\Delta t_n}; t_{\text{duration,n}} \right\} (p_n(t)) \tag{7.1}$$

and a corresponding measured static energy meter error/deviation, e_n. Here, the errors are determined using,

$$e_n\,[\%] = \frac{P_{\mathrm{SM}} - P_{\mathrm{ref}}}{P_{\mathrm{ref}}} \cdot 100\% \tag{7.2}$$

where P_{SM} is the power measured by the static energy meter under test and P_{ref} is the power of the reference power analyzer, according to the measurement procedure explained in Chapter 3. From the ten selected specimen of static energy meters, it was observed that not all result in the same magnitude of errors. Therefore, the estimator will be referred to the worst case, as the maximum error represents the most critical interference case.

7.3.2 Inverse distance weighting function

For the estimation of errors it is assumed that similar waveforms will result in similar interference. In this regard, similar waveforms are those characterized by parameters that are close to each other in terms of their euclidean distance. Therefore, it is reasonable to assume that an unknown waveform, $p_u(t)$, having a set of parameters, $\mathbf{S}_u$,

$$\mathbf{S}_u = \left\{ CF_u; \frac{\Delta i_u}{\Delta t_u}; t_{\mathrm{duration,u}} \right\} (p_u(t)) \tag{7.3}$$

will result in a metering error, e_u, that can be estimated through an interpolation function, that is, $\tilde{e}_u = f(\mathbf{S}_u)$. In this regard, a suitable alternative for the interpolation method is the IDW function [130]. Because the data set interpolates the parameters to the static energy meter errors, $\{\mathbf{S}_1, \mathbf{S}_2, ..., \mathbf{S}_{138}\} \rightarrow \{e_1, e_2, ..., e_{138}\}$, according to a deterministic relationship and also because the points in the data set are scattered in the study region. And thus weights the similarities between the parameters of the interpolated (unknown) waveforms with the reference data set indirectly. Accordingly,

$$f(\mathbf{S}_u) = \begin{cases} \dfrac{\sum_{n=1}^{N} w_n(\mathbf{S}_u) e_n}{\sum_{n=1}^{N} w_n(\mathbf{S}_u)} & \text{if } d(\mathbf{S}_u, \mathbf{S}_n) \neq 0 \ \forall \ n \\ e_n & \text{if } \exists \ n \in d(\mathbf{S}_u, \mathbf{S}_n) = 0 \end{cases} \tag{7.4}$$

where the weighting function, $w_n\,(\mathbf{S}_u)$,

$$w_n\,(\mathbf{S}_u) = \frac{1}{d(\mathbf{S}_u, \mathbf{S}_u)^{\alpha}}, \tag{7.5}$$

d is the metric operator (in this case the euclidean distance) and α is the power parameter. The equations above indicate that the weight decreases as distance increases from the interpolated points. Moreover, greater values of α assign greater influence to values closest to the interpolated point. A power parameter value of 4 is found to provide a good fit between the reference data set and the validation experiments provided in the next subsection. This translates into an appropriate neighboring region for interpolating the unknown waveforms and a reasonable importance of outliers.

Table 7.1. Time-domain parameters, estimated ($\tilde{e}_{\text{est}}$), and real error (e_{real}) of the validation measurements.

	Negative error					No error				
Index	1	2	3	4	5	6	7	8	9	10
q **(mC)**	3.3	3.0	4.5	5.2	5.5	0.2	11.4	4.6	4.1	2.6
CF	29	29	19	24	21	4	3	3	3	3
$\Delta i/\Delta t$ **(A/µs)**	9.0	8.4	9.3	8.4	8.7	0.01	0.02	0.03	0.08	0.01
i_{pk} **(A)**	18	18	17	20	20	0.2	2	2	2	2
t_{duration} **(ms)**	0.9	1.0	0.9	1.8	1.8	7.9	5.3	3.9	18.3	1.8
$\tilde{e}_{\text{est}}$ **(%)**	-76	-74	-36	-28	-9	0	0	0	0	0
e_{real} **(%)**	-64	-30	-10	-26	-18	-2	1	-1	-2	0

	Positive error									
Index	11	12	13	14	15	16	17	18	19	20
q **(mC)**	2.8	5.3	3.3	7.1	6.4	4.1	6.2	7.2	7.1	3.8
CF	7	7	7	6	6	8	6	6	8	11
$\Delta i/\Delta t$ **(A/µs)**	0.3	0.9	1.3	1.1	0.9	0.9	0.9	0.6	0.4	0.6
i_{pk} **(A)**	12	15	10	15	15	12	14	15	16	19
t_{duration} **(ms)**	3.0	0.8	2.6	0.9	0.9	0.7	0.9	0.9	1.0	0.4
$\tilde{e}_{\text{est}}$ **(%)**	78	143	188	199	203	212	214	229	331	1608
e_{real} **(%)**	28	239	183	301	276	266	304	211	331	1087

7.3.3 Validation of the error estimator

Twenty experiments which are not included in the reference data set are used to validate the accuracy of the estimator. The experiments were performed using the same methodology as the data in the reference data set. Five cases with negative errors (index = 1-5), five cases with no error outside the limits for electricity meters [56] (index = 6-10), and ten cases with positive errors (index = 11-20) are included. The associated waveforms for index 1, 6, 8, 9, and 12 are visualized in Figure 7.4, and Table 7.1 shows the parameters. These wave-shapes repeat every mains cycle during the whole measurement period. The waveforms resulting in a negative error all have a similar shape as the waveform with index 1, however there is a slight difference in the parameters. It is remarkable that all those waveforms have a sharp transient that contains almost no charge in the positive part of the fundamental voltage (as the voltage is in-phase with the waveform with index 9). The waveforms resulting in no error show a chopped sinusoidal waveform (index 6 and 7), a relatively wide pulse with low peak value (index 8 and 10) or a clear sinusoidal waveform (index 9). The waveforms resulting in a positive error all have a similar shape as index 12, but with slightly different parameters, which affects the magnitude of the error. The estimated and real error are presented in Figure 7.5 and Table 7.1, respectively. The estimator matches the real errors well, as for all indices it was correctly estimated if the error was negative, non-existing, or positive. This is thus a valuable tool for selecting critical waveforms from a large set of on-site captured data, after which more concise and precise measurements can be performed effectively.

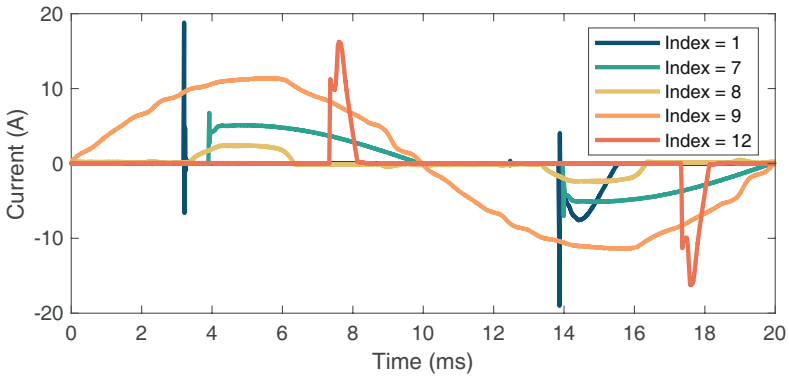

Figure 7.4. Waveforms of the validation measurements.

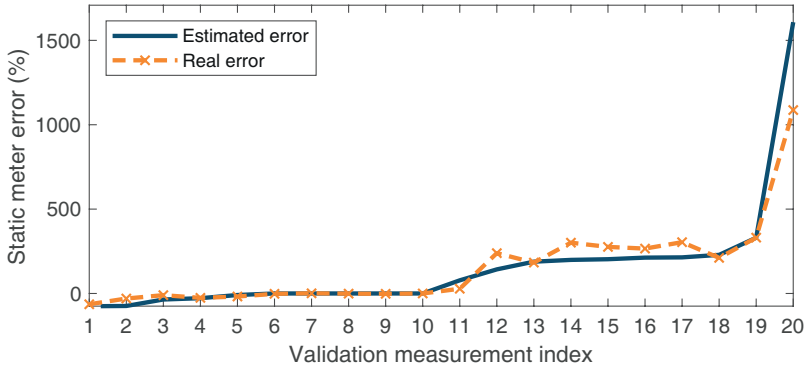

Figure 7.5. Estimated and real error of the validation experiments.

7.4 Method for on-site survey

To indicate the existence of pulsed currents that could interfere with static energy meters in on-site situations, a survey was conducted. Three different test sites were surveyed, which consists of: an industrial plant using EV charging stations in Viladecavalls (Barcelona), Spain (site 1), a consumer residence that includes PV installation in Gelida (Barcelona), Spain (site 2), and an apartment in Enschede, The Netherlands (site 3). Site 1 uses a three-phase system, while site 2 and 3 use a single-phase system. Some preliminary results of site 1 and 2 were already published in [106], [107].

7.4.1 Measurement setup

Measurements were performed at the meter connection point, to measure the complete low-voltage system, and thus the signals to which installed static energy meters are exposed to. During the measurement survey it was not known which appliances were turned on. For the three-phase system (site 1) the currents on all three lines (L1, L2, L3) were measured, for the single-phase systems (site 2 and 3) the current on the line and the neutral conductor were measured. The current was measured using flexible current probes model TA325 from Pico Technology, and are within 0.5 dB accuracy in the frequency range up to 20 kHz, calibrated according to Chapter 4. It was verified that the probe's response time was sufficient to measure fast changing pulsed currents without major influences on the measured waveform. The transducers were connected to a 5444B Picoscope digitizer from the same manufacturer. Time-domain EMI measurement and processing system (TEMPS) software [131] was controlling the digitizer via a laptop. Figure 7.6 shows the installed measurement setup at the consumers' meter connection point.

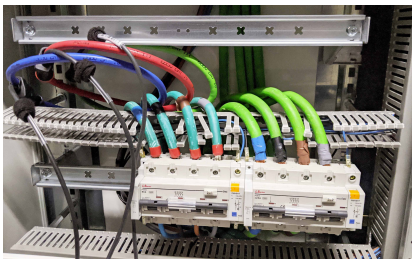

(a) Site 1

(b) Site 2

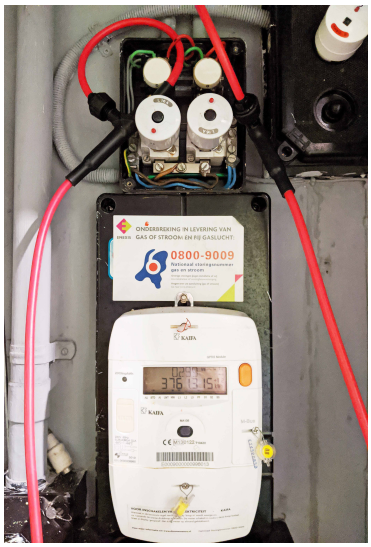

(c) Site 3

Figure 7.6. Installed measurement setup at the consumer's meter connection point.

7.4.2 Measurement settings

The on-site locations were monitored during an interval of ten days. The acquired waveforms were analyzed in order to preselect and store meaningful data only. For that purpose, specific triggering settings were used based upon the pulsed waveforms of interest following the procedure in [107]. That are amplitude probability distribution (APD) [132] and DWT [116], which have shown to be strong indicators for pulsed waveforms. Furthermore, snapshots (instantaneous acquisitions) were made every ten minutes. In this way, a representative set of waveforms (events) in the surveyed sites is gathered. The measurement time for each triggered acquisition was ten cycles at mains frequency (50 Hz), which is equivalent to 200 ms. The waveform sampling rate was set to 1 MS/s.

7.5 Results obtained from on-site survey

The time-domain parameters are extracted from on-site surveyed waveforms and are presented statistically in Figure 7.7, using the Turkey's boxplot method [127]. Points with a value of 1.5 times the interquartile range from the median are marked as outliers and are visible with a dot. The value of the median (Q2), lower (Q1) and upper (Q3) quartile, and the minimum (min) and maximum (max) are presented in the graph. The range in which parameters are found to be critical in relation to static energy meter errors, according to Table 5.3, is indicated in red. For the peak value no critical range is included, as this

parameter individually does not correlate to meter readings, e.g. a large value could relate to a large pulse but also to a linear waveform with high peak value. The charge and peak value are not included in the estimator, but are provided here for a complete statistical overview of the waveforms. The graph shows the typical ranges of the parameters and their variability. In 74% of the captured events at least one parameter was inside the critical area of static energy meter errors. An overview of events containing at least one critical parameters, and events where a static energy meter error is estimated, is provided in Table 7.2. These are explained per test site hereafter.

Table 7.2. Overview of on-site survey, showing the captured events, events containing critical parameters and events having estimated errors.

Site	Events	Critical parameters	Estimated errors
1	14295	13304	3
2	1230	404	44
3	4006	779	332

7.5.1 Test site 1

For site 1 the APD trigger captured a large number of low amplitude noisy waveforms, which explains the considerably higher number of triggered events compared to the other sites. Consequently, the crest factor is inside the critical red area and explains the 13304 events with a critical parameter. However, these pulses have a low charge, slope, and peak value, while the pulse duration is large. Still for three events an error is estimated, which are 19%, 86%, and 333%, respectively. The corresponding waveforms are distorted sinusoidal as shown in Figure 7.8(a). The wave-shape repeats for multiple consecutive cycles as long as the source of interference is turned on. Where the extremity of the waveforms' rising slope determines the magnitude of the error. No pattern was recognized in the occurrence of these events containing estimated errors, so these peaks occur seemingly at random.

7.5.2 Test site 2

In site 2 1230 events are captured of which a third of them (32.8%) contain critical parameters. The pulses contain more charge and have a higher peak value compared to site 1. For 44 events an error is estimated, mostly because of fast rising slopes combined with a high crest factor. Figure 7.8(b) shows an example waveform for which an error is estimated, it shows a pulse that is present in a distorted sinusoidal waveform, which repeats for multiple consecutive cycles. The other waveforms of which errors are estimated contain similar pulses and the extremity of the time-domain parameters, being the combination of the crest factor, maximum slope, and pulse duration, determines the magnitude of the error. The estimated errors range from -29% to 464%, where the

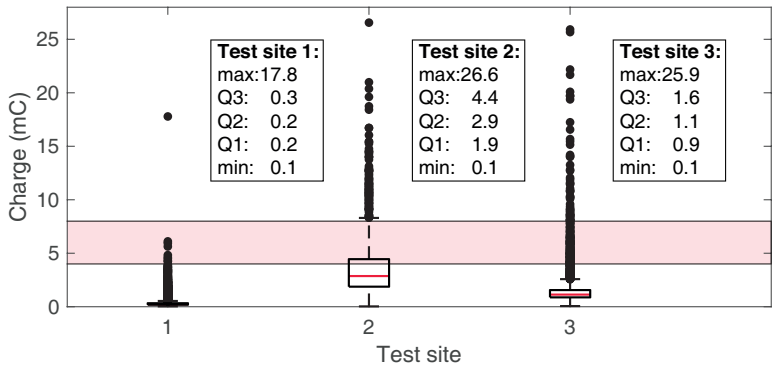

(a) Charge

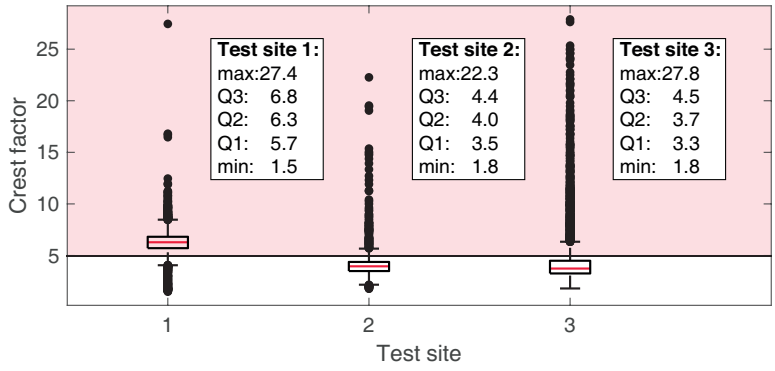

(b) Crest factor

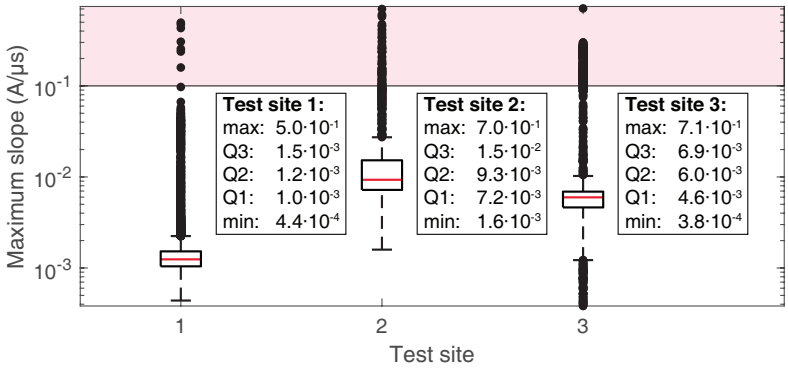

(c) Maximum slope

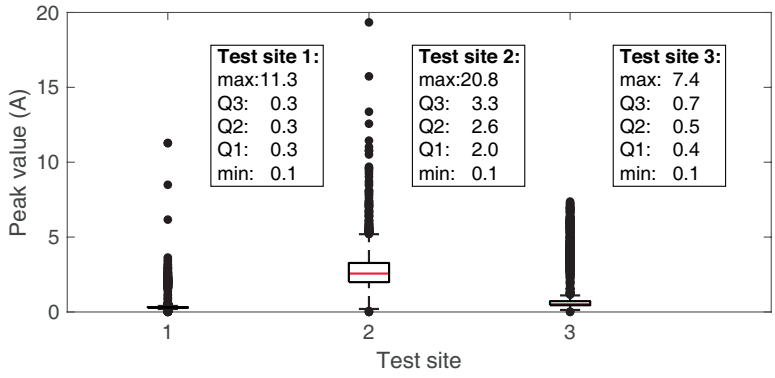

(d) Peak value

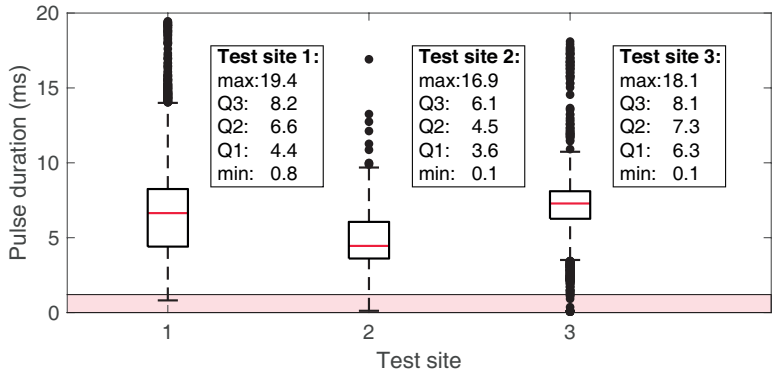

(e) Pulse duration

Figure 7.7. Statistical overview of the time-domain parameters that occurred in the three surveyed test sites.

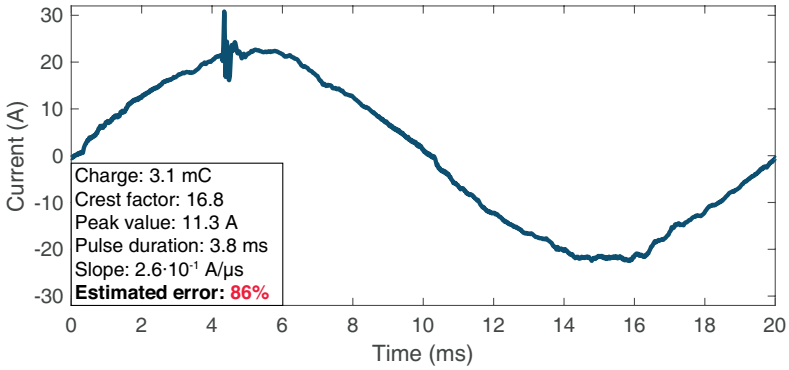

(a) Site 1

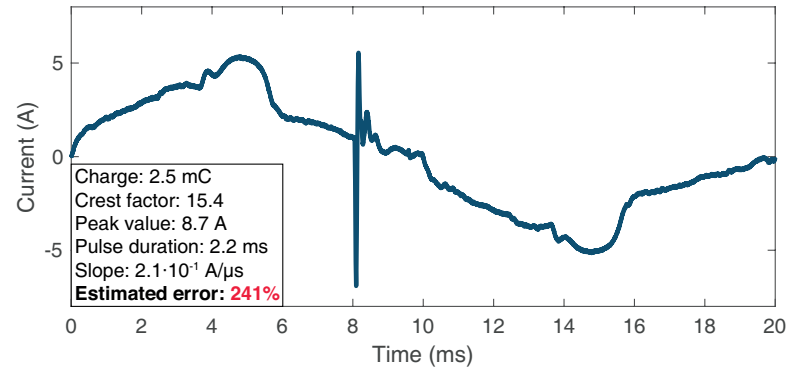

(b) Site 2

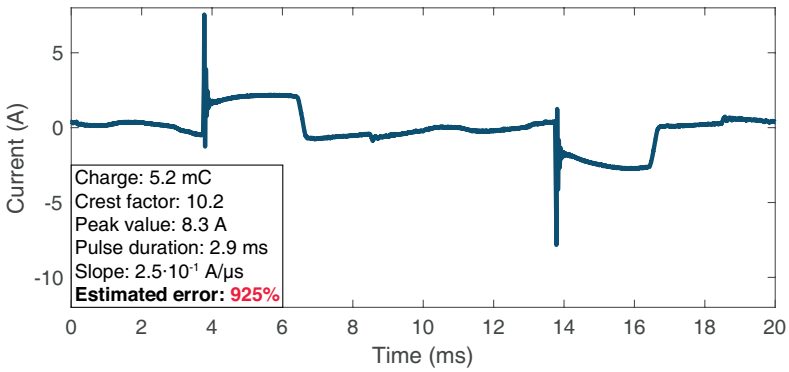

(c) Site 3

Figure 7.8. Waveforms with an estimated static energy meter error surveyed in the sites.

highest estimated interference corresponds to the most extreme combination of the time-domain parameters. Similar to site 1 these pulses occur seemingly at random, as there is no pattern observed in its occurrence.

7.5.3 Test site 3

For site 3 a total of 4006 events was captured of which 779 contain critical parameters, and for 332 an error was estimated. This is mostly because of the high crest factor and high rising slope found in these waveforms. A waveform for which an error was estimated is exemplified in Figure 7.8(c), the interference repeats during multiple consecutive cycles. It shows a pulsed current waveform without a clear sinusoidal component present, this represents a similar situation as the pulses causing static energy meter interference in lab experiments. During the ten day survey in site 3, similar pulses were identified five times during intervals of 1.5 to 3 hours. This indicates the pulse is resulting from equipment which is not running continuously, however the pulses occurred during different times of the day. The estimated errors for site 3 range from -35% to 925%. The variation of the estimated error occurs mainly due to a difference in crest factor and rising slope between the different occurrences of the event.

7.6 Discussion and conclusion

In this chapter, waveforms likely to be critical in relation with static energy meter interference are detected in on-site surveyed waveforms. This is done using a parametric waveform model for the characterization of pulses in on-site scenarios. That separates the pulsed part from the linear part of the waveform, as the pulsed part was correlated to the interference on static energy meters in Chapter 5 and is therefore of interest to analyze. Consecutively, the time-domain parameters of interest are determined, which are: charge, crest factor, maximum slope, peak value, and pulse duration. Then, a data set of laboratory experiments of which static energy meter errors are known is interpolated to the unknown surveyed waveforms using an IDW function to estimate the interference. As a result, surveyed waveform data with similar characteristics is detected. During the on-site survey, at three sites the waveforms occurring at the meter connection points are measured. These sites cover an EV charging station, a consumer's residence that includes a PV installation, and an apartment premise. From this data the waveforms that contain time-domain parameters of interest considering the interference of static energy meters are detected. These detected waveforms show the existence of several waveforms in on-site situations that have similar characteristics as the waveforms proven to result in static energy meter interference. For example, waveforms with a slope larger than 0.1 A/µs and crest factors way above 5, even reaching 27.8, are found. In 74% of the surveyed waveforms parameters in the critical range were found. The estimated errors range from -35% to 925% depending on the extremity of the time-domain parameters of the pulse. Furthermore, the

presented parameters in the on-site data show that, in general, a variety of non-linear waveforms are present in low-voltage networks and are thus encountered by the static energy meters. These non-linearities are outside the requirements as included in immunity standards such as the IEC 61000-4-19 [29]. This can become problematic as equipment inside such systems, e.g. the static energy meter, is characterized using frequency-domain tests. As these tests assume a LTI system, which the low-voltage grid is clearly not, according to the results in this chapter. And as was already identified to be critical when looking at the applicable standards for static energy meters in Chapter 2.

Chapter 8

Conclusion

This chapter outlines the conclusions that can be drawn from the research presented in this thesis. Moreover some directions for future work are provided.

8.1 Conclusions

In this thesis it was shown that EMI on static energy meters occurs due to non-linear pulsed currents. These non-linear waveforms have significant differences with the waveforms included in the test standards, which covers linear waveforms that are swept over the frequency range of interest. Furthermore, similar waveforms are found to exist in realistic on-site measurements. This is important as the MID describes that the measurement instrument shall not exceed any permissible errors in its "normal working conditions". That is, the static energy meter should be able to measure realistic waveforms without any problem. In particular, waveforms found to interfere static energy meters are pulsed current waveforms that are narrow and have a fast rising slope. The existence of similar waveforms in a realistic on-site environment was shown by a broad survey of the waveforms from individual appliances present in a typical residential system, with a special focus on the emissions of (modern) light equipment. Additionally, waveforms were surveyed at the metering connection point of three representative (modern) systems. These realistic on-site waveforms are comparable with the waveforms the result in interference on static energy meters. That is, the parameters of the waveforms as surveyed in a realistic on-site situation are similar to the waveforms resulting in metering errors. In that sense, realistic waveforms that result in EMI on static energy meters have a non-linear behavior and do not represent the sinusoidal CW signals that are swept over the frequency range of interest as used in the harmonized standards.

Next, the conclusions of the individual chapters are presented one-by-one.

8.1.1 Chapter 2

In Chapter 2, the lack in standardization for the immunity of the static energy meter and the emissions generated in the electrical environment where the meter is placed in is shown. First, the EMC directive is not applicable to measurement instruments, including the static energy meter. Besides, the MID states that the measurement instrument shall not exceed any permissible errors in its "normal working conditions". Thus the signals that are present in the low-voltage grid should be measured by the static energy meter without any problems. Second, for the relevant standards that consider the immunity of static energy meters, and the emissions of the connected equipment and the low-voltage grid, a lack of standardization is observed, especially from 2 kHz till 150 kHz. Which is an important frequency range as many power electronic devices switch at these frequencies. In the current standards only ideal conditions are covered, which are represented by sinusoidal voltages and currents. These test conditions are not representative for today's realistic situation which combines many non-linearities. Also, due to the adoption of many power electronic devices, the low-voltage grid is typically more low impedant than considered in standardization.

8.1.2 Chapter 3

In Chapter 3, several cases of EMI on static energy meters are presented. Which are due to modern appliances, that are: dimmed lighting equipment of LED and CFL technology, a speed controlled water pump, and multimedia equipment. As a result several under- or over-estimations of the energy consumption as measured by the static energy meter are found, that could result in incorrect billing of consumers. The currents that cause the interference are non-linear pulses, that have fast rise times in the range between 2 µs and 150 µs, and current slopes higher than 0.1 A/µs. In that sense, higher slopes contribute to higher static energy meter errors. Furthermore, the impedance of the grid affects the interference, i.e. a capacitive grid result in higher errors, as high frequency currents are drawn easier as the grid has a lower impedance for higher frequencies. Additionally, for meters using the Rogowski coil as their current sensing element, the phase firing angle between the current and voltage alters the interference. That is, for a phase firing angle above 90° positive errors (over-estimation) are found and for a phase firing angle below 90° negative errors (under-estimation) are found. Consequently, even an incorrect power delivery back to the grid is found when no power delivery equipment is connected. This occurs when the under-estimation is so large that the negative error is higher than the actual consumption.

Next to this, incorrect energy measurements are found due to an unbalance between the line and neutral conductor, while the static energy meter is working according to its specification. As energy measurements are performed according to the Blondel theorem, which states that for a system containing N conductors, only *N-1* current measuring elements are needed. And as the

residential system is earthed, no current can flow through the protective-earth conductor. Consequently, only *N-2* current elements are used, i.e. in a one-phase system only the line current is measured. However, two cases are shown where a protective-earth current was flowing, creating an unbalance between the line and neutral conductor, and incorrect energy measurements. In the first case, a current could flow through the protective-earth due to a broken RCD. Creating a very unsafe situation and a difference in the energy measurement dependent on whether the line or neutral is measured, which are both true considering the Blondel theorem with the assumption that no current flows through the protective-earth conductor. In the second case, leakage currents are found when using non-linear appliances. For example, due to the filter capacitors (Y-capacitors) in modern appliances. Which could cause malfunction of different components within the system. Again, a difference in energy measurement is observed dependent on whether a current element on the line or neutral is used. To overcome these problems, both the line and neutral conductor should be measured.

8.1.3 Chapter 4

In Chapter 4, an impulsive test method for the characterization of CTs shows a good alternative compared to conventional CW testing. In particular, square-wave signals are generated using a half bridge, and thus cover a wide frequency range. Hence, for two square-wave signals only 35% measurement points are found compared to the CW test in the bandwidth up to 1 MHz. The chosen square-wave signals have a repetition frequency of 50 Hz to resemble currents at mains frequency, and of 10 kHz to resemble critical currents in relation to EMI on static energy meters, respectively. A fairly good spread of frequency points could be achieved by increasing the number of square-wave signals. Furthermore, the impulsive test method allows to generate test signals up to 30 A with a bandwidth of 10 MHz without using a high power wide-band amplifier, and thus the novel impulsive test method is more cost effective.

Additional tests using realistic on-site pulsed currents show discrepancies with the current response of several CTs. More specifically, when no pulse is present, i.e. the signal value is zero, a saw-tooth is present due to droop of the CTs. The product of the voltage with this discrepant saw-tooth pattern in the current, results in an additional energy that is measured. Which results in the occurrence of energy errors outside the permissible limits for electricity meters. While linear sinusoidal currents, of different frequencies inside the same frequency band, form no problems for the CTs under test. This shows that the energy errors are only observed when using pulsed test signals. And thus, the sinusoidal signals as included in the immunity test standards do not indicate these problems.

8.1.4 Chapter 5

In Chapter 5, a simplified description of the interfering non-linear waveforms is made using a parametric waveform model. The interference waveform is described by a limited amount of data-points, rather than a highly sampled complex waveform. Using the parametric waveform model the critical parameters are identified. An increase in metering errors is shown due to a higher crest factor, narrower pulse width, higher peak amplitude, less charge, and higher slopes. However, no parameter could be individually correlated to the interference, a combination of those critical parameters will determine the extend of the error. Also it is found that static energy meters utilizing a Rogowski coil as their current sensing element will contribute to the highest interference cases. Followed by the current transformer, and the shunt resistor and Hall effect sensor have lower errors. Furthermore, the simplified modelled waveform provides a proper candidate for arbitrary test signals for future standardization, as the modelled waveform had similar errors as the original on-site waveform. And thus, the modelled waveform correctly describes the critical features of the original interference waveform in a simplified manner.

8.1.5 Chapter 6

In Chapter 6, the survey of emissions of typical (household) equipment shows many similar parameters as the waveforms found to interfere with static energy meters. First, the emissions of different dimmer technologies combined with lighting equipment of LED technology is analyzed. For the rising edge dimmers that use the TRIAC or MOSFET for dimming the emissions are larger compared to the falling edge dimming of a MOSFET dimmer. These emissions contain many similar parameters as the waveforms causing interference on static energy meters. Furthermore, there is a general lack of standardization for dimmers observed. Besides, due to a lack of knowledge of consumers non-advised combinations of dimmers and luminaries can occur. In those cases the luminary still works, however it is creating an unwanted pulsed current that can harm other equipment (e.g. the static energy meter).

Second, an extensive survey of typical equipment that is present in a realistic situation, shows that 43% of the equipment has parameters inside the critical range related to the EMI on static energy meters. And the majority of surveyed equipment is non-linear and time-varying. Consequently, a realistic system combines those non-linearities and emissions are created that are not covered by the current standards, for example the IEC 61000-4-19 for the immunity of static energy meters.

8.1.6 Chapter 7

In Chapter 7, many non-linearities and current waveforms with similar parameters as the earlier interference cases, are found during a survey of typical waveforms that occur at the meter connection point. Those similarities were

identified by comparing the on-site waveforms with the waveforms that are causing interference on static energy meters as measured in the lab. The survey of typical waveforms at the meter connection point includes modern installations such as an EV charging station and a PV installation, but also a more conventional apartment without energy generating equipment was included. Using the parametric waveform model the similarities with the lab study are identified. Similar waveforms are found that have a slope larger than 0.1 A/µs and a crest factor above 5, which were found to be critical to interference on static energy meters in Chapter 5. In 74% of the waveforms critical parameters are found. Based on the lab study, i.e. which combination of parameters result in the largest interference, the criticalness of the on-site waveforms is determined. Errors between -35% and 925% were estimated, so critical waveforms are present in a real-world situation. Hence, the survey shows that the realistic on-site waveforms contain many EMI that is not covered in the standards, as those focus on frequency-domain tests and do not cover pulsed waveforms.

8.2 Recommendations

Research on the EMI on static energy meters will continue in the future. Based on the work as presented in this thesis, directions for future work are provided as:

- Explore testing of the immunity of static energy meters with practical pulsed currents in future standardization. As the present immunity standards focus on frequency-domain test, and do not cover waveforms with a pulsed behavior that are found to interfere the energy readings of the static energy meter. In that sense, the test standards do not match the electromagnetic environment. Therefore, the improved standardization should focus on time-domain testing of pulses that include a wide-spread of frequency components.

- Further explore the root cause of the interference problems with the static energy meters. The problems with meters utilizing a Rogowski coil were analyzed in [82], and it was found that the pulsed currents create a $\mathrm{d}i/\mathrm{d}t$ at the output of the Rogowski coil that is so high that the signal will clip at the amplifier. However, the root cause for other current sensing elements, e.g. the current transformer, Hall effect sensor, and shunt resistor, should be explored. Especially the current transformer is of interest as meters utilizing this element also show significant metering errors. Furthermore, measurements on the response of CTs using practical pulsed currents, show droop problems resulting in incorrect energy measurements.

- The suitability of the Hall effect sensor as a current sensing element for energy measurements should be further explored. As in Chapter 4 no problems were found when using a Hall effect sensor for energy measurements, in contrast to the current transformer and Rogowski coil. In that

sense, the Hall effect sensor could be a suitable choice to be implemented in a static energy meter or a low-cost energy monitor (used as reference instrument in cases of consumer disputes). However, also static energy meters with a Hall effect sensor can be prone to EMI, so the drawbacks of this sensor should also be explored.

References

[1] "Stepping up Europe's 2030 climate ambition Investing in a climate-neutral future for the benefit of our people", COM (2020) 562 final, Tech. Rep., 2020.

[2] "Roadmap 2050 - A Practical Guide to a Prosperous Low-Carbon Europe", European Climate Foundation (ECF), Tech. Rep., 2010.

[3] M. Pourarab, S. Alishahi, and M. H. Sadeghi, "Analysis of harmonic distortion in distribution networks injected by nonlinear loads", in *21st International Conference on Electricity Distribution*, Frankfurt, Germany, 2011, pp. 1–4.

[4] M. Olofsson, "Power Quality and EMC in Smart Grid", in *2009 10th International Conference on Electrical Power Quality and Utilisation*, Lodz, Poland, 2009, pp. 1–6.

[5] *Electromagnetic compatibility (EMC) - Environment - Compatibility levels for low-frequency conducted disturbances and signalling in public low-voltage power supply systems*, IEC 61000-2-2:2002 Std., 2002.

[6] *Voltage characteristics of electricity supplied by public electricity networks*, EN 50160:2010 Std., 2010.

[7] R. B. Timens, "Electromagnetic interference of equipment in power supply networks", PhD thesis, University of Twente, Enschede, The Netherlands, 2013.

[8] R. B. Timens, F. J. Buesink, and F. Leferink, "Effect of energy saving lights on power supply", in *International Symposium on Electromagnetic Compatibility - EMC EUROPE*, Rome, Italy, 2012, pp. 1–4.

[9] K. Murakawa, N. Hirasawa, H. Ito, and Y. Ogura, "Electromagnetic interference examples of telecommunications system in the frequency range from 2kHz to 150kHz", in *2014 International Symposium on Electromagnetic Compatibility, Tokyo*, Tokyo, Japan, 2014, pp. 581–584.

[10] B. Zhang and S. Wang, "A Survey of EMI Research in Power Electronics Systems With Wide-Bandgap", *IEEE Journal of Emerging and Selected Topics in Power Electronics*, vol. 8, no. 1, pp. 626–643, Mar. 2020.

[11] R. Smolenski, *Conducted Electromagnetic Interference (EMI) in Smart Grids*. Smart Grids, Springer, 2012.

[12] V. Khokhlov, J. Meyer, P. Schegner, D. Agudelo-Martínez, and A. Pavas, "Immunity Assessment of Household Appliances in the Frequency Range from 2 to 150 kHz", in *25th International Conference on Electricity Distribution (CIRED)*, Madrid, Spain, 2019, pp. 1–5.

[13] S. Sakar, S. Rönnberg, and M. Bollen, "Interferences in AC–DC LED Drivers Exposed to Voltage Disturbances in the Frequency Range 2–150 kHz", *IEEE Transactions on Power Electronics*, vol. 34, no. 11, pp. 11 171–11 181, 2019.

[14] "Study Report on Electromagnetic Interference between Electrical Equipment/Systems in the Frequency Range Below 150 kHz", CLC/TR 50627, Tech. Rep., 2015.

[15] M. A. Wibisono, T. Hartman, N. Moonen, D. Hamdani, and F. Leferink, "The Effect of the Current Pulse Width from LEDs on Narrowband Power Line Communication and its Analysis in Time and Frequency Domain", in *2020 International Symposium on Electromagnetic Compatibility (EMC Europe 2020)*, Rome, Italy, 2020, pp. 1–6.

[16] S. Rönnberg, "Emission and Interaction from Domestic Installations in the Low Voltage Electricity Network, up to 150 kHz", PhD thesis, Luleå University of Technology, Luleå, Sweden, 2013.

[17] F. Leferink, "Conducted interference, challenges and interference cases", *IEEE Electromagnetic Compatibility Magazine*, vol. 4, no. 1, pp. 78–85, Apr. 2015.

[18] R. Quijano Cetina, A. J. Roscoe, and P. S. Wright, "Challenges for Smart Electricity Meters due to Dynamic Power Quality Conditions of the Grid: A Review", in *2017 IEEE International Workshop on Applied Measurements for Power Systems (AMPS)*, Liverpool, UK, 2017, pp. 1–6.

[19] P. Siano, "Demand response and smart grids — A survey", *Renewable and Sustainable Energy Reviews*, vol. 30, pp. 461–478, 2014.

[20] Q. Sun, H. Li, Z. Ma, C. Wang, J. Campillo, Q. Zhang, F. Wallin, and J. Guo, "A Comprehensive Review of Smart Energy Meters in Intelligent Energy Networks", *IEEE Internet of Things Journal*, vol. 3, no. 4, pp. 464–479, 2016.

[21] Tounquet, Frédéric and Alaton Clément, "Benchmarking smart metering deployment in the EU-28 ", European Comission, Tech. Rep., 2020.

[22] D. Gallo, C. Landi, N. Pasquino, and N. Polese, "A New Methodological Approach to Quality Assurance of Energy Meters Under Nonsinusoidal Conditions", *IEEE Transactions on Instrumentation and Measurement*, vol. 56, no. 5, pp. 1694–1702, Sep. 2007.

[23] A. Cataliotti, V. Cosentino, and S. Nuccio, "Static Meters for the Reactive Energy in the Presence of Harmonics: An Experimental Metrological Characterization", *IEEE Transactions on Instrumentation and Measurement*, vol. 58, no. 8, pp. 2574–2579, Aug. 2009.

[24] A. Cataliotti, V. Cosentino, A. Lipari, and S. Nuccio, "Metrological characterization and operating principle identification of static meters for reactive energy: An experimental approach under nonsinusoidal test conditions", *IEEE Transactions on Instrumentation and Measurement*, vol. 58, no. 5, pp. 1427–1435, May 2009.

[25] J. Kirchhof and G. Klein, "EMV - Grenzwertlücke – Wechselrichter stört Zähler", in *24. Symposium Photovoltaische Solarenergy*, Bad Staffelstein, Germany, 2009, pp. 1–8.

[26] J. Kirchhof, "Grenzwertlücke - Wechselrichter stört Elektrizitätszähler", in *EMV*, Düsseldorf, Germany, 2010, pp. 1–9.

[27] P. Kotsampopoulos, A. Rigas, J. Kirchhof, G. Messinis, A. Dimeas, N. Hatziargyriou, V. Rogakos, and K. Andreadis, "EMC Issues in the Interaction Between Smart Meters and Power-Electronic Interfaces", *IEEE Transactions on Power Delivery*, vol. 32, no. 2, pp. 822–831, Apr. 2017.

[28] "Electricity metering equipment - Severity levels, immunity requirements and test methods for conducted disturbances in the frequency range 2 -150 kHz", CLC/TR 50579, Tech. Rep., 2012.

[29] *Electromagnetic Compatibility (EMC) - Part 4-19: Testing and measurement techniques - Test for immunity to conducted, differential mode disturbances and signalling in the frequency range from 2 kHz to 150 kHz, at a.c. power port*, IEC 61000-4-19 Std., 2014.

[30] F. Leferink, C. Keyer, and A. Melentjev, "Runaway energy meters due to conducted electromagnetic interference", in *2016 International Symposium on Electromagnetic Compatibility - EMC EUROPE*, Wroclaw, Poland, 2016, pp. 172–175.

[31] F. Leferink, C. Keyer, and A. Melentjev, "Static energy meter errors caused by conducted electromagnetic interference", *IEEE Electromagnetic Compatibility Magazine*, vol. 5, no. 4, pp. 49–55, Oct. 2016.

[32] C. Keyer and F. Leferink, "Conducted interference on smart meters", in *2017 IEEE International Symposium on Electromagnetic Compatibility & Signal/Power Integrity (EMCSI)*, Washington, DC, USA, 2017, pp. 608–611.

[33] G. Rietveld, D. Hoogenboom, and M. Acanski, "Conducted EMI Causing Error Readings of Static Electricity Meters", in *2018 Conference on Precision Electromagnetic Measurements (CPEM 2018)*, Paris, France, 2018, pp. 1–2.

[34] R. Steiner, M. Farrell, S. Edwards, T. Nelson, J. Codere, and S. Sarwat, "Testing Electric Utility Smart Meters with High Harmonic Current Waveforms", in *2020 Conference on Precision Electromagnetic Measurements (CPEM)*, Denver, CO, USA, 2020, pp. 1–2.

[35] J. R. Macedo Jr., G. L. Xavier, I. N. Gondin, L. T. S. Oliveira, and R. F. B. de Oliveira, "An update on the performance of active energy meters under non-sinusoidal conditions", *Electrical Engineering*, vol. 102, pp. 1785–1794, Apr. 2020.

[36] B. ten Have, T. Hartman, N. Moonen, C. Keyer, and F. Leferink, "Faulty Readings of Static Energy Meters Caused by Conducted Electromagnetic Interference from a Water Pump", in *Renewable Energy and Power Quality Journal (RE&PQJ)*, Santa Cruz de Tenerife, Spain, 2019, pp. 15–19.

[37] T. Hartman, B. ten Have, N. Moonen, and F. Leferink, "How to Earn Money with an EMI Problem: Static Energy Meters Running Backwards", in *How to Earn Money with an EMI Problem: Static Energy Meters Running Backwards*, Raleigh, NC, USA, 2021, pp. 788–793.

[38] R. van Leeuwen, H. E. van den Brom, D. Hoogenboom, G. Kok, and G. Rietveld, "Current waveforms of household appliances for advanced meter testing", *2019 IEEE 10th International Workshop on Applied Measurements for Power Systems (AMPS)*, pp. 1–6, Aachen, Germany, 2019.

[39] L. Bartolomei, D. Cavaliere, A. Mingott, L. Peretto, and R. Tinarelli, "Testing of Electrical Energy Meters in Off-Nominal Frequency Conditions", in *2019 IEEE 10th International Workshop on Applied Measurements for Power Systems (AMPS)*, Aachen, Germany, 2019, pp. 1–6.

[40] I. Diahovechenko, B. Dolník, M. Kanálik, and J. Kurimský, "Contemporary electric energy meters testing under simulated nonsinusoidal field conditions", *Electrical Engineering*, pp. 1–16, Aug. 2021.

[41] R. Quijano Cetina, Y. Seferi, S. M. Blair, and P. S. Wright, "Energy metering integrated circuit behavior beyond standards requirements", *Energies*, vol. 14, no. 2, pp. 1–19, Jan. 2021.

[42] M. Brignall,"I can't charge my electric car cheaply because I'm too close to an RAF base," The Guardian, United Kingdom, Dec. 6, 2021. [Online]. Available: https://www.theguardian.com/money/2021/dec/06/i-cant-charge-my-electric-car-cheaply-because-im-too-close-to-an-raf-base, Accessed on: Dec. 6, 2021.

[43] "Publishable Summary for 17NRM02 MeterEMI Electromagnetic Interference on Static Electricity Meters", National Physical Laboratory, Czech Metrology Institute, Justervesenet, Federal Institute Of Metrology METAS, VSL, Universitat Politècnica de Catalunya, University of Twente, Tech. Rep., 2019.

[44] *Electromagnetic compatibility (EMC) - Part 3-2: Limits - Limits for harmonic current emissions (equipment input current ≤16 A per phase)*, IEC 61000-3-2 Std., 2005.

[45] B. ten Have, T. Hartman, N. Moonen, and F. Leferink, "Why Frequency Domain Tests Like IEC 61000-4-19 Are Not Valid; a Call for Time Domain Testing", in *2019 International Symposium on Electromagnetic Compatibility (EMC Europe 2019)*, Barcelona, Spain, 2019, pp. 124–128.

[46] B. ten Have, T. Hartman, N. Moonen, and F. Leferink, "Static Energy Meters and the Electrical Environment Comply to the Standards but Are Not Compatible", *[Manuscript submitted for publication] IEEE Electromagnetic Compatibility Magazine*, pp. 1–8, 2022.

[47] F. Gronwald, R. Conrads, R. Janssen, and T. Weber, "Efficient immunity testing of smart meter devices in the frequency range 2–150 khz", in *22nd International Conference and Exhibition on Electricity Distribution (CIRED 2013)*, Stockholm, Sweden, 2013, pp. 1–4.

[48] F. Gronwald, "Frequency versus time domain immunity testing of smart grid components", *Advances in Radio Science*, vol. 12, pp. 149–153, Nov. 2014.

[49] P. Davari, F. Blaabjerg, E. Hoene, and F. Zare, "Improving 9-150 khz emi performance of single-phase pfc rectifier", in *CIPS 2018; 10th International Conference on Integrated Power Electronics Systems*, Stuttgart, Germany, 2018, pp. 1–6.

[50] M. Bollen, M. Olofsson, A. Larsson, S. Rönnberg, and M. Lundmark, "Standards for supraharmonics (2 to 150 kHz)", *IEEE Electromagnetic Compatibility Magazine*, vol. 3, no. 1, pp. 114–119, Apr. 2014.

[51] P. T. Jensen and P. Davari, "Power converter impedance and emission characterization below 150 khz", in *2021 IEEE International Joint EMC/SI/PI and EMC Europe Symposium*, Raleigh, NC, USA, 2021, pp. 255–260.

[52] E. O. A. Larsson, M. H. J. Bollen, M. G. Wahlberg, C. M. Lundmark, and S. K. Rönnberg, "Measurements of High-Frequency (2–150 kHz) Distortion in Low-Voltage Networks", *IEEE Transactions on Power Delivery*, vol. 25, no. 3, pp. 1749–1757, Jul. 2010.

[53] S. K. Rönnberg, M. H. Bollen, H. Amaris, G. W. Chang, I. Y. Gu, Ł. H. Kocewiak, J. Meyer, M. Olofsson, P. F. Ribeiro, and J. Desmet, "On waveform distortion in the frequency range of 2kHz–150kHz—Review and research challenges", *Electric Power Systems Research*, vol. 150, pp. 1–10, Sep. 2017.

[54] "CEN and CENELEC Position Paper on the implementation and future of the Construction Product Regulation", CEN and CENELEC Technical Committees, Tech. Rep., 2020.

[55] *Directive 2014/30/EU of the European Parliament and of the Council on the harmonisation of the laws of the Member States relating to electromagnetic compatibility*, Feb. 2014.

[56] *Directive 2014/32/EU of the European Parliament and of the Council on the harmonisation of the laws of the Member States relating to the making available on the market of measuring instruments*, Feb. 2014.

[57] A. Bernieri, G. Betta, L. Ferrigno, M. Laracca, and R. Schiano Lo Moriello, "Electrical energy metering: Some challenges of the European Directive on Measuring Instruments (MID)", *Measurement*, vol. 46, no. 9, pp. 3347–3354, 2013.

[58] *Electricity metering equipment - Particular requirements - Part 21: Static meters for AC active energy (classes 0,5, 1 and 2)*, IEC 62053-21 b:2020 Std., 2020.

[59] *Electricity metering equipment - Particular requirements - Part 22: Static meters for AC active energy (classes 0,1S, 0,2S and 0,5S)*, IEC 62053-22 b:2020 Std., 2020.

[60] *Electricity metering equipment (AC) - General requirements, tests and test conditions - Part 11: Metering equipment*, IEC 62052-11 2020 Std., 2020.

[61] *Electricity metering equipment (a.c.) – Part 1: General requirements, tests and test conditions - Metering equipment (class indexes A, B and C*, EN 50470-1:2006 Std., 2006.

[62] *Electricity metering equipment (a.c.) – Part 3: Particular requirements - Static meters for active energy (class indexes A, B and C)*, EN 50470-3:2006 Std., 2006.

[63] *Electromagnetic compatibility (EMC) – Part 4-6: Testing and measurement techniques – Immunity to conducted disturbances, induced by radio-frequency fields*, IEC 61000-4-6 Std., 2014.

[64] M. I. Sudrajat, N. Moonen, H. Bergsma, and F. Leferink, "EMI Mitigation Technique for Warship Power Distribution Systems in the Frequency Range Below 150 kHz", in *2021 Asia-Pacific International Symposium on Electromagnetic Compatibility (APEMC)*, Nusa Dua - Bali, Indonesia, 2021, pp. 1–4.

[65] *Electromagnetic compatibility (EMC) - Part 3-12: Limits - Limits for harmonic current emissions produced by equipment connected to public low-voltage systems with input current >16 A and ≤75 A per phase*, IEC 61000-3-12 Std., 2011.

[66] *Electromagnetic compatibility - Requirements for household appliances, electric tools and similar apparatus - Part 1: Emission*, CISPR 14-1:2020 Std., 2020.

[67] *Electromagnetic compatibility - Requirements for household appliances, electric tools and similar apparatus - Part 2: Immunity*, CISPR 14-2:2020 Std., 2020.

[68] *Limits and methods of measurement of radio disturbance characteristics of electrical lighting and similar equipment*, CISPR 15:2018 Std., 2018.

[69] *Industrial, scientific and medical equipment - Radio-frequency disturbance characteristics - Limits and methods of measurement*, CISPR 11:2015 Std., 2015.

[70] *Electromagnetic compatibility of multimedia equipment - Emission requirements*, CISPR 32:2015 Std., 2015.

[71] F. Zare, H. Soltani, D. Kumar, P. Davari, H. A. M. Delpino, and F. Blaabjerg, "Harmonic emissions of three-phase diode rectifiers in distribution networks", *IEEE Access*, vol. 5, pp. 2819–2833, Feb. 2017.

[72] *Specification for radio disturbance and immunity measuring apparatus and methods - Part 1-1: Radio disturbance and immunity measuring apparatus - Measuring apparatus*, CISPR 16-1-1:2019 Std., 2019.

[73] *Consideration of reference impedances and public supply network impedances for use in determining the disturbance characteristics of electrical equipment having a rated current $\leq$ 75 A per phase*, IEC TR 60725:2012 Std., 2012.

[74] *Electromagnetic compatibility (EMC) – Part 4-7: Testing and measurement techniques – General guide on harmonics and interharmonics measurements and instrumentation, for power supply systems and equipment connected thereto*, IEC 61000-4-7:2002 Std., 2002.

[75] *Specification for radio disturbance and immunity measuring apparatus and methods - Part 1-2: Radio disturbance and immunity measuring apparatus - Coupling devices for conducted disturbance measurements*, EN 55016-1-2:2014 Std., 2014.

[76] *Specification for radio disturbance and immunity measuring apparatus and methods - Part 1-2: Radio disturbance and immunity measuring apparatus - Coupling devices for conducted disturbance measurements*, CISPR 16-1-2:2014 Std., 2014.

[77] R. Stiegler, J. Meyer, S. Schori, M. Höckel, K. Scheida, J. Drápela, and T. Hanžlík, "Survey of network impedance in the frequency range 2-9 kHz in public low voltage networks in AT/CH/CZ/GE", in *25th International Conference on Electricity Distribution*, Madrid, Spain, 2019, pp. 1–5.

[78] B. ten Have, C. Keyer, and F. Leferink, "Monitoring of Power Measured by Static Energy Meters for Observing EMI Issues", in *2018 International Symposium on Electromagnetic Compatibility (EMC Europe)*, Amsterdam, The Netherlands, 2018, pp. 903–907.

[79] B. ten Have, T. Hartman, N. Moonen, and F. Leferink, "Misreadings of Static Energy Meters due to Conducted EMI caused by Fast Changing Current", in *2019 Joint International Symposium on Electromagnetic Compatibility and Asia-Pacific International Symposium on Electromagnetic Compatibility*, Sapporo, Japan, 2019, pp. 445–448.

[80] B. ten Have, T. Hartman, N. Moonen, and F. Leferink, "Inclination of Fast Changing Currents Effect the Readings of Static Energy Meters", in *2019 International Symposium on Electromagnetic Compatibility (EMC Europe 2019)*, Barcelona, Spain, 2019, pp. 208–213.

[81] B. ten Have, T. Hartman, N. Moonen, and F. Leferink, "Unfairly Faulty Energy Meter Reading due to Inappropriate Use of the Blondel Theorem", in *2020 International Symposium on Electromagnetic Compatibility - EMC EUROPE*, Rome, Italy, 2020, pp. 1–5.

[82] T. Hartman, B. ten Have, J. Dijkstra, R. Grootjans, N. Moonen, and F. Leferink, "Susceptibility of Static Energy Meters Due to Clipping Caused by a Rogowski Coil", *IEEE Transactions on Electromagnetic Compatibility*, pp. 1–9, 2022.

[83] B. J. Van Leersum, R. B. Timens, F. J. Buesink, and F. B. Leferink, "Time domain methods for the analysis of conducted interference on the power supply network of complex installations", in *2014 International Symposium on Electromagnetic Compatibility*, IEEE, Gothenburg, Sweden, 2014, pp. 605–610.

[84] *Electromagnetic compatibility (EMC) - Part 4-30: Testing and measurement techniques - Power quality measurement methods*, 2012.

[85] *IEEE Standard for Transitions, Pulses, and Related Waveforms*, IEEE Std 181-2011 (*Revision of IEEE Std 181-2003*) Std., 2011.

[86] Z. Marais, H. E. Van den Brom, G. Rietveld, R. Van Leeuwen, D. Hoogenboom, and J. Rens, "Sensitivity of static energy meter reading errors to changes in non-sinusoidal load conditions", in *2019 International Symposium on Electromagnetic Compatibility (EMC Europe 2019)*, Barcelona, Spain, 2019, pp. 202–207.

[87] STMicroelectronics, "Programmable single phase energy metering IC with tamper detection", STPM01 datasheet, Jun. 2011, Doc ID 10853 Rev 8.

[88] A. Blondel, "Measurement of the energy of polyphase currents", in *Proceedings of the International Electrical Congress Held in the City of Chicago*, Chicago, USA, 1893, pp. 112–116.

[89] "Progress in the art of metering electric energy: III — Special applications", *Electrical Engineering*, vol. 60, no. 11, pp. 540–546, Nov. 1941.

[90] Y. Xiang, V. Cuk, and J. F. Cobben, "Impact of residual harmonic current on operation of residual current devices", in *2011 10th International Conference on Environment and Electrical Engineering*, Rome, Italy, 2011, pp. 1–4.

[91] A. Liew, "Nuisance trippings of residual current circuit breakers or ground fault protectors of power sources connected to computer and electronic loads", *Electric Power Systems Research*, vol. 20, no. 1, pp. 23–30, 1990.

[92] A. M. Blanco, F. Möller, J. Meyer, and P. Schegner, "Characterization of the leakage currents produced by household electronic devices", in *2020 19th International Conference on Harmonics and Quality of Power (ICHQP)*, Dubai, United Arab Emirates, 2020, pp. 1–6.

[93] B. ten Have, N. Moonen, and F. Leferink, "Time Domain Analysis of Current Transducer Responses using Impulsive Signals", *IEEE Letters on Electromagnetic Compatibility Practice and Applications*, vol. 3, no. 1, pp. 19–23, Mar. 2021.

[94] B. ten Have, N. Moonen, and F. Leferink, "Electromagnetically Interfered Energy Metering Resulting from Droop of Current Transducers", in *2021 IEEE International Joint EMC/SI/PI and EMC Europe Symposium*, Raleigh, NC, USA, 2021, pp. 250–254.

[95] *IEEE Standard Requirements for Instrument Transformers*, IEEE Std C57.13-2016 Std., 2016.

[96] C. Narduzzi and C. Offelli, "A time-domain method for the accurate characterization of linear systems", *IEEE Transactions on Instrumentation and Measurement*, vol. 40, no. 2, pp. 415–419, 1991.

[97] A. Cataliotti, D. Di Cara, A. E. Emanuel, and S. Nuccio, "A novel approach to current transformer characterization in the presence of harmonic distortion", *IEEE Transactions on Instrumentation and Measurement*, vol. 58, no. 5, pp. 1446–1453, 2009.

[98] A. Cataliotti, D. Di Cara, A. E. Emanuel, and S. Nuccio, "Characterization of clamp-on current transformers under nonsinusoidal conditions", *IEEE Transactions on Power Delivery*, vol. 24, no. 1, pp. 373–380, 2009.

[99] L. Shi, J. Tan, and B. Zhou, "Time domain calibration of pulsed current probe", in *17th International Zurich Symposium on Electromagnetic Compatibility*, Singapore, Singapore, 2006, pp. 296–299.

[100] M. Appelman, M. A. Wibisono, W. Shalannanda, N. Moonen, and F. Leferink, "Comparison of Time-domain Measurement Techniques for Interference Analysis in Power Line Communication", in *2019 IEEE 5th International Conference on Wireless and Telematics (ICWT)*, Yogyakarta, Indonesia, 2019, pp. 1–5.

[101] T. Van Leersum, "Characterization Method Using Square Wave Signals for Testing Current Transducer Responses", B.Sc. thesis, University of Twente, Enschede, The Netherlands, 2021.

[102] B. ten Have, M. A. Azpúrua, T. Hartman, M. Pous, N. Moonen, F. Silva, and F. Leferink, "Waveform Model to Characterize Time-Domain Pulses Resulting in EMI on Static Energy Meters", *IEEE Transactions on Electromagnetic Compatibility*, vol. 63, no. 5, pp. 1542–1549, Oct. 2021.

[103] H. E. van den Brom, R. van Leeuwen, Z. Marais, B. ten Have, T. Hartman, M. A. Azpúrua, M. Pous, G. J. P. Kok, M. G. A. van Veghel, I. Kolevatov, H. Malmbekk, F. Silva, and F. Leferink, "EMC Testing of Electricity Meters Using Real World and Artificial Current Waveforms", *IEEE Transactions on Electromagnetic Compatibility*, vol. 63, no. 6, pp. 1865–1874, Dec. 2021.

[104] S. Lodetti, D. Ritzmann, P. Davis, P. Wright, H. van den Brom, Z. Marais, and B. ten Have, "Wavelet-based sparse representation of waveforms for type-testing of static electricity meters", *IEEE Transactions on Instrumentation and Measurement*, vol. 71, pp. 1–10, Feb. 2022.

[105] P. Jaques, R. Kolander, R. Hartig, R. Stiegler, A. Fröbel, and J. Meyer, "Survey of current gradient at public low voltage customer terminals in Germany", in *25th International Conference on Electricity Distribution*, Madrid, Spain, 2019, pp. 1–5.

[106] T. Hartman, M. Pous, M. A. Azpúrua, F. Silva, and F. Leferink, "On-site Waveform Characterization at Static Meters Loaded with Electrical Vehicle Chargers", in *2019 International Symposium on Electromagnetic Compatibility (EMC Europe 2019)*, Barcelona, Spain, 2019, pp. 191–196.

[107] B. ten Have, M. A. Azpúrua, M. Pous, F. Silva, and F. Leferink, "On-Site Waveform Survey in LV Distribution Network using a Photovoltaic Installation", in *2020 International Symposium on Electromagnetic Compatibility (EMC Europe 2020)*, Rome, Italy, 2020, pp. 1–6.

[108] L. Yang, S. Liu, S. Tsoka, and L. G. Papageorgiou, "Mathematical programming for piecewise linear regression analysis", *Expert Systems with Applications*, vol. 44, pp. 156–167, Feb. 2016.

[109] R. Killick, P. Fearnhead, and I. A. Eckley, "Optimal detection of changepoints with a linear computational cost", *Journal of the American Statistical Association*, vol. 107, no. 500, pp. 1590–1598, Dec. 2012.

[110] M. Sabarimalai Manikandan, S. R. Samantaray, and I. Kamwa, "Detection and Classification of Power Quality Disturbances Using Sparse Signal Decomposition on Hybrid Dictionaries", *IEEE Transactions on Instrumentation and Measurement*, vol. 64, no. 1, pp. 27–38, 2015.

[111] W. Yao, Q. Tang, Z. Teng, Y. Gao, and H. Wen, "Fast S-Transform for Time-Varying Voltage Flicker Analysis", *IEEE Transactions on Instrumentation and Measurement*, vol. 63, no. 1, pp. 72–79, 2014.

[112] S. Lodetti, J. Bruna, J. J. Melero, V. Khokhlov, and J. Meyer, "A Robust Wavelet-Based Hybrid Method for the Simultaneous Measurement of Harmonic and Supraharmonic Distortion", *IEEE Transactions on Instrumentation and Measurement*, vol. 69, no. 9, pp. 6704–6712, 2020.

[113] M. P. Tcheou, L. Lovisolo, M. V. Ribeiro, E. A. B. da Silva, M. A. M. Rodrigues, J. M. T. Romano, and P. S. R. Diniz, "The Compression of Electric Signal Waveforms for Smart Grids: State of the Art and Future Trends", *IEEE Transactions on Smart Grid*, vol. 5, no. 1, pp. 291–302, 2014.

[114] M. Zhang, K. Li, and Y. Hu, "A High Efficient Compression Method for Power Quality Applications", *IEEE Transactions on Instrumentation and Measurement*, vol. 60, no. 6, pp. 1976–1985, 2011.

[115] D. Ritzmann and P. Wright, "Specification of New Test Waveforms for Static Electricity Meters", in *2020 Conference on Precision Electromagnetic Measurements (CPEM)*, Denver, CO, USA, 2020, pp. 1–2.

[116] F. Barakou, P. S. Wright, H. E. van den Brom, G. Kok, and G. Rietveld, "Detection Methods for Current Signals Causing Errors in Static Electricity Meters", *2019 International Symposium on Electromagnetic Compatibility (EMC Europe 2019)*, pp. 273–278, Barcelona, Spain, 2019.

[117] B. ten Have, N. Moonen, and F. Leferink, "Current Emissions Generated by Dimmed Lighting Equipment of Different Technologies", in *2021 Asia-Pacific International Symposium on Electromagnetic Compatibility (APEMC)*, Nusa Dua - Bali, Indonesia, 2021, pp. 1–4.

[118] B. ten Have, T. Hartman, N. Moonen, and F. Leferink, "Statistical Time-Domain Analysis of Equipment in Low-Voltage Networks", *IEEE Letters on Electromagnetic Compatibility Practice and Applications*, vol. 3, no. 4, pp. 114–117, Dec. 2021.

[119] W. El Sayed, H. Loschi, C. L. Lok, P. Lezynski, and R. Smolenski, "Prospective Analysis of the effect of Silicon based and Silicon-Carbide based Converter on G3 Power Line Communication", in *2020 International Symposium on Electromagnetic Compatibility (EMC Europe 2020)*, Rome, Italy, 2020, pp. 1–6.

[120] A. M. Blanco, E. Gasch, J. Meyer, and P. Schegner, "Web-based Platform for Exchanging Harmonic Emission Measurements of Electronic Equipment", *2012 IEEE 15th International Conference on Harmonics and Quality of Power*, pp. 943–948, Hong Kong, China, 2012.

[121] G. Dreyfus and C. Gallinat, "Rise and Shine: Lighting the World with 10 Billion LED Bulbs," U.S. Department of Energy, United States, Dec. 7, 2015. [Online]. Available: https://www.energy.gov/articles/rise-and-shine-lighting-world-10-billion-led-bulbs, Accessed on: Jun. 24, 2022.

[122] S. Uddin, H. Shareef, A. Mohamed, and M. A. Hannan, "An Analysis of Harmonics from LED Lamps", in *2012 Asia-Pacific Symposium on Electromagnetic Compatibility*, Singapore, Singapore, 2012, pp. 837–840.

[123] A. Gil-De-Castro, R. Medina-Gracia, S. K. Ronnberg, A. M. Blanco, and J. Meyer, "Differences in the performance between CFL and LED lamps under different voltage distortions", in *Proceedings of International Conference on Harmonics and Quality of Power, ICHQP*, IEEE, Ljubljana, Slovenia, 2018, pp. 1–6.

[124] M. A. Azpúrua, M. Pous, and F. Silva, "Decomposition of Electromagnetic Interferences in the Time-Domain", *IEEE Transactions on Electromagnetic Compatibility*, vol. 58, no. 2, pp. 385–392, January, 2016.

[125] T. Hartman, N. Moonen, and F. Leferink, "Evaluation of Multichannel Synchronous Conducted TDEMI Measurements for High Voltage Power Electronics", *2018 International Symposium on Electromagnetic Compatibility (EMC EUROPE)*, pp. 839–843, Amsterdam, The Netherlands, 2018.

[126] B. Audone, R. Colombo, I. Marziali, and O. Losito, "The Short Time Fourier Transform and the Spectrograms to Characterize EMI Emissions", *2016 International Symposium on Electromagnetic Compatibility - EMC EUROPE*, pp. 882–888, Wroclaw, Poland, 2016.

[127] H. Wickham and L. Stryjewski, "40 years of boxplots", had.co.nz, Tech. Rep., 2012.

[128] T. Wohlfahrt, C. Waniek, J. M. Myrzik, J. Meyer, and P. Schegner, "Supraharmonic disturbances: Lifetime reduction of electronic mass-market equipment by the aging of electrolytic capacitors", in *2018 18th International Conference on Harmonics and Quality of Power (ICHQP)*, Ljubljana, Slovenia, 2018, pp. 1–6.

[129] B. ten Have, M. A. Azpúrua, T. Hartman, M. Pous, N. Moonen, F. Silva, and F. Leferink, "Estimation of Static Energy Meter Interference in Waveforms Obtained in On-Site Scenarios", *IEEE Transactions on Electromagnetic Compatibility*, vol. 64, no. 1, pp. 19–26, Feb. 2022.

[130] M. A. Azpúrua and K. D. Ramos, "A comparison of spatial interpolation methods for estimation of average electromagnetic field magnitude", *Progress In Electromagnetics Research*, vol. 14, pp. 135–145, 2010.

[131] M. A. Azpúrua, M. Pous, J. A. Oliva, B. Pinter, M. Hudlicka, and F. Silva, "Waveform Approach for Assessing Conformity of CISPR 16-1-1 Measuring Receivers", *IEEE Transactions on Instrumentation and Measurement*, vol. 67, no. 5, pp. 1187–1198, May 2018.

[132] M. Pous, M. A. Azpúrua, and F. Silva, "APD oudoors time-domain measurements for impulsive noise characterization", *2017 International Symposium on Electromagnetic Compatibility - EMC EUROPE 2017, EMC Europe 2017*, pp. 1–6, Angers, France, 2017.

List of publications

Peer-reviewed journal papers

1. **B. ten Have**, T. Hartman, N. Moonen, and F. Leferink, "Static Energy Meters and the Electrical Environment Comply to the Standards but Are Not Compatible", *[Manuscript submitted for publication] IEEE Electromagnetic Compatibility Magazine*, pp. 1-8, 2022.

2. **B. ten Have**, M. A. Azpúrua, T. Hartman, M. Pous, N. Moonen, F. Silva, and F. Leferink, "Estimation of Static Energy Meter Interference in Waveforms Obtained in On-Site Scenarios", *IEEE Transactions on Electromagnetic Compatibility*, vol. 64, no. 1, pp. 19-26, Feb. 2022.

3. **B. ten Have**, T. Hartman, N. Moonen, and F. Leferink, "Statistical Time-Domain Analysis of Equipment in Low-Voltage Networks", *IEEE Letters on Electromagnetic Compatibility Practice and Applications*, vol. 3, no. 4, pp. 114-117, Dec. 2021.

4. **B. ten Have**, M. A. Azpúrua, T. Hartman, M. Pous, N. Moonen, F. Silva, and F. Leferink, "Waveform Model to Characterize Time-Domain Pulses Resulting in EMI on Static Energy Meters", *IEEE Transactions on Electromagnetic Compatibility*, vol. 63, no. 5, pp. 1542-1549, Oct. 2021.

5. **B. ten Have**, N. Moonen, and F. Leferink, "Time Domain Analysis of Current Transducer Responses using Impulsive Signals", *IEEE Letters on Electromagnetic Compatibility Practice and Applications*, vol. 3, no. 1, pp. 19-23, Mar. 2021.

6. T. Hartman, **B. ten Have**, J. Dijkstra, R. Grootjans, N. Moonen, and F. Leferink, "Susceptibility of Static Energy Meters Due to Clipping Caused by a Rogowski Coil", *IEEE Transactions on Electromagnetic Compatibility*, pp. 1-9, 2022.

7. S. Lodetti, D. Ritzmann, P. Davis, P. Wright, H. van den Brom, Z. Marais, **B. ten Have**, "Wavelet-Based Sparse Representation of Waveforms for Type-Testing of Static Electricity Meters", *IEEE Transactions on Instrumentation and Measurements*, vol. 71, pp. 1-10, Feb. 2022.

8. H. E. van den Brom, R. van Leeuwen, Z. Marais, **B. ten Have**, T. Hartman, M. A. Azpúrua, M. Pous, G. J. P. Kok, M. G. A. van Veghel, I. Kolevatov, H. Malmbekk, F. Silva, and F. Leferink, "EMC Testing of Electricity Meters Using Real-World and Artificial Current Waveforms", *IEEE Transactions on Electromagnetic Compatibility*, vol. 63, no. 6, pp. 1865-1874, Dec. 2021.

Peer-reviewed conference papers

9. **B. ten Have**, N. Moonen, and F. Leferink, "Current Emissions Generated by Dimmed Lighting Equipment of Different Technologies", in *2021 Asia-Pacific International Symposium on Electromagnetic Compatibility (APEMC)*, Nusa Dua - Bali, Indonesia, 2021, pp. 1-4.

10. **B. ten Have**, N. Moonen, and F. Leferink, "Electromagnetically Interfered Energy Metering Resulting from Droop of Current Transducers", in *2021 IEEE International Joint EMC/SI/PI and EMC Europe Symposium*, Raleigh, NC, USA, 2021, pp. 250-254. [1]

11. **B. ten Have**, M. A. Azpúrua, M. Pous, F. Silva, and F. Leferink, "On-Site Waveform Survey in LV Distribution Network using a Photovoltaic Installation", in *2020 International Symposium on Electromagnetic Compatibility (EMC Europe 2020)*, Rome, Italy, 2020, pp. 1-6.

12. **B. ten Have**, T. Hartman, N. Moonen, and F. Leferink, "Unfairly Faulty Energy Meter Reading due to Inappropiate Use of the Blondel Theorem", in *2020 International Symposium on Electromagnetic Compatibility (EMC Europe 2020)*, Rome, Italy, 2020, pp. 1-5.

13. **B. ten Have**, N. Moonen, and F. Leferink, "On-Site Efficiency Analysis in a Generator in the Millisecond Range", in *2020 IEEE International Symposium on Electromagnetic Compatibility Signal/Power Integrity (EMCSI)*, Reno, USA, 2020, pp. 209-212.

14. **B. ten Have**, T. Hartman, N. Moonen, and F. Leferink, "Why Frequency Domain Tests Like IEC 61000-4-19 Are Not Valid; a Call for Time Domain Testing", in *2019 International Symposium on Electromagnetic Compatibility (EMC Europe 2019)*, Barcelona, Spain, 2019, pp. 124-128.

15. **B. ten Have**, T. Hartman, N. Moonen, and F. Leferink, "Inclination of Fast Changing Currents Effect the Readings of Static Energy Meters", in *2019 International Symposium on Electromagnetic Compatibility (EMC Europe 2019)*, Barcelona, Spain, 2019, pp. 445-448.

[1] Finalist for the Best EMC Paper at the 2021 IEEE International Joint EMC/SI/PI and EMC Europe Symposium.

16. **B. ten Have**, T. Hartman, N. Moonen, and F. Leferink, "Misreadings of Static Energy Meters due to Conducted EMI caused by Fast Changing Current", in *2019 Joint International Symposium on Electromagnetic Compatibility and Asia-Pacific International Symposium on Electromagnetic Compatibility*, Sapporo, Japan, 2019, pp. 445-448.

17. **B. ten Have**, T. Hartman, N. Moonen, C. Keyer, and F. Leferink, "Faulty Readings of Static Energy Meters Caused by Conducted Electromagnetic Interference from a Water Pump", in *Renewable Energy and Power Quality Journal (RE&PQJ)*, Santa Cruz de Tenerife, Spain, 2019, pp. 15-19.

18. **B. ten Have**, C. Keyer, and F. Leferink, "Monitoring of Power Measured by Static Energy Meters for Observing EMI Issues", in *2018 International Symposium on Electromagnetic Compatibility (EMC Europe)*, Amsterdam, The Netherlands, 2018, pp. 903-907.

19. M. A. Wibisono, **B. ten Have**, W. El Sayed, N. Moonen, D. Hamdani, and F. Leferink, "Impact of a Speed-Controlled Water Pump on Power Line Communication of Smart Energy Meters", in *2021 Asia-Pacific International Symposium on Electromagnetic Compatibility (APEMC)*, Nusa Dua - Bali, Indonesia, 2021, pp. 1-4. [2]

20. T. Hartman, **B. ten Have**, N. Moonen, and F. Leferink, "How to Earn Money with an EMI Problem: Static Energy Meters Running Backwards", in *2021 IEEE International Joint EMC/SI/PI and EMC Europe Symposium*, Raleigh, NC, USA, 2021, pp. 788-793.

21. T. Hartman, N. Moonen, **B. ten Have**, and F. Leferink, "Fast Magnetic Emission Tests for Continuous Measurements Around an Equipment Under Test", in *2019 ESA Workshop on Aerospace EMC (Aerospace EMC)*, Budapest, Hungary, 2019, pp. 1-5.

[2]Nominated for the Best Student Paper Award at the 2021 Asia-Pacific International Symposium on Electromagnetic Compatibility (APEMC).

Acknowledgement

When starting this journey towards a Doctor of Philosophy degree I did not know were it would take me. Sometimes it felt like a *Grand Tour* with flat, hilly, and mountain stages. With quite tough mountains, *hors catégory* conclusively. At some moments the roads seemed endless, its climbs seemed pointless, or just too steep. Not to mention the many detours, or taking roads back and forth. I did not understand it many times, frustrating. But at some moment I managed to connect the countless obstacles and saw were I was going. Afterwards, it was a pleasure to try and get to the finish and to compile the notable results into this thesis. Luckily the route was not an individual pursuit, but there was a peloton guiding me through it. Therefore, I would like to thank the people that supported me.

First of all, I would like to thank my promoter Frank for giving me the opportunity to do a PhD. Something I had not taught about myself at the moment you proposed this position to me. You have always motivated me to do my best, push me to really finish my tasks, which I was not that good in at the start, trigger me to become an academic researcher and not only to complete certain tasks, and also to pursue on developing non-scientific qualities. Furthermore, many thanks for allowing me to visit conferences and meetings abroad (unluckily lots of them were online due to COVID-19), after which I could explore the area by bike, e.g. Sapporo, Barcelona, and Spokane.

Second, I would like to thank my co-promoter Niek M. for the technical discussions that we had and for the thorough paper reviews. That has improved my work quite significant. Furthermore, you are approachable and respond quickly, which was very helpful especially in times of COVID-19 (a large part of my PhD) when human interaction was not self-evident. I only had to message you on MS Teams to get any help or a discussion started.

Over the last years a lot of things changed in our research group, from Telecommunication Engineering in the beginning towards Power Electronics and Electromagnetic Compatibility group at the end. Therefore, I had the opportunity to work and socialize with a lot of colleagues. It is always super cozy to enjoy the coffee, lunch, or whatever break, coffee+ses, the Friday afternoon drinks (I mean talks), the Christmas diner, drinks at the conferences, and many more socializing things together with all of you, thanks!

Lillian, I would like to thank you for always being so helpful and friendly.

If we have to register for a conference, book a trip, reserve a room, or just anything else, you did it as if it was the natural thing to, this makes life so much easier. And most importantly the personal aspect, just asking how I am doing, it makes you feel so comfortable and welcome. Many thanks!

Next, I would like to thank Tom for our collaboration over the past years. We started together working towards a PhD in the MeterEMI project and it was really nice not to be alone in this project and attending meetings, conferences, etc. together. Maybe at the beginning our collaboration did not always work, but towards the end it was a pleasure to collaborate on so many articles and also other things like supervising students among others.

Vervolgens wil ik graag Chris, de oude man uit Renkum, bedanken voor zijn toewijding in het opsporen en doorspitten van alle door consumenten gerapporteerde problemen omtrent de kilowattuurmeter. Jouw expertise heeft ons heel erg geholpen in de analyse van al deze gemelde problemen. Dit heeft ons bovendien een aantal erg interessante casussen opgeleverd waar we uiteindelijk in-situ metingen bij de consument hebben uitgevoerd, waarvan een aantal zijn benoemd in dit proefschrift. Daarnaast hebben jou contacten ons ook geholpen om een aantal 'van de vrachtwagen gevallen' meters te verkrijgen om te testen in ons lab, en diverse meetcampagnes zoals in jou lokale bouwmarkt.

Next, I would like to thank Marc and Marco from UPC for our enjoyable collaboration in the MeterEMI project. During which I went to Barcelona to perform on-site measurements. This was one of the "working" weeks that I really enjoyed, especially the back-heel goal of Suárez in Camp Nou after an assist of Frenkie (and watching Messi of course). This week also directly resulted in a collaborated conference paper. Luckily afterwards we managed to continue our collaboration and even wrote two Transaction articles together! I have experience our collaboration on those articles as extremely fruitful and I have learned a lot on writing technical articles. Both of you always had time to discuss and to contribute to the waveform model that resulted from it, I could never have figured that alone.

I would like to thank Cees, although not longer with us, for his practical help during installation of the measurement setup in the on-site. You helped me on your own way and told me *"this is a metering cabinet, good luck"*. You advised me to wear insulating safety gloves, which you did not wear yourself. But after your "tutorial" I was quite confident that I could repeat it myself.

Next, I would like to thank Roelof B.T. for providing his premise as one of the first on-site labs, for verifying the correct operation of the installed static energy meter with your solar panels. And Frits for performing electric field measurements during that visit. I have gained a lot of practical experience there, and it was also quite an experience to watch the two of you collaborating.

Furthermore, I would like to thank all the consumers that trusted me to perform on-site measurements at their premise, with the aim to verify the readings of the installed static energy meters. This was really helpful in understanding the metering problem, by gaining access to what was occurring in the "real" world and discussing our and also your observations. Besides, these measure-

ment locations through the whole country also provided opportunities to cycle in other areas, which was very enjoyable, e.g. Limburg and Schoorl.

Ik wil graag mijn familie bedanken voor de steun en hulp die ze mij hebben geboden bij de keuzes die ik heb gemaakt. Mama, ik kan onze belletjes op zondag avond altijd erg waarderen, of samen wandelen, of gezellig spelletjes spelen, het laatste ook vaak met Birgit en Niek. Papa, ik geniet altijd erg van onze fietstochten samen door het Groninger land of zelfs over de Mont Ventoux, of het geneuzel over wat dan ook. Birgit, het is altijd erg gezellig om deels samen te reizen op zondagavond, met de auto of trein, vaak ook met Niek. Dan konden we nog even praten over je studie, mijn PhD, planten, series, enzovoort. En de voorkant van dit boek, die jij hebt gemaakt, is gewoon geweldig geworden, bedankt! Niek, het is altijd gezellig om samen te ouwehoeren over voetbal, wielrennen, of iets dergelijks, daarnaast is het ook altijd mooi om samen een rondje te fietsen bijvoorbeeld recent op de Mont Ventoux of over de Zevenheuvelenweg!

Daarnaast wil ik graag mijn vrienden bedanken. Het Studieclubje, Arjan, Douwe, en Idzard, of het nou een barbeque of een illegale corona spelletjes avond (met één man te veel) was, het is altijd gezellig! En natuurlijk Klein Verzet voor de talloze fietstochten en ook activiteiten naast het fietsen. In het bijzonder Jesse Jan, Nick, Harmen, Jesse H., Arjan, Simon, en Philip, voor de verschillende fietsvakanties (of martelkampen). En Jesse Jan, als lokalmatador, voor de rondleiding door het mooie Drenthe, in 200 km op de MTB, twee keer... Daarnaast natuurlijk de verschillende commissies waarin ik heb mogen deelnemen, in het bijzonder de KoersCom voor het organiseren van de Ronde van Enschede in 2021 en de Ronde van Lonneker in 2022, het was erg tof om ook dit soort dingen naast mijn PhD te doen, allemaal erg bedankt!

Biography

Bas ten Have was born on 2 October 1994 in Grijpskerk, The Netherlands. He received the Bachelor of Science degree in 2015 and the Master of Science degree in 2018, both in electrical engineering, from the University of Twente, Enschede, The Netherlands. During his masters graduation project he researched a control meter that can be used to verify the readings of an already installed static energy meter at consumer's disputes. Since June 2018 he has been working towards the Doctor of Philosophy degree in electromagnetic compatibility with the Power Electronics and Electromagnetic Compatibility Group, at the University of Twente. He was involved in the MeterEMI project that focuses on the electromagnetic interference of static energy meters. In this project he was involved in the laboratory study that investigates cases resulting in misreadings of static energy meters, and in the on-site testing to capture signals to which static energy meters are typically exposed to in a real-world environment. Since August 2021 he works as a Researcher with the Power Electronics and Electromagnetic Compatibility Group, at the University of Twente. There he is involved in the STEPS project, that focuses on the storage of energy and power systems. His main focus is on supporting SMEs to advance the technical readiness level of their energy storage solution by providing knowledge in the field of EMC.
He was a finalist for the Best EMC Paper at the 2021 IEEE International Joint EMC/SI/PI and EMC Europe Symposium. And he co-authored a paper that was nominated for the Best Student Paper Award at the 2021 Asia Pacific International Symposium on Electromagnetic Compatibility.

bas.tenhave@utwente.nl ‖ bthave@gmail.com
linkedin.com/in/bas-ten-have